Susceptibility to Libby Amphibole-Induced Pulmonary Disease in the Cardiovascular-Compromised Subpopulation

Jonathan Henry Shannahan

A dissertation submitted to the faculty of the University of North Carolina at Chapel Hill in partial fulfillment of the requirements for the degree of Doctor of Philosophy in the Curriculum in Toxicology.

Chapel Hill
2011

Approved by:

Advisor: Dr. Urmila Kodavanti

Reader: Dr. Louise Ball

Reader: Dr. Andrew Ghio

Reader: Dr. Alan Hinderliter

Reader: Dr. Ilona Jaspers

ABSTRACT

Jonathan Henry Shannahan: Susceptibility to Libby Amphibole Induced Pulmonary Disease in the Cardiovascular-Compromised Subpopulation
(Under the direction of Dr. Urmila Kodavanti)

Human exposure to asbestos is known to cause the development of mesothelioma, asbestosis and lung cancer. Asbestos toxicity is thought to be mediated through reactive oxygen species (ROS) production by surface available iron (Fe). Within the lung asbestos can complex endogenous Fe possibly increasing toxicity. We hypothesized that asbsestos-induced inflammation and injury would be greater in rat models of human cardiovascular disease (CVD) with Fe-overload. We characterized the baseline pulmonary disease of normotensive Wistar Kyoto, spontaneously hypertensive (SH), and SH heart failure (SHHF) rats. SH and SHHF were found to exist with pulmonary inflammation, oxidative stress, and Fe-overload (SHHF>SH). Libby amphibole (LA) was used to examine the role of Fe in asbestos-induced toxicity. LA complexed Fe in an acellular system, which enhanced ROS production. In *in vitro* and *in vivo* models the inflammatory response to LA decreased with increased cellular and fiber-complexed Fe. The chelation of Fe from fibers and cells exacerbated LA-induced inflammation. To determine the role of increased host Fe in LA-induced inflammation, and lung pathology WKY, SH, and SHHF were intratracheally-instilled with LA (0.0, 0.25, and 1mg/rat). LA-induced neutrophilic inflammation was not exacerbated although persistent through 1-month in CVD models compared to WKY. SH and SHHF failed to increase antioxidants but increased Fe-binding proteins after LA exposure. Progressive pulmonary fibrosis was noted over 3-months in all strains, whereas the accumulation of Fe in fiber-laden macrophages occurred primarily in SHHF. At 3-months, only SHHF exposed to LA demonstrated atypical hyperplastic lesions of bronchiolar epithelial origin. Gene expression

profiling at 3-months indicated baseline differences reflective of pulmonary inflammation, and immune dysregulation in CVD models. Changes in genes involved in cell-cycle control and cancer pathways correlated with atypical hyperplasia in SHHF. We concluded LA can bind Fe and produce ROS in an acellular system but this process does not exacerbate the inflammatory response in cells or animals. Furthermore, in Fe-overload conditions, more Fe accumulates at sites of fiber deposition without enhancing the inflammatory response. In the presence of baseline lung pathology, the inability to further induce inflammation in response to LA may predispose those with Fe-overload to proliferative lung pathology.

TABLE OF CONTENTS

LIST OF TABLES

LIST OF FIGURES

LIST OF ABBREVIATIONS

AALAC	Association for the Assessment and Accreditation of Laboratory Animal Care
AP-1	Activator Protein-1
ASC	Apoptotic Speck Protein
BALF	Bronchoalveolar Lavage Fluid
CARD	Caspase Recruitment Domain
CCL-5	Chemokine Ligand-5
CCL-7	Chemokine Ligand-7
CCL-11	Chemokine Ligand-11
CCL-12	Chemokine Ligand-12
COX-2	Cyclooxygenase-2
CXCL-3	Chemokine Ligand-3
CXCL-14	Chemokine Ligand-14
CVD	Cardiovascular Disease
DAVID	Database for Annotation Visualization and Integrated Discovery
DEF	Deferoxamine
DEG	Differentially Expressed Gene
DMT-1	Divalent Metal Transporter-1
EGF	Epidermal Growth Factor
EPA	Environmental Protection Agency
F	Frequency
FAC	Ferric Ammonium Citrate
Fe	Iron

FeLA	Iron Loaded Libby Amphibole
FHC	Ferritin Heavy Chain
FLC	Ferritin Light Chain
GAPDH	Glyceraldehyde 3-Phosphate Dehydrogenase
GGT	Gamma glutamyl transferase
GSH	Glutathione
H & E	Hematoxylin and Eosin
HPLC	High Performance Liquid Chromatography
HO-1	Hemeoxygenase-1
HWKY	Hypertrophic Wistar Kyoto
ICP-MS	Inductively-Coupled Plasma Mass Spectrometry
IACUC	Institutional Animal Care and Use Committee
IFN-λ	Interferon-λ
IL-1α	Interleukin-1 Alpha
IL-1β	Interleukin-1 Beta
IL-6	Interleukin-6
IL-8	Interleukin-8
IL-18	Interleukin-18
ip	Intraperitoneal
IT	Inspiratory Time
KEGG	Kyoto Encyclopedia of Genes
KRAS	Kirsten Rat Sarcoma Viral Oncogene
LA	Libby Amphibole

LDH	Lactate Dehydrogenase
MIP-2	Macrophage Inflammatory Protein-2
MV	Minute Volume
NAG	N-acetyl-beta-D-glucosaminidase
NALP3	NACHT, LRR and PYD Domains-Containing Protein 3
NfκB	Nuclear Factor Kappa B
NHEERL	National Health and Environmental Effects Research Laboratory
NOX-2	NAPDH Oxidase-2
PAU	Pause
PEF	Peak Expiratory Flow
Penh	Enhanced Pause
PIF	Peak Inspiratory Flow
PM	Particulate Matter
ROS	Reactive Oxygen Species
RT-PCR	Reverse Transcriptase Polymerase Chain Reaction
S.E.	Standard Error
SH	Spontaneously Hypertensive
SHHF	Spontaneously Hypertensive Heart Failure
TE	Expiratory Time
TFR-1	Transferrin Receptor-1
TFR-2	Transferrin Receptor-2
TIBC	Total Iron Binding Capacity
TIMP-1	Tissue Inhibitor of metalloproteinase-1

TNF-α	Tumor Necrosis Factor Alpha
TP53	Tumor Protein p53
TRF	Transferrin
UIBC	Unsaturated Iron Binding Capacity
WKY	Wistar Kyoto

CHAPTER 1. INTRODUCTION

Asbestos is a well-known air pollutant associated with a number of pulmonary abnormalities and diseases including mesothelioma and asbestosis. Asbestos refers to a group of naturally occurring fibrous minerals that are divided into different sub-classes based on their chemical formulas. The serpentine family includes only chrysotile and the amphibole family includes tremolite, crocidolite, actinolite, richerite, and winchite. Chrysotile has a curly structure and is flexible; whereas the amphiboles consist of straight, inflexible, rod-like fibers. Prior to the 1970s, mined fibrous asbestos minerals were widely used in building materials, brake shoes, electrical wiring, and insulation. Because of the unique properties of asbestos minerals such as their durability, flexibility, and resistance to heat, electrical, and chemical damage, these materials had a variety of commercial applications. However, due to a strong correlation between asbestos exposure and the health risk of mesothelioma and other pulmonary diseases, its use has diminished in most developed countries.

Human exposure to asbestos takes place mainly in occupational settings; however, since it is naturally occurring, some environmental exposure does occur. Libby, Montana is currently an EPA superfund site and has been declared as the first public health emergency by the United States EPA. Because of the extensive history of mining operations of amphibole asbestos-contaminated vermiculite, significant asbestos exposure has taken place in Libby. The residents of Libby have shown orders of magnitude higher numbers of

asbestos-related diseases, such as asbestosis, lung cancer, and mesothelioma in comparison to the rest of the United States (Sullivan 2007). Furthermore epidemiological research has demonstrated a dose-dependent correlation between Libby amphibole (LA) exposure and cardiovascular disease (CVD) mortality (Larson et al. 2010), as well as an increase in the incidence of systemic autoimmune disease in Libby residents (Pfau et al. 2005). Because the asbestos-contaminated vermiculite was shipped, processed, and used all over the country, primarily for insulation in the attics of homes, exposure to LA is not limited to Libby, Montana. The physicochemistry of LA asbestos (Figure 1.1) is unique in that it is a complex mixture of different amphiboles, primarily winchite, and richterite with trace amounts of tremolite (Figure 1.2) (Meeker et al. 2003). It is currently not known how the toxicity of this mineral fibrous mix differs from the toxicity of other well-classified asbestos materials.

Figure 1.1

Figure 1.1. Scanning Electron microscope image of Libby amphibole asbestos at 10 μm resolution. Image from USGS Denver Microbeam Laboratory, G.P. Meeker.

Figure 1.2

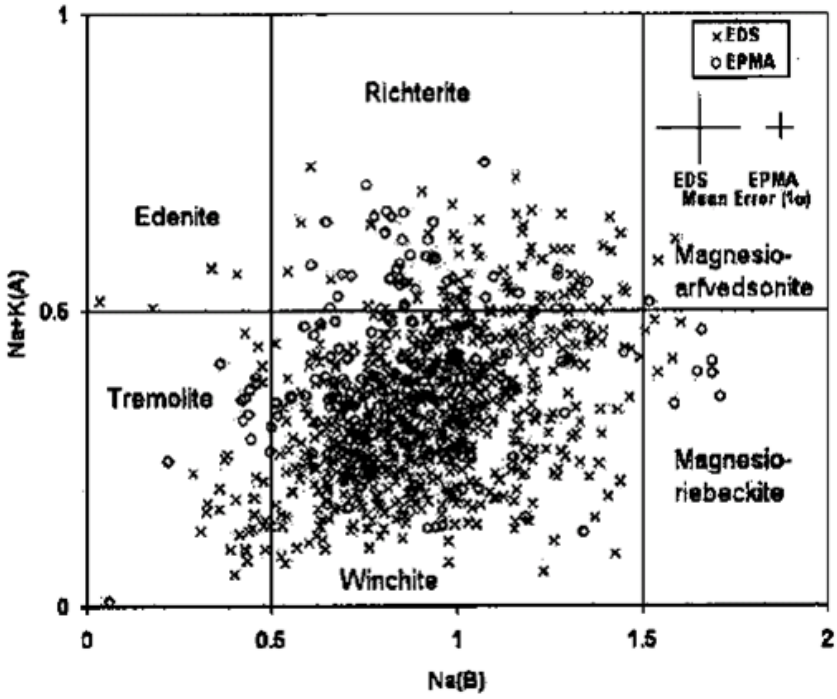

Figure 1.2. Specific fiber types found to compose the Libby amphibole fiber mix. (Meeker et al. 2003).

Chemical Formulas of Primary Fiber Components of Libby Amphibole

Winchite: $(CaNa)Mg_4(Al,Fe^{3+})Si_8O_{22}(OH)_2$

Richterite: $Na(CaNa)(Mg,Fe^{2+})_5[Si_8O_{22}](OH)_2$

Tremolite: $Ca_2Mg_5Si_8O_{22}(OH)_2$

In general, asbestos is known to cause pulmonary toxicity upon inhalation which leads to a variety of diseases. It has been estimated that the cumulative deaths associated

with asbestos exposure will surpass 200,000 by the year 2030 in the United States (Nicholson et al. 1982). A number of pulmonary diseases have been attributed specifically to asbestos exposure. Mesothelioma, a cancer of the mesothelium, is the most well-known asbestos associated disease. Mesothelioma usually arises in the pleural surface decades after exposure to asbestos in humans and decreases the functionality of the lung. The mode of action by which asbestos causes mesothelioma is currently unknown. The majority of mesothelioma cases occur in people who have been exposed occupationally to asbestos. Furthermore, inhalation of asbestos fibers has been linked to increases in the development of lung tumors, which is enhanced upon co-exposure with tobacco smoke (Vaino and Buffetta 1994, Mossman and Churg 1998). Exposure to asbestos can also cause the development of asbestosis leading to dyspnea, restrictive outcomes, and ultimately respiratory failure. Asbestosis is a chronic inflammatory condition of the lung resulting in fibrosis and is directly related to the biopersistence of asbestos within the lung.

Asbestos toxicity and eventually the development of asbestos-related diseases are thought to be mediated through the production of reactive oxygen species (ROS). ROS can cause direct cellular damage through the oxidation of lipids, proteins, and DNA. This damage can activate many pathways and transcription factors which in turn cause a variety of gene expression changes. Asbestos exposure is known to modify the expression of genes related to antioxidants, apoptosis, inflammatory cytokines, growth factors, and stress response (Kamp and Weitzman 1999) (Figure 1.3).

Figure 1.3

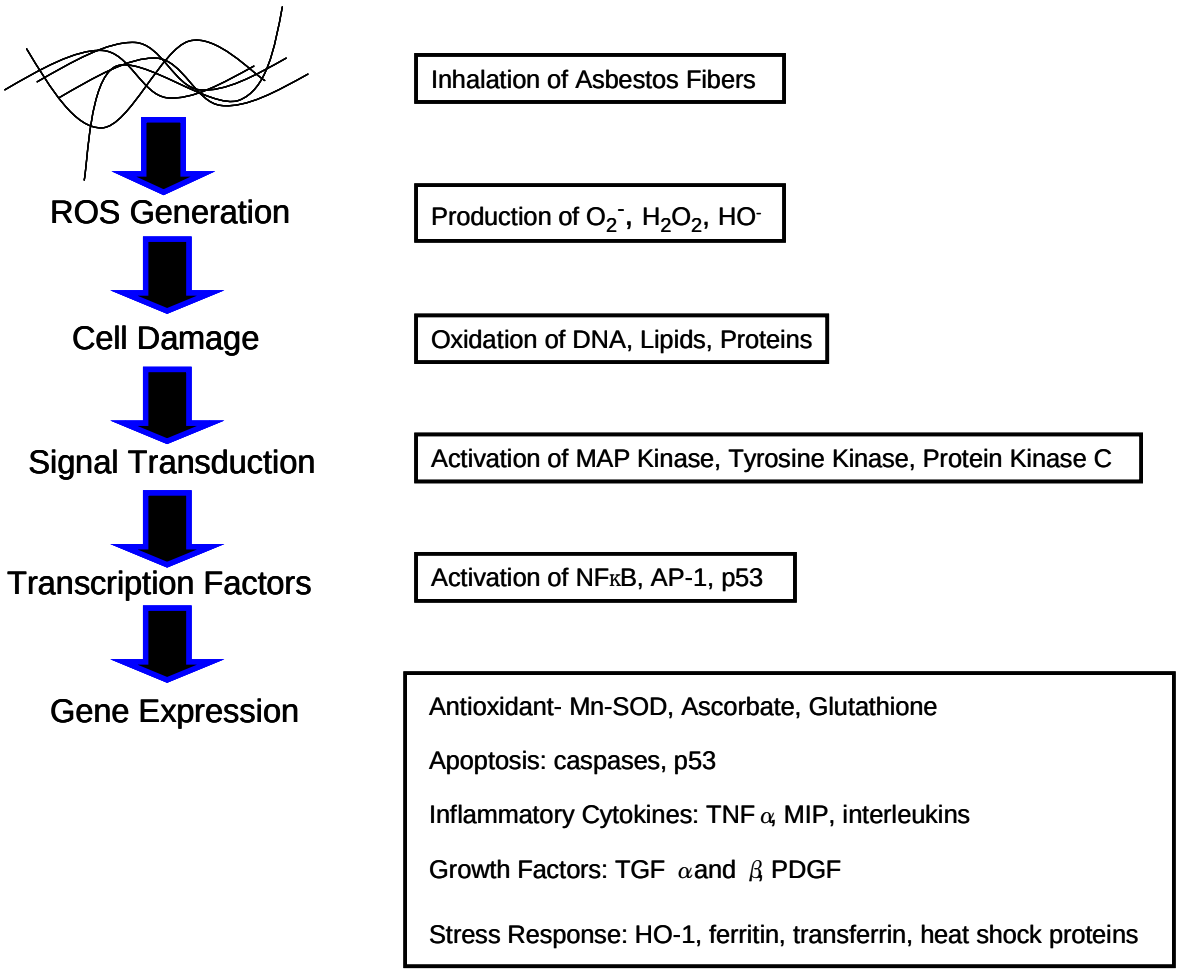

Figure 1.3. Effects of asbestos and generated reactive species in causing pulmonary toxicity.

In general, asbestos produces ROS through 1) frustrated phagocytosis, 2) redox cycling of surface available transition metals, 3) complexation of endogenous iron. Frustrated phagocytosis is directly related to the biopersistence of asbestos and the continual activation of inflammatory cells. Typically, foreign particles are removed from the lung via recognition and phagocytosis by alveolar macrophages. Asbestos fibers are usually too long and rigid to be completely engulfed and phagocytozed by alveolar macrophages. This inability of alveolar macrophages to clear fibers allows them more time within the lung to

induce toxicity. Fibers often can penetrate epithelial cells and the interstitium thereby contributing to the inflammatory cascade as well as causing extracellular matrix turnover. The inability to engulf the fiber leads to the further recruitment and activation of other inflammatory cells and causes continual production of ROS through activation of NADPH oxidase. This constant inflammation and production of ROS by inflammatory cells leads to damage of cells in the lung through oxidative stress. Besides initiating an inflammatory response, mediators released from alveolar macrophages also stimulate proliferation, production of growth factors and collagen synthesis by interstitial fibroblasts. This state of chronic inflammation eventually leads to thickening of the alveolar walls of the lung and filling of the alveolar spaces with scar tissue and fibrous connective tissue leading to fibrosis or asbestosis.

Asbestos itself is able to produce ROS through the redox cycling of iron (Fe) and other transition metals associated with its surface. Asbestos has been shown to generate ROS in cellular and acellular systems. Researchers have demonstrated that increasing the amount of Fe available on the surface of the fiber leads to increased oxidative damage, such as DNA double strand breaks and lipid oxidation. Furthermore chelation of Fe has been shown to reduce this damage *in vitro* and to lessen *in vivo* fiber-induced inflammation and DNA damage (Kamp 1995). Amphiboles typically have been shown to have increased amounts of Fe on their surfaces compared to chrysotile which may facilitate the production of ROS and enhance their toxicity. Fe on the surface of fibers is able to continually generate ROS through facilitating Fenton chemistry/Haber-Weiss reactions.

Fenton Reaction: $Fe^{2+} + H_2O_2 \rightarrow Fe^{3+} + HO^- + HO^\cdot$

Haber-Weiss Reaction: $O_2^- + H_2O_2 \rightarrow Fe \rightarrow HO^- + HO^\cdot + O_2$

Reduction of ferric iron to ferrous iron: $Fe^{3+} + O_2^- \rightarrow Fe^{2+} + O_2$

This output of ROS by the fiber producing an environment of oxidative stress within the lung that can lead to the progression of asbestos-induced diseases. Additionally, superoxide produced by inflammatory cells can assist in the production of hydroxyl radicals by driving Fenton reaction occurring on the surface of the fibers (Figure 1.4). Superoxide in an attempt to remove iron from the surface of the fiber reduces ferric iron to ferrous iron. This allows for the oxidation of hydrogen peroxide by ferrous iron to highly reactive hydroxyl radicals.

Figure 1.4

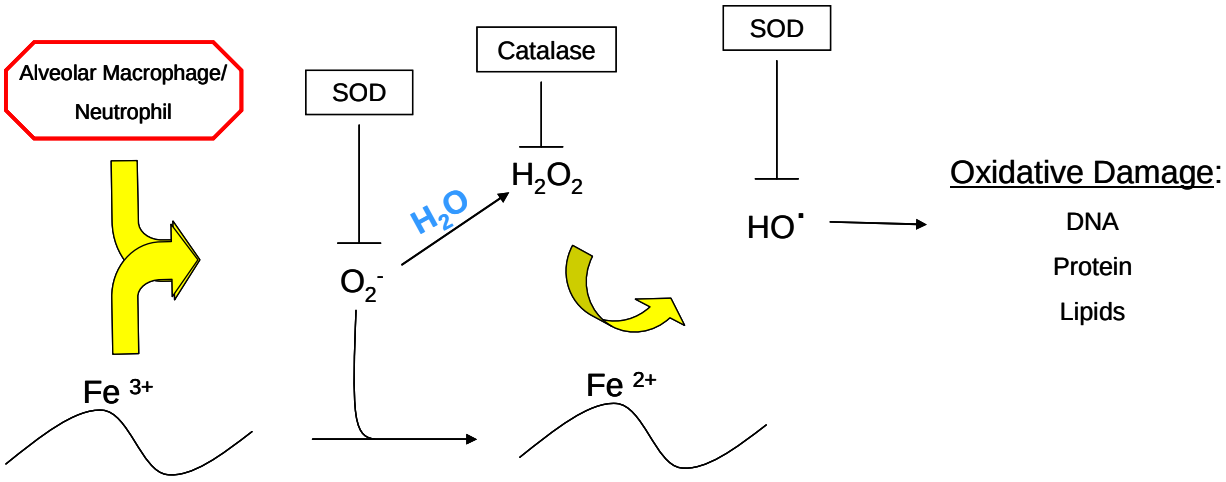

Figure 1.4. Mechanism of asbestos-induced free radical production via inflammatory cell activation and cycling of iron associated with the surface of the fiber.

Interestingly, asbestos has demonstrated an ability to bind catalytically active Fe from the endogenous labile Fe pool upon deposition into the airways and thereby potentiating the production of ROS (Ghio et al. 2004). At physiological pH there is a dissociation of hydrogens from Si-OH groups associated with the surface of asbestos leaving a net negative charge across the surface of the fiber allowing for ionic binding of cations. Due to the

bioavailability of Fe and the high stability constant for Si-O^- and Fe cations, inhaled asbestos becomes saturated by exogenous Fe in the lung forming ferriginous bodies (Figure 1.5). As long as one of the coordination sites on this Fe remains available it is still able to redox cycle and produce ROS. Through this mechanism the ability of the fiber to produce ROS is enhanced after inhalation. Due to the ability of asbestos to bind endogenous Fe we believe that individuals existing in a state of Fe-overload may be increasingly sensitive to the toxic effects of asbestos. Diseases and conditions associated with Fe-overload include thalassamia patients or others receiving repeated blood transfusions, diabetics, and individuals with cardiovascular disease (CVD).

Figure 1.5

Figure 1.5. Scanning Electron microscope image of asbestos fiber with ferringinous bodies associated with its surface at a magnification of 2,000.

Cardiovascular disease (CVD) is the number one cause of mortality and morbidity worldwide (Lopez et al. 2006, Sans et al. 1997). It is estimated that out of 300 million people in the United States, 80.7 million suffer from one or more forms of CVD. In the United

States, 35% of total deaths are attributable to CVD. Types of CVD include atherosclerosis, myocardial ischemia, congestive heart failure, hypertension, cerebrovascular disease, stroke, angina and others. In general, risk factors for the development of CVD include tobacco smoking, high blood pressure, diabetes mellitus, physical inactivity, high cholesterol, and obesity. Chronic cardiopulmonary diseases are associated with common multiple systemic alterations, including a dysregulation of Fe homeostasis, inflammation, microvascular thrombosis, and oxidative stress (Blum 2009; Omiya et al. 2009). This dysregulation of Fe homeostasis associated with chronic CVD is known to cause an increase in the systemic labile Fe pool (Kruszewski 2004). The labile Fe pool is an intracellular chelatable pool composed of both ferrous and ferric ions associated with a variety of ligands. The labile Fe loosely bound to ligands is able to potentially engage in reduction-oxidation, cycling which may be one of the factors increasing systemic oxidative stress in these individuals (Kakhlon and Cabantchik 2002). Due to these alterations, this population of individuals may compose a sub-group that is significantly more susceptible to the negative health effects of a variety of pollutants including asbestos.

Epidemiological studies have demonstrated that individuals with chronic diseases such as chronic obstructive pulmonary disease, diabetes, asthma, and CVD exhibit increased mortality and morbidity upon exposure to particulate matter. These findings have driven both the development and the increased use of animal models to study variations in human susceptibility to inhaled pollutants. A number of experimentally created and genetically predisposed rodent models have been used in the investigation of air pollution health effects (Nikula and Green 2000; Kodavanti and Costa 2001; Doggrell and Brown 1998). Our laboratory introduced the use of the genetically predisposed spontaneously hypertensive (SH)

rat for understanding CVD-related susceptibility to air pollution-induced injury a decade ago (Kodavanti et al. 2000). The SH rat as a model for human CVD is now accepted and extensively used to study air pollution health effects. Specifically, the SH rat mimics human hypertension and CVD in its pathogenesis, progression, and failure mechanisms (Schmid-Schonbein et al. 1991; Suzuki et al. 1995; Harjai 1999). Even though the hypertension displayed by the SH rat is similar to human hypertension, neither the number of gene polymorphisms nor the mechanism by which hypertension is initiated is currently known. Unlike the SH rat, the spontaneously hypertensive heart failure (SHHF) rat model of human CVD has not been used in air pollution susceptibility studies. The SHHF model was produced by breeding an obese SH rat with a non-obese SH rat and then inbreeding the offspring and selecting for the unique trait of congestive heart failure (McCune et al. 1990). The SHHF rat is a model of more severe CVD compared to SH because it presents with heart failure along with diastolic dysfunction in addition to hypertension (Cheng et al. 2009). The SHHF is known to exhibit hypertension and myocardial hypertrophy at 4 months of age or earlier. By 9 months of age, the SHHF demonstrates increased left ventricular wall thickness and enhanced markers of inflammation, hypertrophy and stress. Usually by approximately 18 months of age, they begin to present with dilated heart failure (Emter et al. 2005; Heyen et al. 2002). Most animal studies typically use the Wistar Kyoto (WKY) rat as the normotensive reference strain in conjunction with the SH or SHHF due to the WKY being the genetic background for both models (Okomoto and Akoto 1963). The use of the SH rat has generally supported epidemiological studies in that the SH rat model has demonstrated exacerbated cardiac outcomes, oxidative stress, and pulmonary injury/inflammation in response to a number of air pollutants (Yu et al. 2008; Kodavanti et al. 2002; Kodavanti et al.

2006; Farraj et al., 2009) compared to WKY rats without CVD. Due to the significant number of individuals suffering from CVD, air pollution susceptibility in this population is of concern to our society. Regulatory agencies often set standards based on the most susceptible group of individuals. This has driven research to assess a variety of pollutants for exacerbated responses in many possible susceptible sub-populations.

LA has been attributed to an increase in mortality and morbidity in exposed individuals. Specifically, exposure to LA has been connected to incidences of autoimmune disease and increases in CVD mortality. Although the toxicity of asbestos has been well studied, it is not known how underlying diseases alter host susceptibility to asbestos-induced lung injury. Because the significant proportion of the population suffers from CVD, any environmental pollutant-induced risk exacerbation will be significant. Individuals suffering from CVD are recognized to have increases in endogenous Fe levels, systemic inflammation, and oxidative stress. Studies have established the ability of Fe to bind to asbestos fibers and possibly potentiate the generation of reactive oxygen species. Due to a dysregulation of Fe homeostasis, individuals with CVD may demonstrate enhanced susceptibility to the toxicity associated with asbestos exposure.

I hypothesize that individuals with CVD are more susceptible to the toxicity of LA exposure due to the ability of their endogenous Fe to bind to the fibers. This binding of Fe to the fibers will enhance their ability to produce ROS leading to increased lung damage. Due to this increased output of ROS, individuals with pre-existing CVD will exhibit enhanced inflammation, oxidative stress, and fibrosis in response to LA-exposure.

CHAPTER 2. PULMONARY OXIDATIVE STRESS, INFLAMMATION, AND DYSREGULATED IRON HOMEOSTASIS IN RAT MODELS OF CARDIOVASCULAR DISEASE

2.1 Introduction

Cardiovascular disease (CVD) is the most prevalent global causes of mortality and morbidity (Lopez et al. 2006; Sans et al. 1997). Many epidemiological studies established that individuals suffering from CVD have increased susceptibility to particulate matter (PM) (Morris et al. 1995; Pope et al. 2004; Dominici et al. 2005; Samet and Krewski 2007) and other air pollutants (Yang et al. 1998; Yang et al. 2004; Zhang et al. 2006). This increased susceptibility may exacerbate the negative respiratory health effects of air pollution compared to individuals without CVD. These findings have driven both the development and the increased use of animal models to study human susceptibility to inhalable pollutants (Kodavanti et al. 2002; Ulrich et al. 2002). A number of experimentally created and genetically predisposed rodent models have been used in the investigation of air pollution health effects (Nikula and Green 2000; Kodavanti and Costa 2001; Doggrell and Brown 1998).

Our lab introduced the use of the genetically predisposed spontaneously hypertensive (SH) rat for understanding susceptibility to air pollution-induced injury a decade ago (Kodavanti et al. 2000). Specifically the SH mimic human hypertension and CVD in its pathogenesis, progression, and failure mechanisms (Schmid-Schonbein et al. 1991; Suzuki et al. 1995; Harjai 1999). As in the case of human CVD patients, neither the number of gene

polymorphisms nor the mechanism by which hypertension is initiated in the SH is known. Unlike SH, the spontaneously hypertensive heart failure (SHHF) rat has not been used in air pollution susceptibility studies. The SHHF model was produced by breeding an obese SH with a non-obese SH and then inbreeding the offspring selecting for the unique trait of congestive heart failure (McCune et al. 1990). The SHHF rat is a more severe model of CVD compared to SH because it presents with both hypertension and heart failure with diastolic dysfunction (Cheng et al. 2009). The SHHF is known to exhibit hypertension and myocardial hypertrophy at 4 months of age or earlier. By 9 months of age the SHHF demonstrates increased left ventricular wall thickness and enhanced markers of inflammation, hypertrophy and stress. Usually by approximately 18 months of age they begin to present with dilated heart failure (Emter et al. 2005; Heyen et al. 2002). Studies generally use the Wistar Kyoto (WKY) rat as the normotensive reference strain in conjunction with the SH or SHHF due to the WKY being the genetic background for both models (Okomoto and Akoto 1963). The use of the SH has generally supported epidemiological studies in that the SH rat demonstrated increased sensitivity to air pollutants, specifically enhanced effects including pulmonary inflammation, vascular permeability, and oxidative stress (Yu et al. 2008; Kodavanti et al. 2002; 2006; Farraj et al., 2009) compared to WKY rats. Although SH showed increased susceptibility to air pollution induced pulmonary injury, the role of their underlying pulmonary disease state has not been thoroughly investigated.

Chronic human CVD and pulmonary diseases share multiple risk factors including systemic inflammation, oxidative stress, and dysregulation of iron (Fe) homeostasis (Blum 2009; Omiya et al. 2009). Dysregulation of Fe homeostasis associated with chronic CVD is

known to increase the systemic labile Fe pool (Kruszewski 2004). The labile Fe pool is an intracellular chelatable pool composed of both ferrous and ferric ions associated with a variety of ligands. The Fe within this pool is able to potentially engage in reduction-oxidation cycling (Kakhlon and Cabantchik 2002). Therefore, this biologically available Fe is tightly controlled by an array of regulatory proteins. Increases in the labile Fe pool can support the production of reactive oxygen species (ROS) through Fenton/Haber-Weiss reactions leading to oxidative stress (Kruszewski 2003). Such oxidant generation mediates inflammatory and fibrotic responses.

The healthy lung is highly sensitive to ROS due to high levels of O_2 and the presence of atmospheric Fe. Studies demonstrated that the pulmonary toxicity associated with ambient PM, tobacco smoke, and asbestos exposure may be associated with to alterations in Fe homeostasis (Ghio and Cohen 2005; Ghio et al. 2008a; 2008b). These alterations are likely a result of an accumulation of catalytically active metal in both cells and the alveolar lining fluid. This endogenous Fe exacerbates Fenton reactions and thereby produces oxidative damage and inflammation (Ghio et al. 2004).

It was postulated that an altered state of Fe homeostasis exists in the lungs of both SH and SHHF rats producing an increase in the availability of Fe. Furthermore, it was postulated that both strains will have higher pulmonary baseline levels of oxidative stress and inflammation than WKY. These disease complications may account for altered susceptibility of SH and SHHF to respirable toxicants relative to WKY. Studies were undertaken to analyze proteins involved in the uptake, storage, and release of Fe to understand each model's regulation of Fe homeostasis along with various markers of baseline pulmonary inflammation and oxidative stress.

2.2 Materials and Methods

Animals. Healthy male, 11 to 12 weeks old, WKY, SH and obese SHHF rats were purchased from Charles River Laboratories, Raleigh, NC; WKY 258 ± 1.38g, SH 266 ± 2.06g, SHHF 391 ± 6.66g, HWKY 271 ± 3.3g (Values mean weight ± S.E.). All rats were maintained in an isolated animal room in an Association for Assessment and Accreditation of Laboratory Animal Care (AALAC) approved animal facility at 21 +/- 1°C, 50 +/- 5% relative humidity, and 12h light/dark cycle. The rats were allowed to acclimate for 4 weeks during their blood pressure and breathing parameters measurements. Rats were housed together in pairs according to strain in polycarbonate cages containing beta chips bedding. Animals received standard (5001) Purina rat chow (Brentwood, MO) and water ad libitum. The protocol for this study was approved by the Environmental Protection Agency's (EPA) Animal Care and Use Committee.

Measurements of Blood Pressure, Heart Rate, and Breathing Parameters.

Systolic blood pressure and heart rate measurements were monitered using tail cuff plethysmography (IITC, Inc., Life Sciences Instruments, Woodland Hills, CA.). Unanesthetized rats were restrained in plastic holding tubes and acclimated for 5 min prior to measurement of blood pressure in a temperature controlled chamber (32°C). The monitoring system uses an automatic scanner, pump, sensing cuff and amplifier to determine the animal's heart rate and compute blood pressure. Three measurements of systolic blood pressure were taken without interfering movements from each rat, and were averaged by the software. These measurements were performed three times per week and repeated over a three week period.

Barometric plethysmography using a whole body plethysmograph system (Buxco Electronics, Inc., Sharon, CT) was used to acquire data on breathing parameters for all animals (Wichers et al. 2004; Kodavanti et al. 2005). This instrument provided continuous monitoring of many breathing parameters including breathing frequency (F), tidal volume (TV), minute ventilation (MV), peak expiratory flow (PEF), peak inspiratory flow (PIF), inspiratory time (TI), expiratory time (TE), pause (Pau), and enhanced pause (Penh).

Necropsy, Sample Collection, and Analysis. Rats were weighed and anesthetized at 14 to 15 weeks of age; WKY 289 ± 3.47g, SH 292 ± 2.89g, SHHF 525 ± 6.28g, HWKY 295 ± 6.84g (Values mean weight ± S.E.). with an overdose of Euthasol (Virbac AH, Inc., Fort Worth, TX)(50-100 mg/kg, ip), and exsanguinated via the abdominal aorta. Blood was then removed from the vasculature of the lung by perfusion of Ca^{2+}/Mg^{2+} free phosphate buffered saline (PBS) via the pulmonary artery. Upon weighing the hearts, it was noted 4 WKY rats presented with non-pathologic cardiac hypertrophy (heart weights >1.3g). All other WKY rats demonstrated heart weights of approximately 1g and were considered to exist without cardiac hypertrophy. Spontaneously occurring non-pathogenic cardiac hypertrophy with the absence of hypertension was previously reported in these rats (Kuribayashi 1987; Leenen and Yuan 1998). It was presumed that this underlying hypertrophy may obscure evaluation of normal baseline values in the control group with which SH and SHHF data are compared. Therefore, these rats were removed from our WKY normotensive control group and used to create another group of hypertrophic Wistar Kyotos (HWKY).

Left ventricular tissues were frozen in liquid nitrogen and stored at -80°C for ascorbate and glutathione (GSH) level analysis. The trachea was then cannulated and the left

lung lobes were tied off. The right lung lobes were lavaged with Ca^{2+}/Mg^{2+} free phosphate buffered saline (pH 7.4, at 37°C) equal to 35 ml/kg body weight (representing total lung capacity) x 0.6 (right lung capacity being 60% of total lung capacity). The lung lobes were lavaged three times with the same PBS aliquot. This bronchoalveolar lavage fluid (BALF) was collected in tubes and kept on ice for additional analysis. The left lung lobes were then removed, placed in liquid nitrogen, and stored at -80°C for real time reverse transcriptase-polymerase reaction (RT-PCR) analysis.

Cell Differential and BALF Analysis. Aliquots of BALF were taken for total cell counts (Coulter Inc., Miami, FL, USA), differential cell determination, and protein analysis. Differential cell determination was conducted by cytospin preparation (Shandon, Pittsburgh, PA), and slides were stained with LeukoStat (Fisher Scientific Co., Pittsburgh, PA). Macrophages and neutrophils were counted under light microscopy and quantified based on total cell count. The remaining BALF was centrifuged at 1500g, and the supernatants were evaluated for the following: protein content (Coomassie plus Protein Assay Kit, Pierce, Rockford, IL), albumin (DiaSorin, Stillwater, MN), lactate dehydrogenase (LDH) activity levels (Thermo Trace Ltd., Melbourne Australia), N-acetyl glucosaminidase (NAG) activity (Roche Diagnostics, Indianapolis IN), γ-glutamyl transferase (GGT) activity (Thermo Trace Ltd., Melbourne Australia), and the Fe-binding proteins, ferritin (Kamiya Biomedical Company, Seattle, Wa) and transferrin (Trf) (DiaSorin, Stillwater, MN). Total Fe-binding capacity (TIBC) was calculated by adding the unsaturated Fe-binding capacity (UIBC) (UIBC Assay, Genzyme Diagnostics, Charlottetown, Prince Edward Island, Canada) and the non-HEME Fe (Serum Fe-SL Assay, Genzyme Diagnostics, Charlottetown, Prince Edward

Island, Canada). All assays were run using commercial kits with only slight modifications for use on the Konelab Arena 30 clinical analyzer (Thermo Chemical Lab Systems, Espoo Finland).

One aliquot of BALF was mixed with an equal volume of 6% perchloric acid and vortexed. After standing on ice for 10 min., it was centrifuged (14,000 g) for 10 min. (4°C) and supernatants were stored at -80°C. Ascorbate was measured in the perchloric acid treated supernatants by high performance liquid chromatography (HPLC) (C-18 Bondpack column, Millipore Waters Chromatography, Milford, MA) using amperometric electrochemical detection (Bioanalytical Systems, W. Layfayette, IN). Total GSH levels were measured using 5,59-dithiobis(2-nitro-benzoic) acid-glutathione disulfide reductase recycling assay via the Konelab clinical analyzer (Anderson 1985).

Lung and Heart Tissue Analysis. Ascorbate and GSH levels were measured in the apical lung lobes, and, heart (left ventricle). Individual samples were homogenized in 3% perchloric acid and then centrifuged (14000 g) for 10 min (4°C). The supernatant was then separated into two tubes, one for GSH analysis via the Konelab clinical analyzer, and the other ascorbate by using HPLC as indicated before.

Frozen tissue was homogenized in Tris-HCl buffer (pH 7.4) with protease inhibitors present. The individual samples were then centrifuged (14000 g) for 20 min (4°C) and the supernatant stored at -80°C. The supernatant was used to determine total protein content, ferritin, transferrin (Trf), total Fe binding capacity (TIBC), and unsaturated Fe-binding capacity (UIBC) using the commercially available kits and the Konelab clinical analyzer as stated above.

RNA Isolation. Total RNA was isolated from caudal lung lobes frozen in liquid nitrogen. The frozen tissue was homogenized in TriReagent (Sigma, St. Louis, MO), and RNA was isolated by RNeasy mini kit by manufacturer's instructions (Qiagen, Valencia, CA). RNA was then dissolved in 50ul of RNase free water with RNase inhibitor present. The quantity of RNA was assessed using a spectrophotometer, Nanodrop 1000 (Thermo Scientific, Wilmington, DE).

Real-Time Quantitative PCR. One-step RT-PCR was carried out using Platinum Quantitative RT-PCR ThermoScript One-Step System (Invitrogen, Carlsbad, CA) following the manufacturer's instructions. PCR was performed for β-actin (Control), macrophage inflammatory protein (MIP-2), tumor necrosis factor-α (TNF-α), interleukin-1α (IL-1α), interleukin-1β (IL-1β), heme-oxygenase-1 (HO-1), transferrin receptor-1 (TFR-1), transferrin receptor-2 (TFR-2), transferrin (Trf), ferritin heavy chain, ferritin light chain, and the divalent metal transporter-1 (DMT-1). Primers for these mRNA were purchased from Applied Biosystems, Inc. (Foster City, CA). Reactions were run using 100 ng of total RNA. RT-PCR was conducted on an ABI Prism 7900 HT Sequence Detection System (Applied Biosystems, Foster City, CA). RT-PCR conditions consisted of 20 min of reverse transcription at 53°C and inactivation of reverse transcriptase activity for 2 min at 95°C. This was followed by 40 amplification cycles at 95°C for 15 sec followed by 60°C for 45 sec. Relative fold mRNA expression was calculated for SH and SHHF rats considering the normal WKY values as control.

Statistical Analysis. Data are expressed as mean ± S.E. (WKY, n = 8; SH, n = 12; SHHF, n = 11; HWKY, n = 4). Values for SH and SHHF were compared with non-hypertrophied WKY rats. Sigma Stat version 3.5 (Systat Software, Inc., Point Richmond, C.A.), commercially available software, was used to determine statistical comparisons via a one-way analysis of variance followed by a post-hoc comparison using the Holm-Sidak method. Statistical significance was determined when p was found to be less than or equal to 0.05 between WKY and SH or SHHF rats.

2.3 Results

2.3.1 Cardiophysiology and breathing parameters

Both the SH and SHHF rat models exhibited increases in heart rate and blood pressure compared to WKY (Figure 2.1) consistent with presence of underlying CVD. HWKY had significantly increased heart weights compared to the normal WKY. Since HWKY rats are not obese, their heart weights normalized for body weights showed an increase compared to WKY demonstrating their hypertrophic cardiac condition (Figure 2.1). However, because age-matched obese SHHF rats had increased body weight due to high amounts of body fat, despite their hearts being larger than non-hypertrophied WKY or SH hearts, heart to body weight ratio failed to indicate their hypertrophic condition (Figure 2.1). HWKY with hypertrophied hearts did not present with altered blood pressure when compared to non-hypertrophied rats, but did have elevated heart rates. Variations in breathing parameters were observed between the groups (Figure 2.2). Most notably, MV was significantly greater in both models of CVD which collaborated with elevation in F and slight increases in TV. HWKY, however, demonstrated significant differences in MV from control WKY (Figure 2.2). TI and TE were also significantly shorter in both SH and SHHF rats relative to WKY.

2.3.2 Pulmonary inflammation, vascular leakage, and injury

SHHF demonstrated significant increases in total protein in BALF when compared to WKY (Figure 2.3). The concentration of total protein in BALF of SH rats was higher than BALF protein in WKY rats which is consistent with our previous studies (Kodavanti et al. 2000; 2001). Interestingly, a significant increase was observed in total protein in the

HWKYs compared to healthy WKY. Albumin levels agreed with this rise in total protein. NAG activity, a marker of macrophage activation, was significantly elevated in SHHF compared to WKY and SH (Figure 2.3). Baseline levels of LDH activities in BALF were also significantly higher in the SHHF than the other strains.

There were no markedly significant differences between the total cells present in the CVD models and the healthy WKY, but HWKY demonstrated an increased number of total cells (Figure 2.4). This divergence in total cells between the WKY and HWKY can be accounted for by higher numbers of alveolar macrophages present in the HWKY as there was no difference in neutrophils compared to WKY; however, both the SH and SHHF had increased numbers of neutrophils in their BALF (Figure 2.4).

2.3.3 Antioxidants in BALF, lung, and heart

Analysis of glutathione in the BALF was attempted, but our assay was not sensitive enough to accurately detect such low amounts. Glutathione concentrations in the lung homogenates were similar between SH and WKY, while GSH in the SHHF rats was significantly reduced (Figure 2.5). BALF ascorbate was higher per given volume of BALF in SHHF than WKY, perhaps due to markedly increased proteins in BALF (Figure 2.5), but ascorbate was significantly lower in the lungs of the SHHF when compared to the WKY and SH. No significant differences in antioxidant levels (GSH, and ascorbate) were observed between the HWKY and the WKY groups. Although the levels of GSH in the hearts did not differ between the 4 groups of rats, the levels of ascorbate was significantly higher in SHHF relative to WKY, SH, or HWKY.

2.3.4 Fe-binding proteins and capacities in BALF

A number of Fe-regulatory proteins and Fe-binding capacities were analyzed in the BALF to evaluate the potential homeostatic mechanisms within the alveolar lining and lung tissue which may be altered as a result of CVD (Figure 2.6). Ferritin, an intracellular Fe storage protein, was significantly increased in BALF of both SHHF and HWKY compared to WKY. Trf, an extracellular Fe transporter, was found to be significantly higher in the BALF of SH and SHHF compared to WKY. HWKY seemed to display a quantitative decrease in Trf in their BALF compared to WKY. BALF from SH demonstrated no significant changes in UIBC and TIBC when compared to WKY, which complements with increased amounts of Trf present in the BALF. SHHF demonstrated significant decreases in UIBC and TIBC in the BALF compared to SH even though they had significantly higher amounts of ferritin and Trf (Figure 2.6). The SHHF exhibited no marked differences when compared to WKY in TIBC in BALF. This could be due to the fact that the Fe regulatory proteins in the BALF of the SHHF are already saturated with Fe, thus accounting for the decreased UIBC but similar TIBC when compared to the WKY. No markedly significant differences occurred between WKY and HWKY in respect to Fe-binding capacities.

2.3.5 Fe-binding proteins and capacities in Lung Tissue

Lung levels of Trf and ferritin proteins were analyzed to evaluate their regulation of Fe in the lung and potentially determine the source of these proteins in BALF. Lung tissue levels of ferritin were decreased in SHHF compared to WKY, while levels of Trf were markedly increased (Figure 2.7). Trf levels were also quantitatively increased in SH compared to WKY. However, the UIBC was below the detection limit in SHHF, further supporting the hypothesis that the available Fe-binding proteins within the lungs of SHHF

were already occupied with non-Heme Fe. Fe-binding proteins and Fe-binding capacities did not differ markedly between HWKY and WKY (Figure 2.7).

2.3.6 Expression of mRNA markers of inflammation, oxidative stress, and Fe homeostasis

Baseline differences in mRNA markers of inflammation, oxidative stress, and Fe homeostasis were analyzed determine pathological complications of the respiratory system secondary to CVD and Fe homeostasis dysregulation. SH showed no significant changes in macrophage inflammatory protein-2 (MIP-2) and tumor necrosis factor α (TNF-α) compared to WKY (Figure 2.8) which corroborated with increased presence of neutrophils in BALF (Figure 2.4). SHHF showed even greater increases in both MIP-2 and TNF-α relative to WKY (Figure 2.8). The lung mRNA expression of IL-1α, and IL-1β in SHHF rats was not statistically different from WKY or SH. HO-1, an inducible marker of oxidative stress, was found at significantly higher levels in the lungs of SHHF compared to WKY and SH. Levels of Trf mRNA were markedly higher in SH than in the WKY and SHHF, but SHHF had lower mRNA for both transferrin receptor 1 (TRF-1) and 2 (TRF-2). The SHHF model exhibited no marked differences in mRNA expression in both ferritin light and heavy chain mRNA when compared to WKY. The HWKY did not demonstrate any significant variations from control WKY in the expression of mRNA for any of the markers.

Figure 2.1

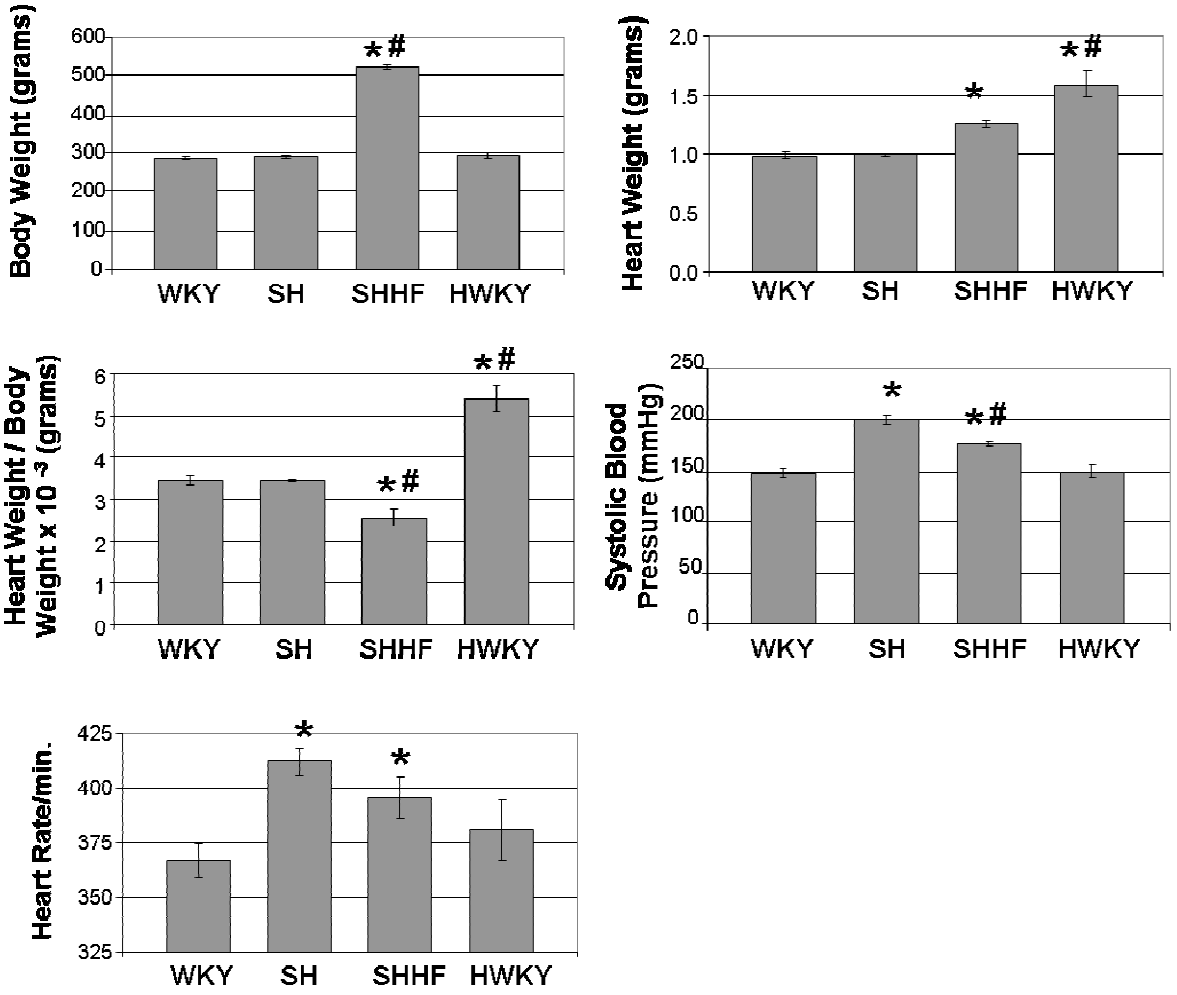

Figure 2.1. Body weight, heart weight, heart weight normalized to body weight, baseline blood pressure, and heart rate in 14-15 week-old healthy male WKY and cardiovascular compromised SH, SHHF and HWKY rats. Cardiovascular function was assessed by heart rate and blood pressure measurements using tail cuff technique. Values are mean ± S.E. (WKY (n =8); HWKY (n = 4); SH (n = 12); SHHF (n = 11)). * Indicates significant difference from WKY (control) ($p<0.05$), # Indicates significant difference between SH and SHHF ($p<0.05$).

Figure 2.2

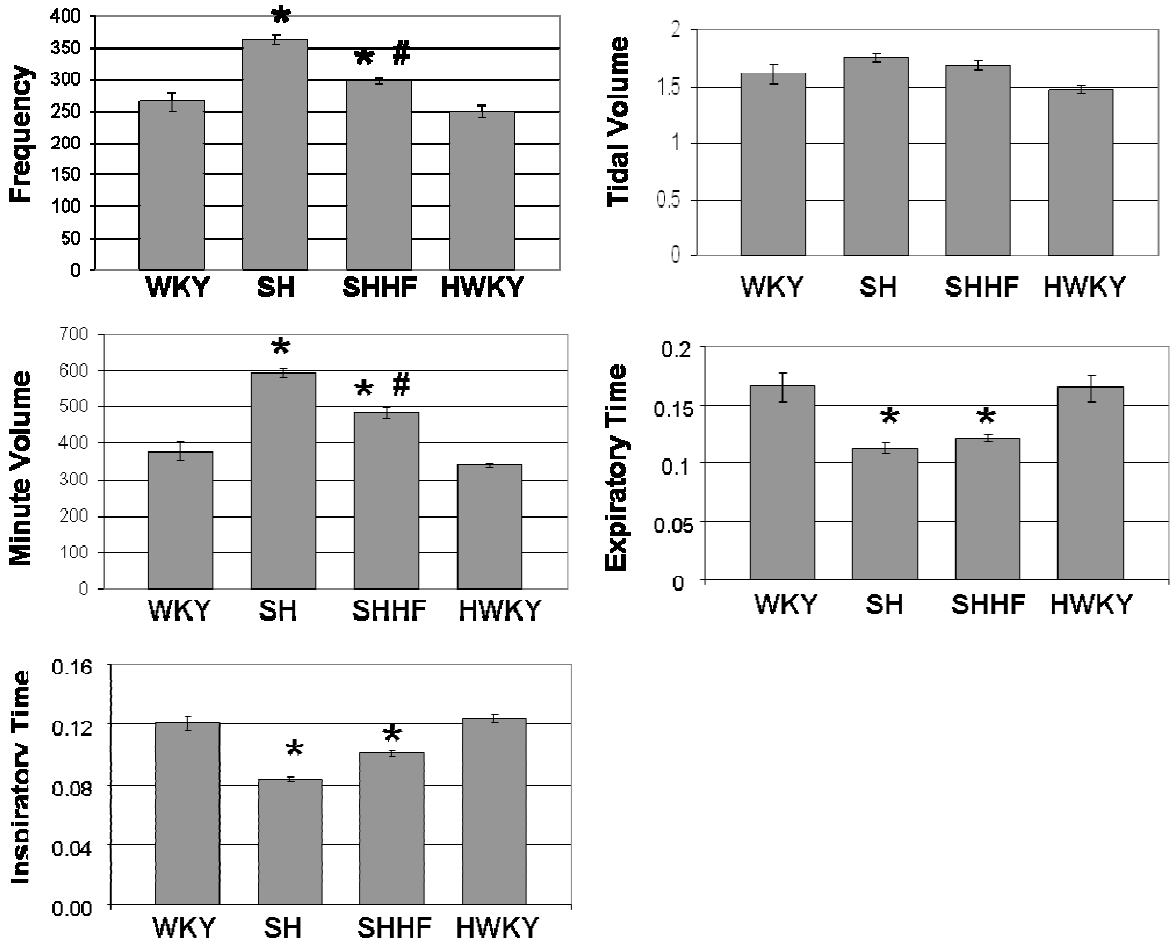

Figure 2.2. Strain-related differences in breathing parameters among male WKY, HWKY, SH and SHHF rats. Breathing parameters were assessed by whole body plethysmography using Buxco System. Pulmonary function illustrated by minute volume a calculated volume (Tidal volume x Frequency). Values are mean ± S.E. (WKY (n =8); HWKY (n = 4); SH (n = 12); SHHF (n = 11)). * Indicates significant difference from WKY (control) ($p<0.05$), # Indicates significant difference between SH and SHHF ($p<0.05$).

Figure 2.3

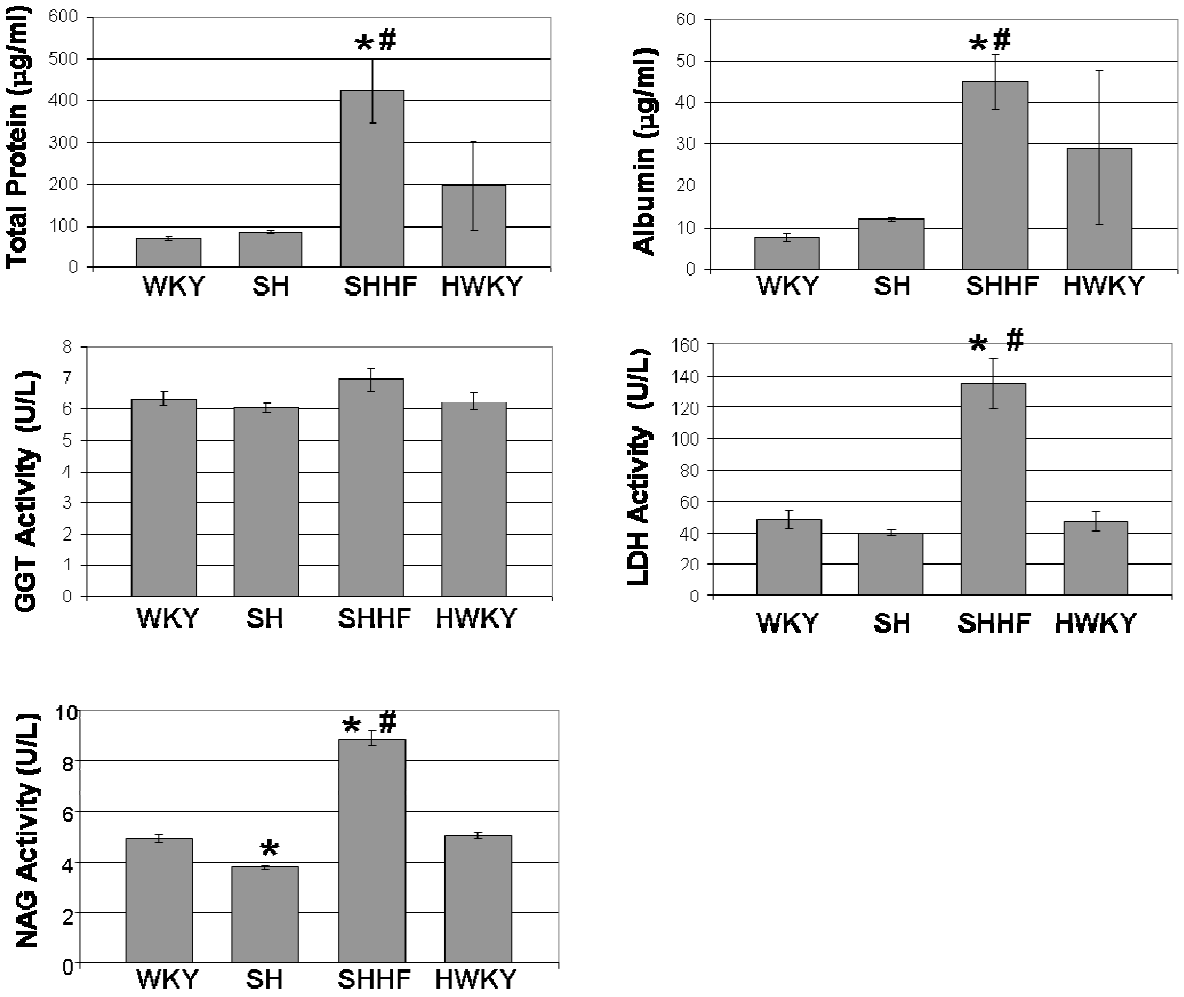

Figure 2.3. BALF concentrations levels of protein, albumin, and LDH, NAG and GGT activities in WKY, HWKY, SH and SHHF rats. Values are mean ± S.E. (WKY (n =8); HWKY (n = 4); SH (n = 12); SHHF (n = 11)). * Indicates significant difference from WKY (control) ($p<0.05$), # Indicates significant difference between SH and SHHF ($p<0.05$).

Figure 2.4

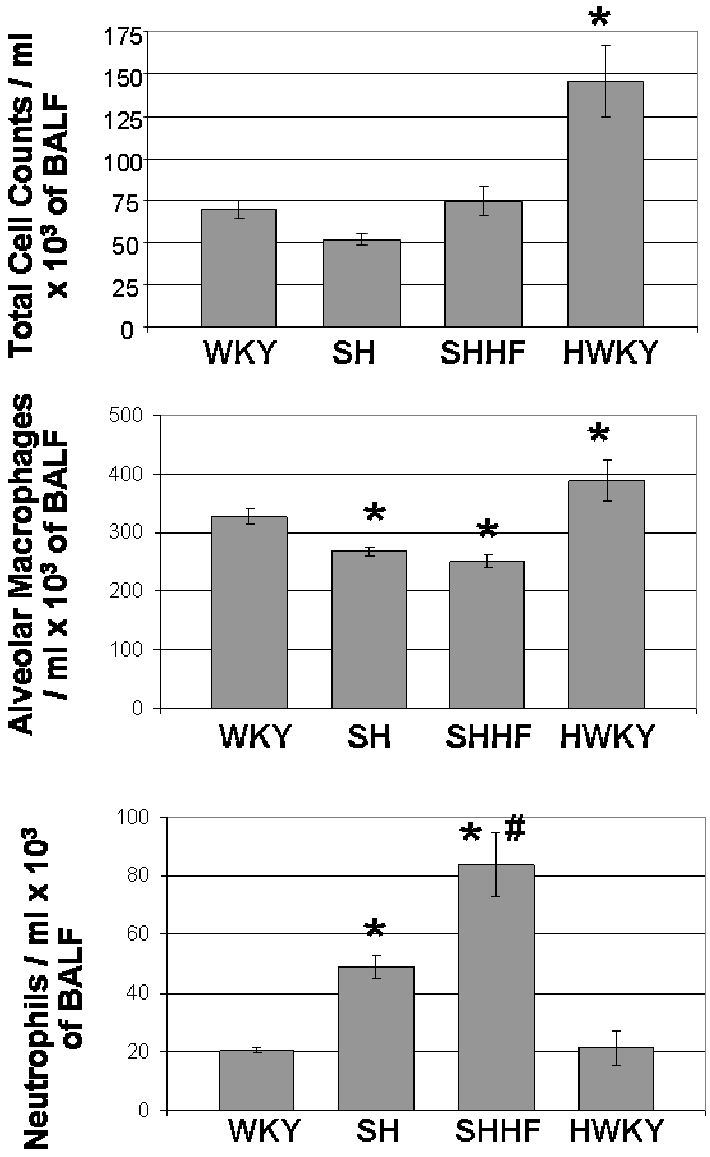

Figure 2.4. Inflammatory cells (macrophages and neutrophils) in BALF of rat models of CVD. Values are mean ± S.E. (WKY (n =8); HWKY (n = 4); SH (n = 12); SHHF (n = 11)). * Indicates significant difference from WKY (control) ($p<0.05$), # Indicates significant difference between SH and SHHF ($p<0.05$).

Figure 2.5

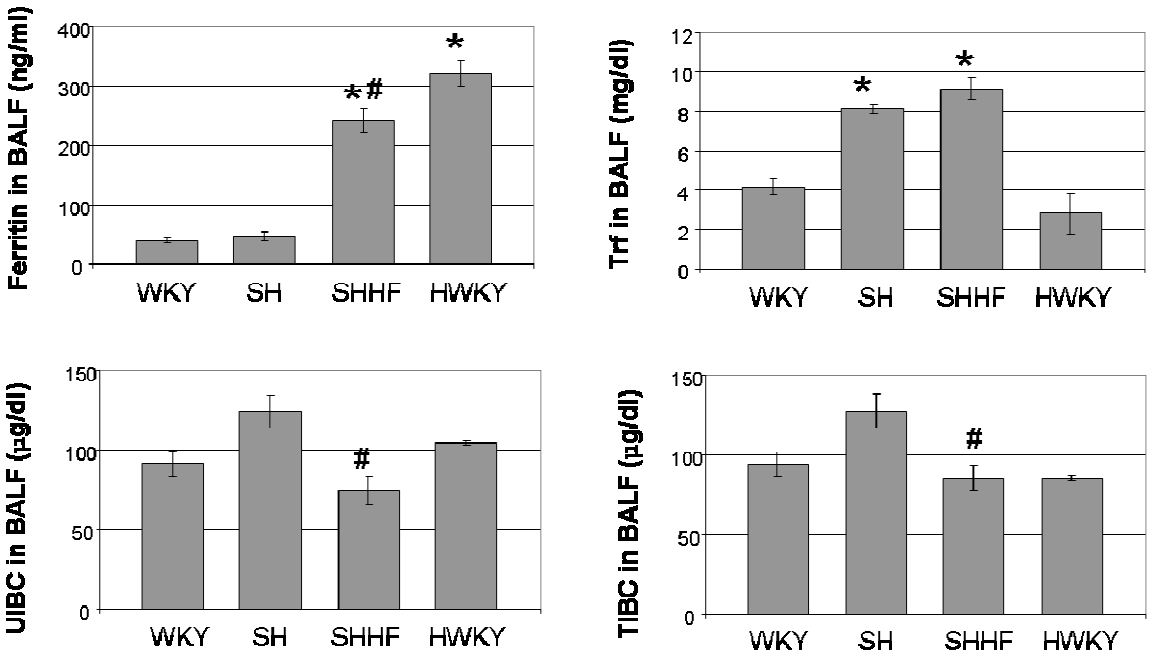

Figure 2.6. Markers of Fe homeostasis in the BALF of rat models of CVD. Unsaturated Fe-binding capacity (UIBC) is a measurement of the capacity of the tissue components to bind non-heme free Fe. TIBC (total Fe-binding capacity), a calculated value (UIBC + non-HEME Fe), is a measurement of all the Fe currently bound within the BALF and the Fe capable of binding. Values are mean ± S.E. (WKY (n =8); HWKY (n = 4); SH (n = 12); SHHF (n = 11)). * Indicates significant difference from WKY (control) ($p<0.05$), # Indicates significant difference between SH and SHHF ($p<0.05$).

Figure 2.6

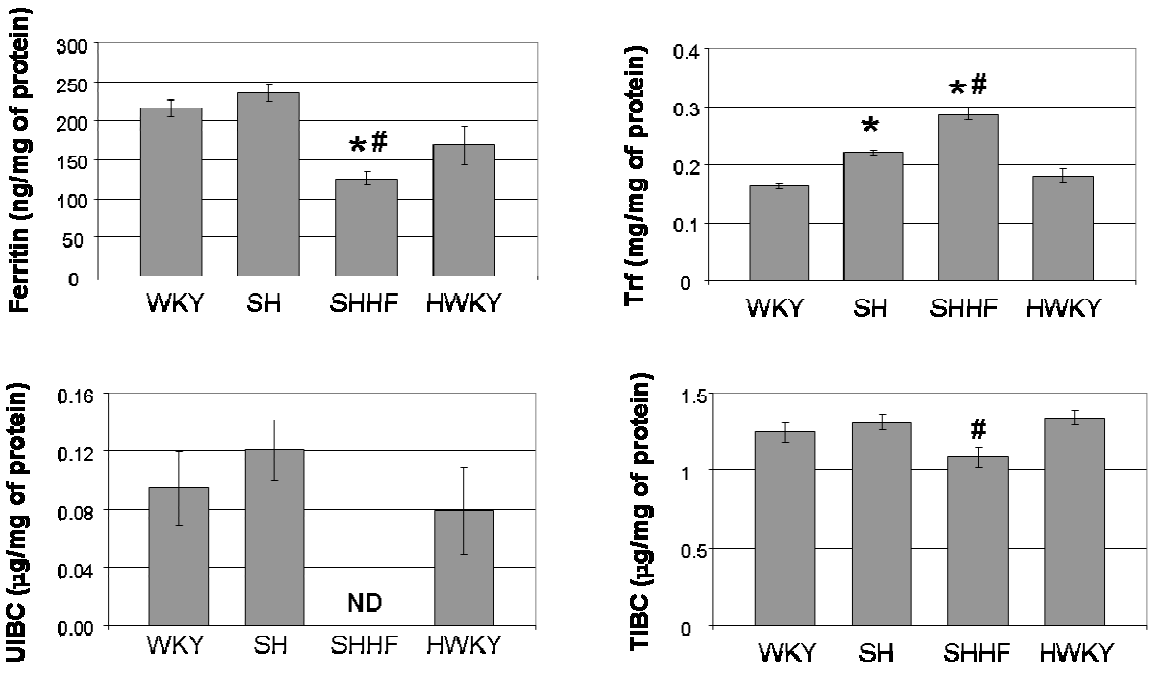

Figure 2.6. Markers of Fe homeostasis in homogenates of lung tissue from rat models of CVD. Unsaturated Fe-binding capacity (UIBC) is a measurement of the capacity of the tissue components to bind non-heme free Fe. TIBC (total Fe-binding capacity), a calculated value (UIBC + non-HEME Fe), is a measurement of all the Fe currently bound within the lung tissue homogenate and the Fe capable of binding. Values are mean ± S.E. (WKY (n =8); HWKY (n = 4); SH (n = 12); SHHF (n = 11)). * Indicates significant difference from WKY (control) ($p<0.05$), # Indicates significant difference between SH and SHHF ($p<0.05$).

Figure 2.7

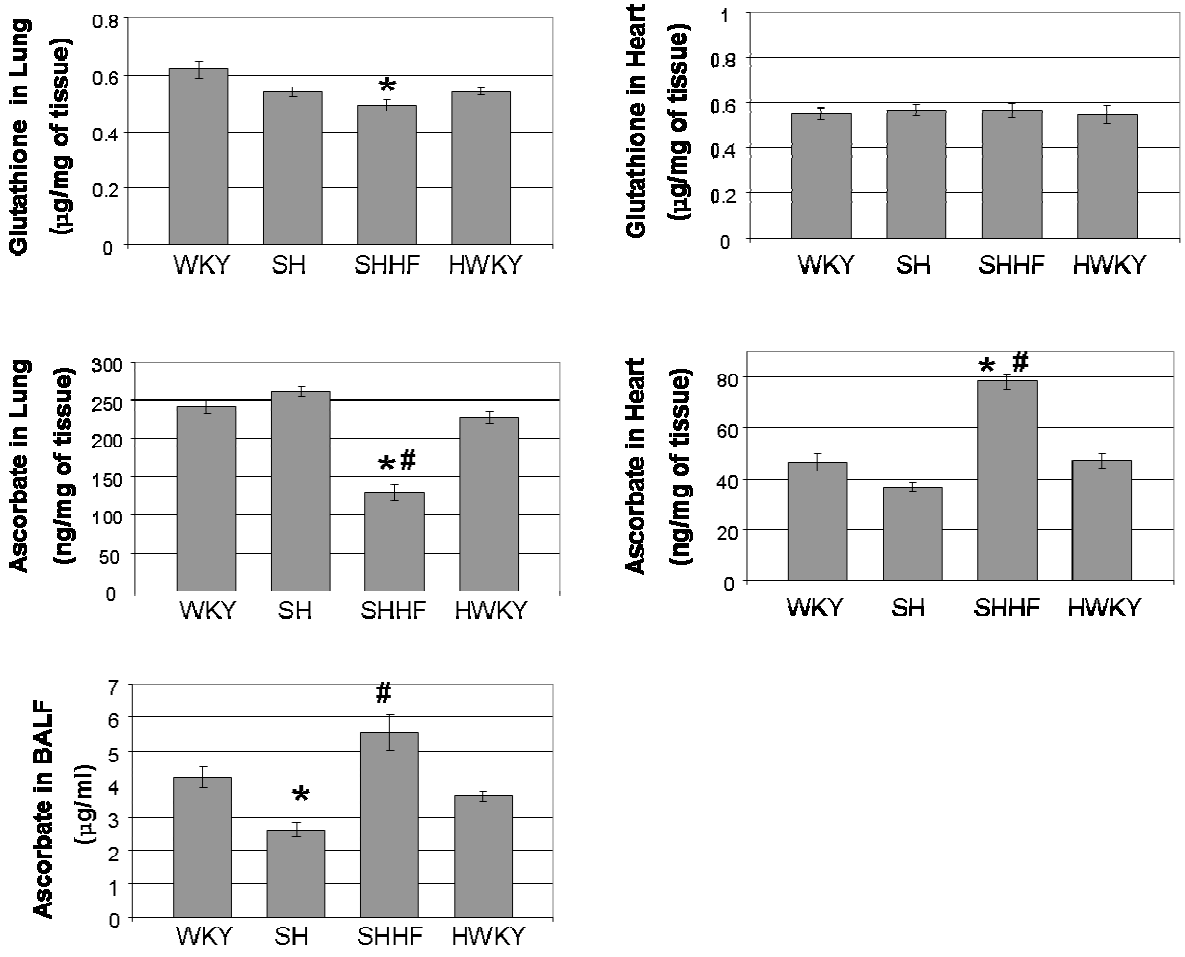

Figure 2.7. Baseline lung, cardiac and BALF glutathione and ascrobate in WKY, HWKY, SH and SHHF rats. Values are mean ± S.E. (WKY (n =8); HWKY (n = 4); SH (n = 12); SHHF (n = 11)). * Indicates significant difference from WKY (control) ($p<0.05$), # Indicates significant difference between SH and SHHF ($p<0.05$).

Figure 2.8

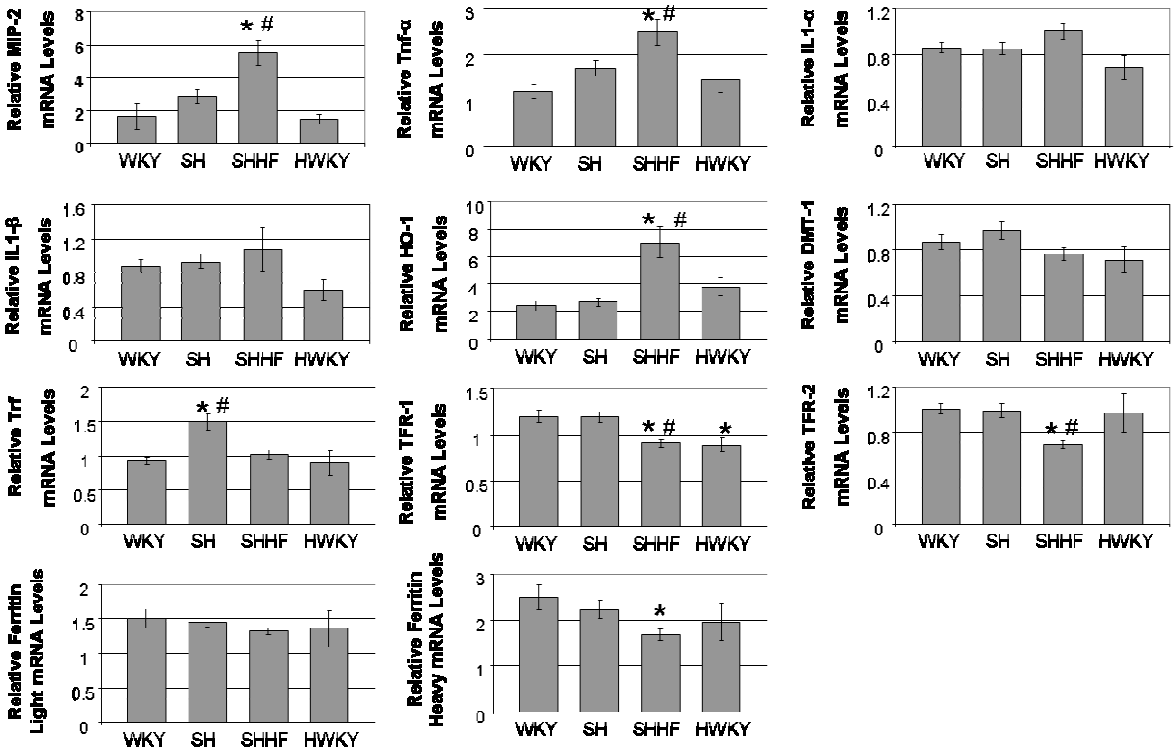

Figure 2.8. Relative mRNA levels for markers of inflammation. Fe homeostasis, and oxidative stress in the lungs of WKY, HWKY, SH and SHHF rats. Real-time reverse transcriptase PCR was used for analysis. MIP-2 (Macrophage Inflammatory Protein-2), Tnf-α (Tumor Necrosis Factor-α), IL-1α (Interleukin-1α), IL-1β (Interleukin-1β), HO-1 (Heme Oxygenase-1), DMT1 (Divalent Metal Transporter 1), Trf (Transferrin), TFR-1 (Transferrin Receptor-1), TFR-2 (Transferrin Receptor-2), Ferritin Light Chain, and Ferritin Heavy Chain. Values are mean ± S.E. (WKY (n =8); HWKY (n = 4); SH (n = 12); SHHF (n = 11)). * Indicates significant difference from WKY (control) ($p<0.05$), # Indicates significant difference between SH and SHHF ($p<0.05$).

2.4 Discussion

Rodent models of human CVD are increasingly being utilized to understand variations in human susceptibility to air pollution exposures (Kodavanti et al. 2005; Kodavanti and Costa 2001). The use of CVD models in these studies requires comprehensive characterization of baseline pulmonary pathobiology in order to elucidate the mechanisms of susceptibility variations. In the current study, it was postulated that two animal models of human CVD, the SH and SHHF rat, would have underlying pulmonary dysregulation of Fe homeostasis, elevated levels of oxidative stress and inflammation compared to healthy WKY. Our data supports this hypothesis in that both rat models displayed pulmonary abnormalities secondary to their CVD that are characterized by a baseline pulmonary dysregulation of Fe homeostasis that may influence their susceptibility to air pollution-induced injuries. Furthermore, the pulmonary tissues of the SH and more so of the SHHF exist in a state of increased inflammation and oxidative stress compared to the WKY. Previous studies showed that SH are more susceptible than WKY to lung injury and airway inflammation induced by PM, tobacco smoke and sulfur dioxide (Yu et al. 2008; Kodavanti et al. 2002; 2006). Our study points to possible contributions of these underlying host abnormalities in their susceptibility to pulmonary injury from air pollutants. Our study also provides evidence that the SHHF rats exists with a dysregulation of Fe homeostasis and diminished antioxidant compensation, which may further enhance their susceptibility to injury from air pollution compared to both the WKY and SH rat strains.

A number of host physiological factors either regulated at gene transcription level or post transcriptionally, influence susceptibility to subsequent environmental exposure. Although the etiology and genetic factors which play a role in CVD predisposition in these

models may not exactly mimic human disease, both the SH and SHHF exhibit unique CVD pathobiologies that have been considered relevant to human conditions and responsive to broad based therapies. The pulmonary complications, secondary to CVD in SH and SHHF models were also observed at physiological and biochemical levels in our study. For example, the SH and SHHF rats demonstrated alterations in breathing patterns (Figure 2.2), which is consistent with alterations of pulmonary function in humans after exercise-induced increases in blood pressure (Fomina et al. 2007).

Numerous studies showed the SH to display systemic oxidative stress and inflammation that mirrors what is seen in the human condition (Turi et al. 2003; Gómez-Amores et al. 2007; Lassègue and Griendling 2004). No studies have investigated, in details, the pulmonary disease secondary to CVD. (Our study provides evidence that these rats have oxidative stress and inflammation within their lungs as evidenced by increased levels of HO-1 (Figure 2.8) and decreased antioxidants (Figure 2.5) secondary to their systemic hypertension. Weakening of the antioxidant response due to a chronic disease such as CVD may cause one to be increasingly susceptible to inhalable pollutant exposure (Scapellato and Lotti 2007). The enhanced inflammation in the lung and the reduced levels of antioxidants are consistent with reported increases in mediators of inflammation and carbonyl content in various tissues in SH (Sun et al. 2006).

SH rats have shown to be more susceptible than WKY rats to increased inflammation and cardiac abnormalities following exposure to a high concentration of inhaled particulate matter, tobacco smoke and sulfur dioxide, however, no air pollution studies have been done using SHHF rats (Kodavanti et al., 2002; 2006; Yu et al., 2008). Because of much greater pulmonary disease and compromised compensatory response in SHHF relative to SH, it is

likely that they might not be able to produce as greater an inflammatory response as WKY to inhaled pollutants, however, they might have more sustained toxicity and oxidative stress. Severe forms of cardiac disease might allow one to look at the failed compensatory mechanisms that are responsible for increased cardiopulmonary mortality, shown in epidemiological studies of air pollution.

Rats with experimentally induced heart failure were shown to have increased oxidative stress and the expression of HO-1 in the lung (Lam et al. 2005). In our study, the genetically predisposed SHHF rat model demonstrated alterations in Fe homeostasis characterized by lower levels of ferritin (Figure 2.7), and decreased Fe-binding capacity within the alveolar lining (Figure 2.6) and the lung tissue (Figure 2.7). These deficiencies were corroborated with decreased lung mRNA expression for ferritin in SHHF, but not SH (Figure 2.8). SHHF, despite having lower lung tissue levels than WKY, had increased ferritin in their BALF. The cause for this difference is unknown but because circulating ferritin levels are generally lower than tissue levels in rats (Othman et al., 2008), vascular leackage might not fully account for increase seen in SHHF rats. It is likely that increased pulmonary cell injury in SHHF might also contribute to increased BALF ferritin. Additionally, decreased clearance of iron-bound ferritin from the airways of the SHHF, might also account for an increase in BALF ferritin. Overall, the actual mechanisms by which Fe metabolism is altered in the lung are not clear, but may involve increase in pulmonary capillary pressure due to existent diastolic dysfunction (Cheng et al. 2009), sheer stress-induced hemolysis, and altered microvascular thrombotic mechanisms. Thus, our data supports the presence of oxidative stress and dysregulated Fe homeostasis in SHHF having both hypertension and heart failure.

There were strain differences in the expression pattern in the markers of Fe homeostasis dysregulation and pulmonary pathology between SH and SHHF rats. The SH, in general, showed milder complications. The Fe-binding capacity in SH was not fully saturated suggesting that the SH may still be able to accommodate exogenous Fe from air pollutants (Figure 2.7). The SH lung was also capable of inducing much greater Trf expression than SHHF rats, suggesting that the lung of SH might not be as severely compromised as that of SHHF rats (Figure 2.8). The SH might possess greater compensatory reserve. However, the SHHF lung based on their more severely dysregulated iron binding capacity and decreased lung ferrrtin might be more vulnerable to oxidative damage and injury following air pollution exposure.

Previous studies have demonstrated the ability of Fe to complex with inhalable PM and fibers (Ghio et al. 2004; Weinrach et al. 2005). The availability of Fe to bind to inhaled particulates or fibers may promote Fenton-like reactions within the reducing environment of the alveolar lining. Based on the baseline pulmonary dysregulation of Fe homeostasis in SH and SHHF rats, it was postulated that these host factors may play roles increasing their susceptibility to air pollutants. Reactive species generated from the above mechanism then go on to damage DNA or oxidize proteins and lipids within the lung. Our data demonstrate a modification of Fe homeostasis in both strains that is consistent with the dysregulation of Fe seen in human CVD (Tuomainen et al. 1998; Salonen et al. 1992).

The elevated levels of oxidative stress and inflammation in this study are likely influenced by decreases in pulmonary antioxidants in SHHF and SH relative to WKY. It is difficult to ascertain from this study if lower level of antioxidants in the lungs are due to their increased utilization in combating existent oxidative stress or reduced production. However,

diminished antioxidants likely contribute to a rise in oxidative stress, which also leads to increases in inflammation. Both the SH and the SHHF showed deficiencies in lung levels of ascorbate and glutathione (Figure 2.5) that is in agreement with the systemic antioxidant deficiencies in CVD patients (Videan et al. 2009; Shih and Lusis 2009).

Upon necropsy during our study a subset was found within the WKY control group suffered from cardiac hypertrophy in absence of increase in blood pressure (Figure 2.1). Our data demonstrate that these rats, due to their hypertrophy, displayed increased vascular leakage in their lungs compared to non-hypertrophic WKY (Figure 2.3). The associated increases in neutrophils and ferritin in the BALF (Figure 2.4), but lack of rise in ferritin in the lung of the HWKY compared to the WKY (Figure 2.7), may relate to its vascular origin from enhanced leakage. The vascular leakage in the HWKY was not as severe as seen in the SHHF. It was noted during necropsy that the hypertrophic hearts in most HWKY rats were due to enlarged right but not left ventricles. This might explain the lack of an increase in systemic blood pressure in HWKY but likely increased pressure in the pulmonary capillaries resulting in pulmonary vascular leakage. The spontaneous cardiac hypertrophy in this strain was noted by other investigators (Kuribayashi 1987; Leenen and Yuan 1998) but the mechanisms are unknown. Separation of HWKY from normal WKY allowed us to precisely compare WKY, SH and SHHF. This separation also allowed us to understand the role of non-pathogenic cardiac hypertrophy in secondary pulmonary complications. The vascular leakage produced by the cardiac hypertrophy may influence the susceptibility of this model and cause the HWKY to be an inadequate control for these studies.

In conclusion, our study provides the characterization of the underlying baseline pulmonary disease of two rat models of human CVD. Data showed increased oxidative

stress, inflammation, and dysregulation of Fe homeostasis in two rat models of CVD. The degree of alterations in the SH model represent effects observed in hypertensive humans with mild cardiovascular complications, and the SHHF represents a more compromised diseased population with susceptibility to heart failure. Results demonstrated that SHHF rats have severely compromised antioxidant compensatory response and diminished Fe-binding capacities in the lung that is associated with oxidative stress and pulmonary vascular leakage at baseline. Overall, this study provides the characterization of pulmonary disease secondary to CVD in SH and SHHF, and lays the foundation for their use in understanding variations in air pollution health effects.

CHAPTER 3. THE ROLE OF IRON IN LIBBY AMPHIBOLE-INDUCED ACUTE LUNG INJURY AND INFLAMMATION

3.1 Introduction

Asbestos has been studied for decades for its ability to induce diseases such as asbestosis, mesothelioma, and lung cancer in humans after inhalation exposure (Mossman *et al.*, 1990). Although the mining and the use of asbestos contaminated materials have been banned in most developed countries, the health issues continue to emerge because of the long latency of the disease and perhaps persistent environmental exposures. Miners in the town of Libby, Montana exposed to fibers during the mining of Libby amphibole (LA)-contaminated vermiculite exhibit increased incidences of asbestos-related diseases (Peipins *et al.*, 2003, Sullivan, 2007). Environmental exposure levels in the vicinity of the mine were also elevated during mining operations possibly contributing to non-occupational exposures and asbestos-related diseases in non-mine workers (Muravov *et al.*, 2005, Whitehouse *et al.*, 2008, Vinikoor *et al.*, 2010). LA contains a mixture of winchite, richterite, tremolite and other minerals of prismatic, acicular, and asbestiform morphologies (Meeker *et al.*, 2003).

The biological effects of asbestos are associated with the production of reactive oxygen species (ROS) and corresponding cellular injury by the oxidation of lipids, proteins, and DNA after exposure (Sanchez *et al.*, 2009). This cellular damage alters host antioxidants, and induces apoptosis, inflammatory cytokine release, growth factor gene expression, and a stress response (Kamp and Weitzman, 1999). Cellular damage caused by

inhalation of asbestos can lead to the development of asbestos-related diseases. Amphibole asbestos fibers are known to be extremely biopersistent within the lung causing chronic oxidative stress and persistent active inflammation (McDonald, 1998, Dostert *et al.*, 2008, Cheng *et al.*, 1999). The persistent inflammation leads to increased pulmonary damage and contributes to the development of chronic pulmonary diseases. Rigid fiber physicochemistry and biopersistence are thought to be necessary for the progression of asbestos-related chronic diseases.

Iron (Fe) is a ubiquitous component of inhalable particulates and fibrous materials; therefore its influence on the inflammation induced by these materials has been a topic of interest. Surface complexed Fe has the ability to produce ROS by providing a redox site for Fenton reactions to occur on the surface of asbestos fibers (Ghio *et al.*, 2008). Furthermore, increases in the amount of Fe associated with the surface of asbestos fibers have been shown *in vivo* due to complexation of endogenous Fe (Ghio *et al.*, 2004, Gibbs *et al.*, 1994). Fe also has the ability to complex the fibers *in vitro* in an acellular system (Shen *et al.*, 2000). This fiber-associated Fe has been postulated to redox cycle enhancing the ROS generation and possibly contributing to toxicity and asbestos-related diseases (Governa *et al.*, 1999, Ghio *et al.*, 2006). Gazzano et al. (2007) demonstrated that chrysotile asbestos loaded with Fe stimulates DNA strand breaks and lipoperoxidation while impairing redox metabolism, and damages cell integrity *in vitro*, while Fe itself has no effect on these parameters. Chelation of Fe from the surface of amosite has been shown to reduce DNA strand breaks *in vitro* (Gilmour *et al.*, 1997, Kamp *et al.*, 1995a). Chelation of endogenous Fe *in vivo* has also been shown to reduce pulmonary inflammation and fibrosis after asbestos exposure (Kamp *et al.*, 1995b).

Because the binding of endogenous Fe to asbestos fibers can increase ROS production and its toxicity, individuals with Fe-overload might be increasingly sensitive to asbestos-induced injury. Systemically disrupted Fe homeostasis and Fe-overload has been noted in individuals with underlying cardiovascular disease due to increased degradation of heme as a result of disruption of red blood cells under sheer stress (Blum, 2009, Kruszewski, 2004). In rodent models of cardiovascular disease, such as spontaneously hypertensive (SH) and SH heart failure (SHHF) rats, we have recently shown that Fe binding proteins are increased and binding capacities have been altered in the lungs in comparison to healthy Wistar Kyoto rats (Shannahan *et al.*, 2010). We have further shown that LA-induced inflammation is more persistent in SH and SHHF rats which is associated with persistent increases in Fe binding proteins (Shannahan *et al.*, 2011a).

We hypothesized that, as with other fibers, Libby amphibole (LA) will bind Fe, and increase the inflammogenic activity of fibers *in vitro* and the acute lung injury and inflammation *in vivo*. In order to address this hypothesis, we examined the ability of LA to bind exogenous Fe in an acellular system and evaluated Fe-related alterations in the production of ROS. Furthermore, we studied the role of Fe in the acute inflammogenic response *in vitro*, using human bronchiolar epithelial cells, and *in vivo*, using SH rats by modulating fiber-associated Fe concentrations.

3.2 Materials and Methods

Libby Amphibole. The Libby amphibole (LA) sample was collected from the Rainy Creek Complex near Libby, Montana in 2007 by the United States Geological Survey (Meeker *et al.*, 2003). The sample was size fractionated by water elutriation as described previously (Webber *et al.*, 2008) in order to isolate a rat respirable fraction ($PM_{2.5}$) using a settling velocity of 3.4×10^{-4} cm s^{-1}. Transmission Electron microscopy showed 97.8% (135/138) of elutriated fibers with aspect ratios ≥ 5, consistent with the composition of fibers obtained from the $PM_{2.5}$ elutriated fraction of the 2000 collection (Meeker *et al.*, 2003, Webber *et al.*, 2008, Lowers and Bern, 2009). Fiber dimensions, as determined using transmission microscopy of the elutriated LA 2007 sample were: mean length 4.99μm ± 4.53 and width 0.28μm ± 0.19; median length = 3.59μm, width = 0.23μm with upper and lower values of length being 0.52μm – 27.30μm and width 0.07μm – 1.15μm (Shannahan *et al.*, 2011a). The estimated fiber count for 1 mg LA sample was 218×10^6. In comparison to the elutriated LA 2007 sample used in the present study air samples from Libby Montana have been shown to contain fibers having a mean length of 7.64μm ± 8.40 and width 0.51μm ± 0.46, and median length 5.2μm and width 0.39μm with upper and lower values of length being 0.5μm – 195μm and width 0.01μm – 10μm; with an aspect ratio of ≥ 5 (U.S. EPA 2010). The median fiber length being smaller than the mean length suggests that there are likely a larger proportion of fibers that are smaller than the mean length.

LA Transition Metal Content. We measured the concentrations of both the water and 1M HCl leachable metals associated with LA in order to gain insight into the surface metal

composition. LA was suspended in saline at a concentration of 5 mg/ml, sonicated for 15 min, vortexed, and mixed for 30 min. Samples were then centrifuged for 15 min at 14,000 rpm and the supernatant removed for evaluation of saline leachable metal content. The pellets were then resuspended in 1M HCl, mixed for 30 min., centrifuged, and the supernatant removed for evaluation of the acid-leachable metal content. All elemental analysis was performed with inductively coupled plasma-atomic emission spectrometry (ICP-AES), following U.S. Environmental Protection Agency (EPA) Method 200.7 rev4.4 protocol (U.S. EPA 2007), using an axially-viewed, simultaneously-measured instrument (PerkinElmer 4300DV ICP-OES, Bridgeport, CT). Fe content was evaluated at duplicate wavelengths of 259.940 nm for reporting and 238.204 nm for confirmation. Independently-sourced, matrix-matched calibration (VHG Labs, Manchester, NH) and quality control (SPEX Certiprep, Metuchen, NJ) standards were used as specified by the analytical protocol. A standard reference material (NIST SRM 1643e, National Institute of Standards, Gaithersburg, MD) solution was included as an additional quality control standard during specified checks. Fe levels measured at the two wavelengths agreed within 10% for all measurements. To demonstrate method proficiency, duplicate samples of bulk solid standard references materials NIST 1648a and 1649b from NIST, Gaithersburg, MD, were digested using aqua regia. Average Fe recoveries were acceptable, with recoveries of 84% and 80%, respectively.

Fe Binding. LA was suspended in saline at a concentration of 5 mg/ml, sonicated for 15 min and vortexed. The LA suspension was then mixed with an equal volume of ferric chloride ($FeCl_3$) (Sigma Aldrich, St. Louis MO) at either 215 μg/ml or 21.5 μg/ml. Samples were incubated at room temperature for 1 hr on a rotator before being centrifuged for 15 min at

14,000 rpm. Supernatant was removed for ICP-AES analysis, to determine the amount of Fe remaining in solution. Through subtracting the amount of Fe in the supernatant from $FeCl_3$ control samples lacking LA, we were able to determine the amount of Fe that associated with the fibers. In order to validate these findings the pellet-associated Fe content was determined using ICP-AES. The pellet was washed 3 times with double distilled water to remove non bound Fe before being digested with aqua regia, (3:1 hydrochloric acid:nitric acid). The amount of Fe bound to LA was then calculated by subtracting Fe released from digested control LA (4.34 μg/mg) without added $FeCl_3$. Results from the two sets of experiments, involving the analysis of Fe lost from the supernatant and Fe bound to the fiber, yielded equivalent results with agreement within 93%.

ROS Measurement. LA was loaded with Fe as described above using 215 μg/ml of $FeCl_3$, the concentration that provided significant Fe binding. After incubation of LA with $FeCl_3$ and before performing the assay fibers were washed 3 times with saline to remove any non-bound $FeCl_3$ and resuspended in saline. Acellular oxidant generation by LA with and without bound Fe was measured by analyzing thiobarbituric acid (TBA)-reactive products generated from the oxidation of deoxyribose. The reaction mixture, containing 1.0 mM deoxyribose, 1.0 mM H_2O_2, 1.0 mM ascorbate, and 2.5 mg of LA was incubated in saline at 37°C for 30 min with agitation and then centrifuged at 1200×g for 10 minutes. One ml of both 1.0% (w/v) TBA and 2.8% (w/v) trichloroacetic acid was added to 1.0 mL of supernatant, heated at 100°C for 10 min, cooled in ice, and the TBA-malondialdehyde adduct concentration was determined by its absorbance at 532 nm.

In Vitro Exposure of Respiratory Epithelial Cells to LA. BEAS-2B cells (passages 70–80) were grown to 90% confluence on tissue culture 12-well plates (Costar) in keratinocyte growth medium (media). In a series of experiments we examined the role of Fe in modulating LA induced toxicity *in vitro*. Initially a dose-response experiment was performed to determine LA-induced cytotoxicity and to set an appropriate dose for subsequent studies. BEAS-2B cells were incubated with 0, 50, 100, or 200 µg LA/mL media and the release of lactate dehydrogenase (LDH) was measured in supernatants.

Next we examined the toxicity of LA loaded with Fe (FeLA) compared to control LA fibers. BEAS-2B cells were incubated with media, 2 µg $FeCl_3$ without LA (2 µg of $FeCl_3$ contains the amount of Fe bound to 50 µg LA), 50 µg LA or 50 µg FeLA. FeLA fibers were produced by the procedure described above including removal of free Fe by washing fibers with distilled water 3 times. In order to further understand the role of fiber bound and endogenous cellular Fe, a Fe chelator, deferoxamine (DEF) was used to alter LA-induced toxicity. BEAS-2B cells were incubated with media, 50 µg LA, 200 µM DEF, or 50 µg LA + 200 µM DEF (LA + DEF). Lastly an experiment was designed to understand how a state of intracellular excess Fe might affect LA-induced toxicity. BEAS-2B cells were Fe-preloaded during a 4hr pre-treatment with 100 µM ferric ammonium citrate (FAC) (Sigma Aldrich, St. Louis MO) or media, then cells were washed and incubated with media or 50 µg LA. The concentrations of LA used are consistent with previous *in vitro* experimentation of other asbestos samples using BEAS-2B cells (Wang *et al.*, 2006a, Wang *et al.*, 2006b) as well as *in vitro* studies examining the toxicity of LA (Duncan *et al.*, 2010). In all experiments supernatants and cells were collected 4 hours after exposure. Cytotoxicity was also measured using LDH release in the supernatant normalized to a positive control (LDH

released from cells lysed with 1 ml of double distilled H_2O) to obtain percent cell viability. Changes in cellular mRNA expression levels of β-actin (Control), interleukin-8 (a rat homolog of macrophage inflammatory protein-2; MIP-2), heme-oxygenase-1 (HO-1), and ferritin heavy chain (FHC) were analyzed at 4 hrs as described below. FHC has been shown to be upregulated following acute insults as a result of mobilization of Fe likely via induction of HO-1 (Koorts and Viljoen, 2007).

Animals. Male, 11-12 week old SH rats were purchased from Charles River Laboratories, Raleigh, NC. All rats were maintained in an isolated animal room within an Association for Assessment and Accreditation of Laboratory Animal Care (AALAC) approved animal facility at 21 ± 1°C, 50 ± 5% relative humidity, and 12 h light/dark cycle. Rats were housed (2/cage) in polycarbonate cages containing beta chip bedding. Animals received standard (5001) Purina rat chow (Brentwood, MO) and water *ad libitum*. The U.S. EPA NHEERL Institutional Animal Care and Use Committee (IACUC) approved the protocol.

Intratracheal Instillation of Libby Amphibole. LA fibers were suspended in saline, sonicated for 15 minutes in a water bath, and vortex mixed in order to obtain uniform suspension of fibers for instillation. To assure that fibers did not settle at the bottom when removing suspension for instillation, the suspension was mixed prior to each instillation. Rats (n=8/time point) were anesthetized with isoflurane and intratracheally instilled as described previously (Wallenborn *et al.*, 2009) with 300 μl saline only or containing 1 mg deferoxamine, 21 μg $FeCl_3$, 0.5 mg of LA, 0.5 mg LA loaded with Fe (FeLA), or 0.5 mg LA + 1 mg deferoxamine (LA + DEF).

Necropsy, Sample Collection, and Analysis. Four hours or 1 day following instillation rats weighed 309 ± 1.46g (Values mean weight ± S.E.) and were anesthetized with an overdose of sodium pentobarbital (Virbac AH, Inc., Fort Worth, TX; 50-100 mg/kg, ip). Animals were exsanguinated via the abdominal aorta. The trachea was then cannulated and the whole lung was lavaged with Ca^{2+}/Mg^{2+} free PBS (pH 7.4, at 37°C) equal to 35 ml/kg body weight (representing total lung capacity). The lung lobes were lavaged three times with the same PBS aliquot. The right lung lobes were then removed, placed in liquid nitrogen, and stored at -80°C for later RNA isolation.

Cell Differential and Bronchoalveolar Lavage Fluid (BALF) Analysis. Aliquots of BALF were taken for total cell counts (Coulter Inc., Miami, FL, USA), and cell differentials. Cell differentials were determined on Cytospin preparations (Shandon, Pittsburgh, PA), of slides stained with LeukoStat (Fisher Scientific Co., Pittsburgh, PA). Macrophages and neutrophils were counted under light microscopy and quantified based on total cell count of at least 300 cells per slide. The remaining BALF was centrifuged, and cell-free BALF was evaluated for the following: total protein (Coomassie plus Protein Assay Kit, Pierce, Rockford, IL), albumin (DiaSorin, Stillwater, MN), lactate dehydrogenase (LDH) activity (Thermo Fischer Diagnostics, Middletown VA), N-acetyl-β-D-glucosaminidase (NAG) activity (Roche Diagnostics, Indianapolis IN), γ-glutamyl-transferase (GGT) activity (Thermo Fischer Diagnostics), ferritin (Kamiya Biomedical Company, Seattle, WA) and transferrin (DiaSorin). Total Fe-binding capacity (TIBC) was calculated by adding the unsaturated Fe-binding capacity (UIBC) (UIBC Assay, Genzyme Diagnostics, Charlottetown, Prince

Edward Island, Canada) and the non-heme Fe (Serum Fe-SL Assay, Genzyme Diagnostics). All assays were normalized for BALF analysis and run using the Konelab Arena 30 clinical analyzer (Thermo Chemical Lab Systems, Espoo Finland).

RNA Isolation and Real-Time Quantitative PCR. Total RNA was isolated from cells using RNeasy micro kits (Qiagen, Valencia, CA), and from caudal lung lobes frozen in liquid nitrogen using RNeasy mini kit (Qiagen). One-step RT-PCR was carried out using Platinum Quantitative RT-PCR ThermoScript One-Step System (Invitrogen, Carlsbad, CA) via manufacturer's instructions (Shannahan *et al.*, 2010). PCR was performed for β-actin (Control), macrophage inflammatory protein (MIP-2), heme-oxygenase-1 (HO-1), ferritin light chain (FLC), and ferritin heavy chain (FHC). Human specific and rat specific primers for these mRNA were purchased from Applied Biosystems, Inc. (Foster City, CA). Relative fold mRNA expression was calculated considering, media exposed cells or saline exposed SH rats as controls.

Statistical Analysis. Data are expressed as mean ± S.E. (BEAS-2B cells, n=9/treatment group; SH rats, n = 8/ group). Sigma Stat version 3.5 (Systat Software, Inc., Point Richmond, C.A.) was used to determine statistical comparisons via a one-way analysis of variance with exposure as the factor followed by a post-hoc comparison using the Holm-Sidak method. Statistical significance was determined when p was found to be less than or equal to 0.05 between treatment groups.

3.3 Results

3.3.1 LA Surface Metal Content, Fe binding and Modulation of ROS Generation by Fe

A very small quantity of water-leachable Fe was present on the surface of LA fibers (6.04 ± 2.96 ng Fe / mg of LA, Table 3.1). When LA fibers were incubated with 1M HCl, the quantity of Fe leached off from LA surface increased by ~100X, however the acid-soluble Fe is still very low relative to total Fe content of LA. Silicon and magnesium, the two major structural elements of LA, were also detected in water and acid leachable fractions of LA. Levels are very low compared to total elemental content, indicating that neither water nor 1M HCl was significantly dissolving the amphibole structure. We observed that upon incubation of LA with $FeCl_3$ additional Fe bound to the fibers, corresponding to 16.6 μg Fe / mg of fiber (Figure 3.1). The additional Fe was not dissociable after three washes with distilled water, demonstrating that Fe can chemically bond with LA which is not dissociable in aqueous media. Since a solution of $FeCl_3$ at a concentration of 215 μg/ml provided a high level of Fe binding to the surface of LA (≈17 μg/mg of LA), all subsequent experiments utilizing Fe-loaded LA were done at this concentration of $FeCl_3$.

LA was found to generate ROS that could be modulated via altering the availability of Fe in a cell free system (Figure 3.1). Incubation of untreated LA in an acellular media produced ROS as determined by presence of TBA reactive substance. Deferoxamine (DEF) reduced the potential of LA to produce ROS by approximately 50%. Furthermore, through loading of LA with Fe, ROS generation was increased 3.5-fold. This increase in ROS generation was also reduced to approximately 75% of untreated LA control levels in the presence of DEF (Figure 3.1).

3.3.2 Effect of Fe Binding and Removal from LA on BEAS-2B Cells

BEAS-2B cells exhibited no changes in cytotoxicity at 4hr post LA exposure at all concentrations (Figure 3.2). Cellular mRNA expression level of IL-8, a neutrophil chemoattractant and marker of inflammation, was elevated 4hr after LA exposure in a concentration-dependent manner. Neither HO-1, a rate limiting enzyme of heme metabolism and a sensor of cellular ROS, nor ferritin, a Fe binding protein transcriptionally activated by increased HO-1, were altered due to LA exposure at any concentration. Since LA at a concentration of 50 μg did not show any cytotoxicity but caused a significant increase in IL-8, further *in vitro* experiments were performed using this concentration of LA.

3.3.3 The Role of Fe Binding to LA on BEAS-2B Cell Expression of mRNA markers of Fe Homeostasis, Oxidative Stress, and Inflammation

LA did not alter cellular mRNA expression levels of HO-1 or ferritin; however significant modifications were demonstrated in IL-8 transcriptional activation (Table 3.2). Exposure of BEAS-2B cells to LA caused a significant induction in IL-8 compared to cells incubated with media without added LA. Fe-loading of LA reduced the level of IL-8 transcriptional activation seen without Fe-loading (Table 3.2A). Exposure of cells to $FeCl_3$ alone (at the level that was bound to LA), did not significantly change IL-8 expression compared to media controls. LA exposure in the presence of DEF caused greater increases in IL-8 expression when compared to LA incubations without DEF (Table 3.2B). Exposure to DEF alone did not change IL-8 expression significantly when compared to media controls. Fe preloading of BEAS-2B cells significantly decreased the ability of LA to induce IL-8 expression (Table 3.2C). Preloading of cells with Fe alone was not found to affect IL-8 expression.

3.3.4 The role of Fe in Modulating *In Vivo* Pulmonary Injury and Inflammation as Determined by Analysis of BALF

In order to determine the role of Fe in altering the toxicity of LA, we intratracheally exposed rats to LA with or without Fe-loading and also in the presence of DEF. Since the transcriptional response was expected to occur earlier than the neutrophilic influx in the lung, we determined changes in transcription of target genes at 4 hr and inflammation at 4hr and 24hr post exposure. BALF total cells collected from rats 24h post-exposure were elevated in LA and LA + DEF exposed animals (Figure 3.3). FeLA however, demonstrated no significant changes from saline controls. No changes were seen in alveolar macrophage counts but they trended to decrease in rats exposed to LA under all conditions. Neutrophil counts were elevated in all LA exposure groups compared to saline controls however variations of neutrophilic influx occurred due to the availability of Fe. In general BALF neutrophil counts were less in rats receiving FeLA than LA by itself. LA + DEF on the other hand caused a marked increase in BALF neutrophils when compared to LA groups without added DEF (LA + DEF > LA > FeLA).

At 4hr post-exposure to LA, FeLA or LA + DEF, BALF LDH and NAG activities, used as the markers of lung cell cytotoxicity and alveolar macrophage activation, respectively, were elevated, whereas total protein, albumin, and GGT activity were unchanged (Data not shown). At 24hr post exposure however, $FeCl_3$ exposed animals demonstrated elevated (though not significantly) BALF total protein levels while all other treatments showed no changes (Figure 3.4). BALF albumin levels followed a similar trend to total protein. GGT and LDH activities at 24hr were unchanged after $FeCl_3$ exposure and were increased in DEF, LA, FeLA, and LA + DEF groups compared to saline controls

(Figure 3.4). Interestingly, animals exposed to FeLA demonstrated less LDH activity when compared to LA alone. NAG activity was uniformly elevated at 24hr in all groups receiving LA (LA, FeLA, LA + DEF) compared to saline. BALF ferritin levels were elevated at 24hr post-exposure to all LA treatments while transferrin levels were unaltered (Figure 3.5). Heme in BALF was increased due to DEF treatment while non-heme Fe levels were increased only in $FeCl_3$ exposed animals (Figure 3.5). No specific pattern of differences in these parameters emerged between LA, FeLA and LA + DEF groups.

3.3.5 Lung Expression of mRNA Markers of Fe Homeostasis, Oxidative Stress, and Inflammation

MIP-2 was significantly elevated in all LA exposed groups at 4hr post-exposure; however variations in induction due to Fe modifications were evident (Figure 3.6). FeLA caused an elevation in MIP-2 that was significantly less than what was observed in LA, whereas LA + DEF caused a significant increase in MIP-2 compared to LA (LA + DEF > LA > FeLA). HO-1 mRNA expression was significantly increased in rats exposed to 21 μg $FeCl_3$ while no changes were seen in any other exposure groups. Ferritin heavy chain (FHC) was markedly elevated only in rats exposed to Fe-loaded LA compared to saline. Ferritin light chain (FLC) was unchanged from control saline in all groups.

Table 3.1. Leachable Metals Associated with LA

	Average Concentration ng Metal / mg of LA (std. error)		
	Fe	Si	Mg
Saline	6.04 ± 2.96	648.48 ± 18.79	317.44 ± 2.75
1M HCl	845.23 ± 6.84	1416.40 ± 23.82	1060.26 ± 8.60

LA was washed with either saline or 1 M HCl and supernatants were measured for leachable iron (Fe), silicon (Si), and Magnesium (Mg). Values represent mean ± S.E.

Figure 3.1

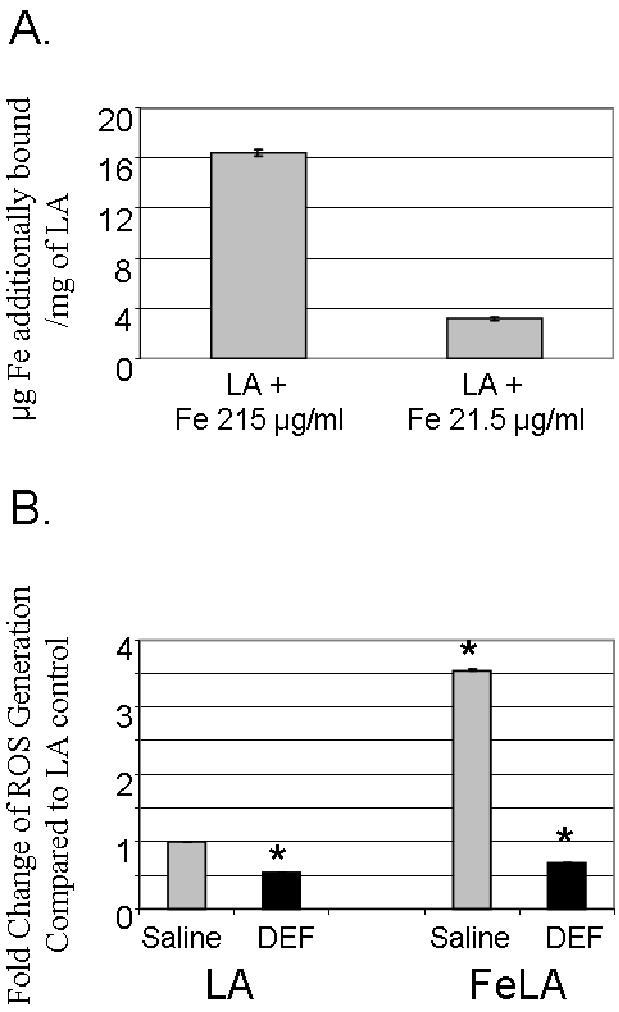

Figure 3.1. The binding of Fe to LA and modulation of ROS generation in a cell-free environment. A) The amount of Fe complexed with LA after an hour incubation with 215 µg/ml or 21.5 µg/ml $FeCl_3$ in an acellular system. Values are mean ± SE (n = 6/ group). B) Reactive oxygen species generation of LA, Fe-loaded LA (FeLA) (produced after incubation with 215 µg/ml $FeCl_3$) and in the presence or absence of an Fe chelator, deferoxamine (DEF) in an acellular system. Values mean ± SE (n= 3/group). * Indicates significant difference from LA controls ($p<0.05$).

Figure 3.2

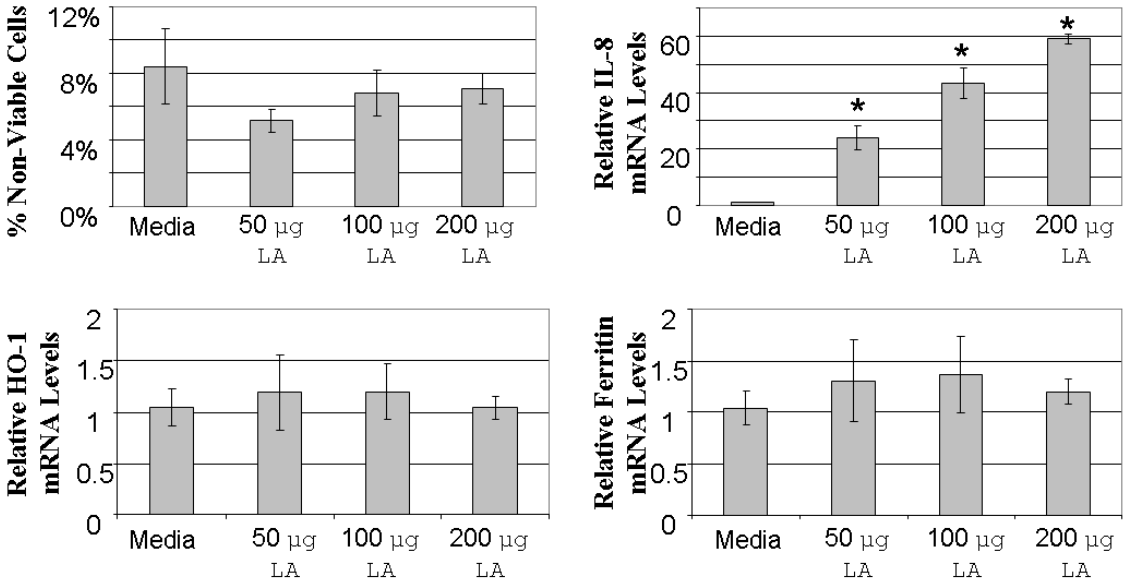

Figure 3.2. Cell viability (LDH), and mRNA expression for biomarkers of inflammation, oxidative stress, and Fe homeostasis in BEAS2B cells at 4 hour following LA exposure. Cells were exposed to 0, 50, 100 or 200 µg/cm^2 of LA and LDH release in the media was analyzed. Real-time reverse transcriptase PCR was used for analysis of IL-8 (Interleukin-8), HO-1 (Heme Oxygenase-1), and Ferritin heavy chain (FHC). Values are mean ± SE (n = 9/ group). * Indicates significant difference from media controls ($p < 0.05$).

Table 3.2. In Vitro Interventional Studies

A.

	Fe loaded LA (Relative mRNA Fold Change ± Std. error)		
	IL-8	HO-1	Ferritin
Media	1.53 ± 0.67	1.07 ± 0.22	1.05 ± 0.14
$FeCl_3$	0.47 ± 0.05	0.91 ± 0.09	1.11 ± 0.14
LA	24.45 ± 1.81 *	0.74 ± 0.04	0.97 ± 0.09
FeLA	14.49 ± 0.60 * #	1.40 ± 0.28	1.50 ± 0.40

B.

	LA and Def Treatment (Relative mRNA Fold Change ± Std. error)		
	IL-8	HO-1	Ferritin
Media	1.07 ± 0.18	1.04 ± 0.13	1.05 ± 0.16
Def	1.62 ± 1.00	0.93 ± 0.13	1.02 ± 0.13
LA	39.90 ± 11.51 *	0.77 ± 0.12	0.92 ± 0.14
LA + Def	83.40 ± 10.69 * #	1.22 ± 0.09	1.23 ± 0.18

C.

	Fe Loaded Cells and LA Exposure (Relative mRNA Fold Change ± Std. error)		
	IL-8	HO-1	Ferritin
Media	1.02 ± 0.10	1.08 ± 0.20	1.07 ± 0.19
Fe loaded cells	1.88 ± 0.74	1.38 ± 0.20	1.30 ± 0.22
LA	50.88 ± 6.54 *	0.87 ± 0.09	1.00 ± 0.09
Fe loaded cells + LA	12.61 ± 2.16 * #	0.95 ± 0.17	0.92 ± 0.23

BEAS-2B cells were exposed for 4h to LA under a number of Fe manipulations and were examined for changes in mRNA expression of interleukin-8 (IL-8) a marker of inflammation, heme-oxygenase-1 (HO-1) a marker of oxidative stress, and ferritin a marker of Fe homeostasis. A) BEAS-2B cells were exposed to media (control), 1 μg $FeCl_3$, 50 μg LA, or 50 μg Fe loaded LA (FeLA). B) BEAS-2B cells were exposed to media (control), 200 μM deferoxamine (DEF), 50 μg LA, or 50 μg LA + DEF. C) BEAS-2B cells were pretreated with 0 or 200 μM ferric ammonium chloride (FAC) in order to Fe preload cells. Then cells were treated with either media (control) or 50 μg LA. Values are mean fold change ± S.E.

Figure 3.3

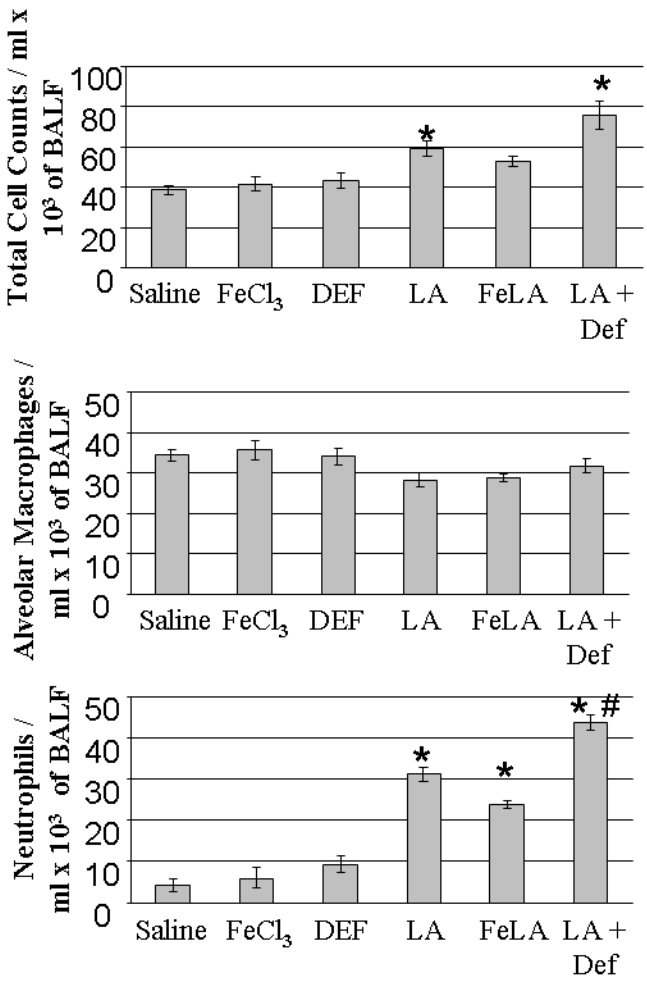

Figure 3.3. The role of Fe binding and chelation in LA-induced influx of inflammatory cells (total cells, macrophages and neutrophils) in BALF of rats 24 h after exposure. Rats were instilled with saline (control), 21 μg $FeCl_3$, 1 mg DEF, 0.5 mg of LA, 0.5 mg Fe-loaded LA (FeLA), or 0.5 mg LA + 1 mg DEF (LA + DEF). Values are mean ± SE (n = 8/group). * Indicates significant difference from saline controls ($p < 0.05$). # Indicates significant difference from LA ($p < 0.05$).

Figure 3.4

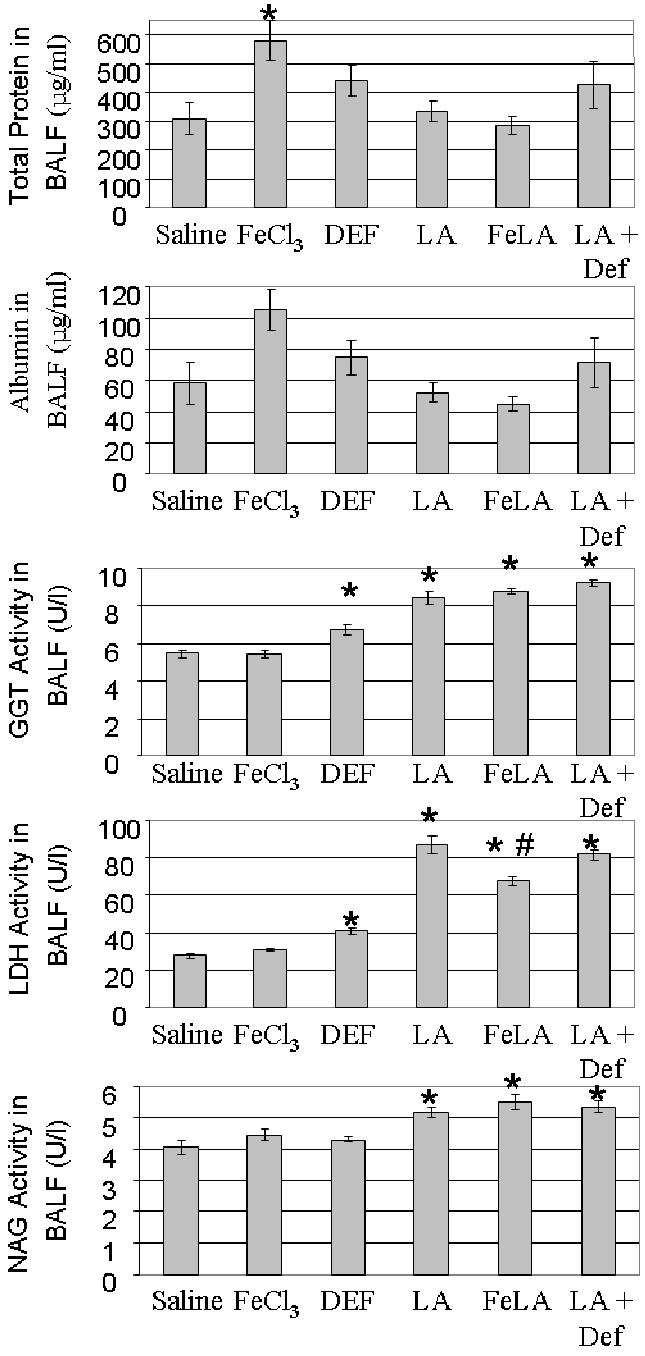

Figure 3.4. The role of Fe binding and chelation in LA-induced changes in BALF protein, albumin and LDH, NAG and GGT activities in rats at 24 hour post exposure. Rats were instilled with saline (control), 21 µg $FeCl_3$, 1 mg DEF, 0.5 mg of LA, 0.5 mg Fe-loaded LA (FeLA), or 0.5 mg LA + 1 mg DEF (LA + DEF). Values are mean ± SE (n = 8/group). *

Indicates significant difference from saline controls ($p < 0.05$). # Indicates significant difference from LA ($p < 0.05$).

Figure 3.5

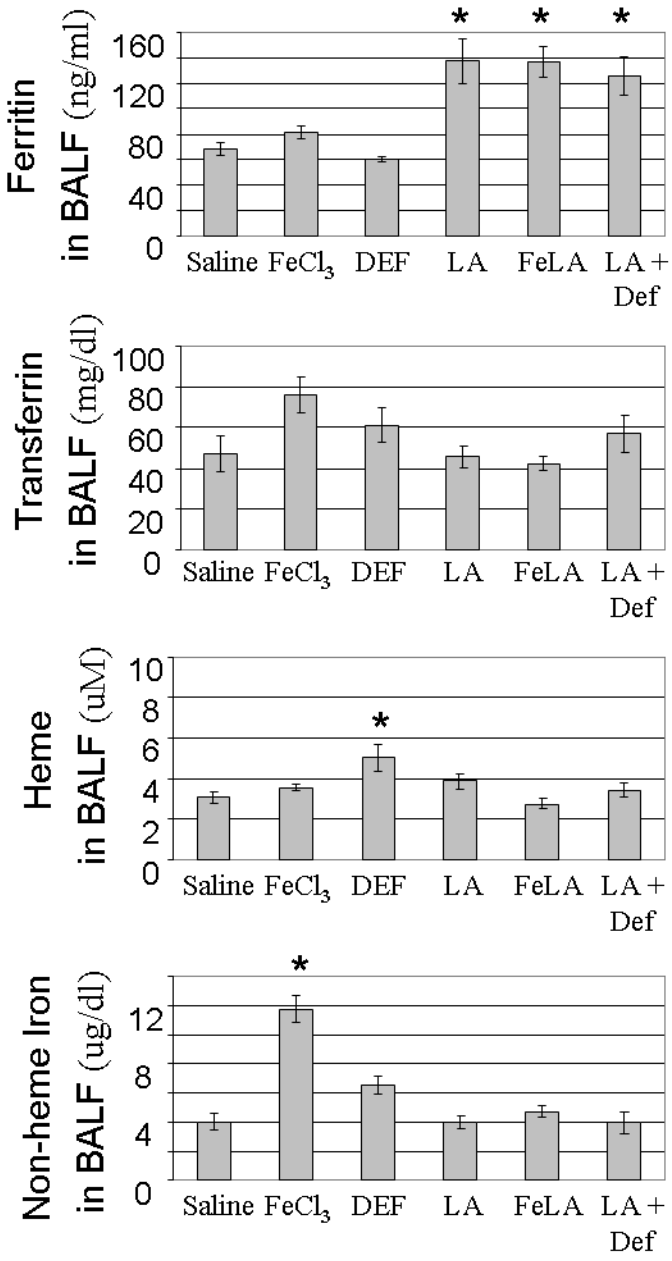

Figure 3.5. Markers of Fe homeostasis in the BALF of rats exposed to saline (control), 21 μg $FeCl_3$, 1 mg DEF, 0.5 mg of LA, 0.5 mg Fe-loaded LA (FeLA), or 0.5 mg LA + 1 mg DEF (LA + DEF). Values are mean ± SE (n = 8/group). * Indicates significant difference from saline controls ($p < 0.05$). # Indicates significant difference from LA ($p < 0.05$).

Figure 3.6

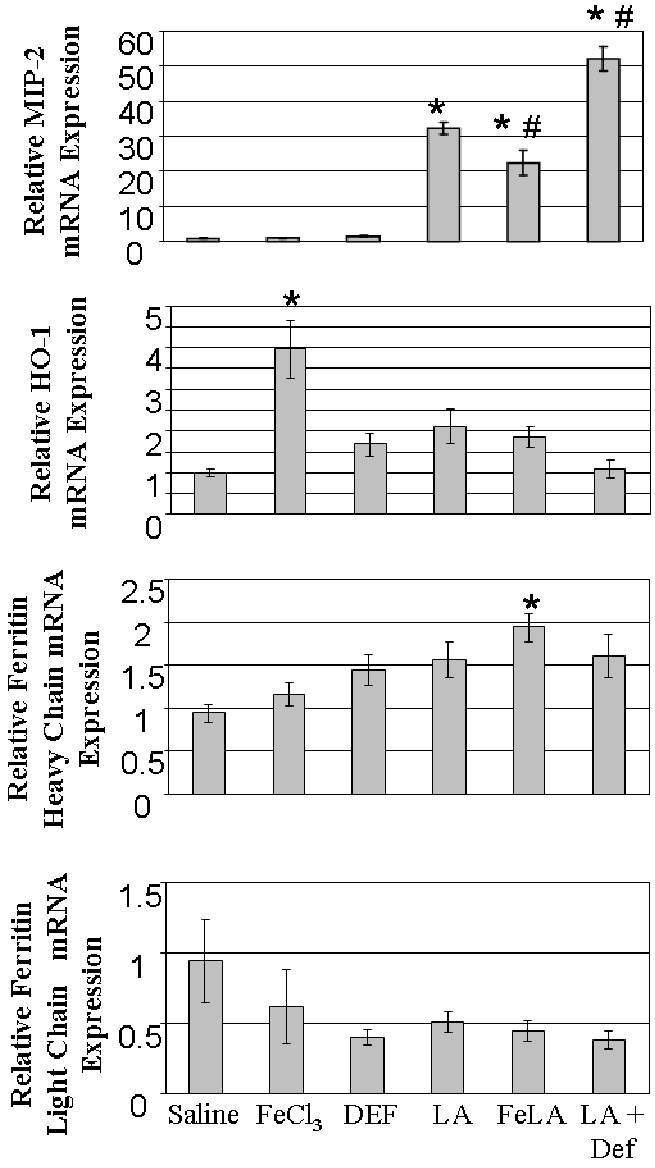

Figure 3.6. Relative mRNA levels for markers of inflammation, oxidative stress, and Fe homeostasis in the lungs of rats exposed to saline (control), 21 μg $FeCl_3$, 1 mg DEF, 0.5 mg of LA, 0.5 mg Fe-loaded LA (FeLA), or 0.5 mg LA + 1 mg DEF (LA + DEF). Real-time reverse transcriptase PCR was used for analysis of MIP-2 (Macrophage Inflammatory Protein-2), HO-1 (Heme Oxygenase-1), FHC (Ferritin Heavy Chain), and FLC (Ferritin

Light Chain). Values are mean ± SE (n = 8/group). * Indicates significant difference from saline controls ($p < 0.05$). # Indicates significant difference from LA ($p < 0.05$).

3.4 Discussion

Fe complexed onto the surface of fibers after inhalation exposure is thought to increase the toxicity of asbestos by increasing ROS production through Fenton reactions. The purpose of this study was to systematically examine the role of surface complexed and endogenous Fe in exacerbating the toxicity of LA. We determined the presence of leachable surface metals, such as Fe and silicon on LA and examined the ability of LA to bind exogenous Fe and produce ROS in an acellular system. Furthermore, we investigated the ability of this additional complexed Fe in modifying LA-induced inflammation *in vitro* (BEAS-2B cells) and *in vivo* (SH rats). As has been reported with other asbestos materials, our data show that a significant quantity of Fe binds to LA. In an acellular system with sufficient quantities of reducing equivalent present, Fe loading of LA increases the production of ROS while removal of the Fe using DEF reduces it. However, *in vitro*, Fe-loading of LA or Fe-preloading of cells reduces the inflammogenic effect of LA as evidenced by a decrease in transcriptional activation of IL-8. Furthermore, *in vivo* Fe loading of LA decreases the neutrophilic inflammation and inflammatory gene expression induced by LA while DEF increases this response. Fe-loading of LA increases ferritin mRNA without inducing HO-1 *in vivo* but not in cells. Thus, increased fiber-bound or cellular catalytically active Fe might reduce the acute inflammatory response caused by LA rather than increasing inflammation through ROS production. In situations where there is a deficiency of catalytically active Fe in cells or more readily available Fe binding sites on the surface of fibers, Fe might be released from cellular proteins that bind Fe tightly which can result in the activation of proteins, and signaling that leads to an inflammatory response.

As with other asbestos fibers (Hardy and Aust, 1995), we noted that LA contained leachable Fe. More importantly, it is likely that because significant amount of silicon is present on the surface of LA (as evidenced by its leaching with 1 M HCl), it can bind exogenous Fe. Silanol groups have been shown in other fiber types to mediate the complexation of endogenous Fe (Ghio *et al.*, 2004). At physiological pH deprotonation of the Si-OH groups leaves a net negative charge across the surface of the fiber allowing for the association of cations. Due to the bioavailability of Fe and the high stability constant for Si-O^- and Fe cations, asbestos fibers could become saturated by exogenous Fe in an acellular system or with endogenous Fe in cellular systems. We show that a substantial amount of Fe could complex LA in an acellular system. Additionally, this Fe was able to redox cycle and increase ROS production in a cell free system consistent with what has been observed with other mineral fibers such as crocidolite and amosite (Ghio *et al.*, 1992, Eborn and Aust, 1995). It has been shown that loading of asbestos fibers with Fe increases asbestos-induced DNA strand breaks and oxidation byproducts via augmentation of ROS production (Gazzano *et al.*, 2007). The Fe chelator, phytic acid, has also been shown to reduce the production of ROS and DNA strand breaks *in vitro* in cellular incubations (Kamp *et al.*, 1995a).

The role of Fe in generating ROS was further demonstrated in our study by a reduction in ROS in the presence of a Fe chelator, DEF, in an acellular system. DEF binds all six available coordination sites of Fe therefore blocking all redox active sites and inhibiting the production of ROS. This ability of DEF to bind Fe at all of coordination sites makes it appropriate for the treatment of Fe-overload diseases and for the study of Fe mediated ROS production (Galanello *et al.*, 2010, Poser *et al.*, 2004).

It is likely that Fe can be released from fibers over time during the dissolution process, as has been shown to occur in case of crocidolite exposure of A549 cells (Fang and Aust, 1997). However dissolution can depend on the type of fiber, the solubility in an intracellular and lysosomal compartment and the duration of incubation. We observed that in case of LA, while a very small quantity of Fe was leached from fibers after water and 1 M HCl washing, a large quantity was Fe was bound in a very short time (1 h) upon incubation with $FeCl_3$. We observed that additional Fe remained bound to LA upon washing with water. Our data show that when rats were exposed to FeLA, Fe remained bound to LA even in the lung. This assumption is supported by the fact that in rats instilled with $FeCl_3$ but not in rats instilled with FeLA, cell-free BALF levels of non heme Fe were increased. The short duration of exposure in our study does not allow us to examine the possibility that endogenous Fe can continue binding LA fibers over time, but our data are consistent in supporting the ability of LA to bind Fe.

The evidence from our study on the role of Fe in LA-induced inflammogenic effects in cells and *in vivo* in rats show that Fe loading of LA decreases the toxicity of LA in cells, contrary to what has been shown to occur involving other asbestos fibers (Kamp *et al.*, 1995b). Since Fe remained associated with fibers after instillation of FeLA in the rat lung, and the inflammatory response of LA was reduced in the presence of surface complexed Fe, we can presume that release of Fe from LA fibers was not associated with a decrease in the inflammatory response. When cells were preloaded with Fe, a decrease in LA-induced inflammogenic effects suggests that the availability of cellular Fe to bind LA, likely in catalytically active form within a low molecular weight fraction of cytoplasm (Fang and Aust, 1997) might decrease the release of Fe from more tightly bound endogenous proteins

thereby causing a decrease in inflammatory response. As DEF removes Fe from the surface of LA and proteins, it is likely that opened Fe binding sites on the surface of LA promotes more tightly bound iron to be released from proteins leading to their activation and signaling for inflammation. The ability to chelate Fe from endogenous sources has been shown to contribute to the inflammatory response to bacteria in the lung as they utilize host Fe resources (Weinberg, 2009). Recent research assessing the role of Fe in quartz-induced toxicity suggests that the movement of Fe is a key component in the inflammatory response (Ghiazza *et* al. 2011). In our study using LA, a mixture of relatively short asbestos fibers, with different physiochemistry yielded similar results. These studies together suggest that the differential inflammation induced by fibrous and non-fibrous particles, each with the ability to bind Fe can be inhibited by readily bioavailable cellular Fe.

Since precise real-time measurement of ROS generation in cells and in lung *in vivo* is technically challenging, we chose to use induction of HO-1 as a marker of oxidative stress and IL-8/MIP-2- as markers for inflammatory response for *in vitro* and *in vivo* experiments. HO-1, an antioxidant, is involved in generating cellular Fe by catabolizing heme. Heme containing proteins are known to be susceptible to damage by ROS causing the release of Fe containing heme groups. Both the release of heme and the presence of ROS cause the transcriptional activation of HO-1. The release of Fe from HO-1 mediated heme catabolism causes the transcriptional upregulation of Fe storage proteins such as ferritin (Gozzelino *et al.*, 2010). The fiber itself and the ROS are known to induce an inflammatory cytokine release causing the recruitment of inflammatory neutrophils in an attempt to clear the foreign fiber (Haegens *et al.*, 2007, Haegens *et al.*, 2005). The primary inflammogenic cytokines

(IL-8 in humans and MIP-2, a human analog of IL-8, in rats) are known to be induced after asbestos exposure (Hillegass *et al.*, 2010, Duncan *et al.*, 2010).

LA was able to markedly induce IL-8 in BEAS-2B cells and MIP-2 in rat lungs. These LA-induced inflammogenic effects were not associated with transcriptional changes in HO-1 regardless of Fe loading. However, $FeCl_3$ by itself increased HO-1 mRNA *in vivo* without inducing ferritin in the lung. It is likely that the kinetics of uptake and the bioavailability of Fe from the airway lining when in loosely-bound chemical form could be different from Fe bound to LA resulting in $FeCl_3$ inducing HO-1. Since Fe loading of LA but not $FeCl_3$ increased ferritin heavy chain mRNA *in vivo*, it is likely that Fe bound to LA triggered a compensatory response in the lung. It is not clear if this response might be involved in reducing the inflammatory response of LA. BALF ferritin was increased in all animals receiving LA, demonstrating the ability of LA to influence host Fe homeostasis. In cells or in the lung lining fluid, the availability of Fe binding proteins might function as antioxidants by sequestering metals. Furthermore, the lack of sufficient reducing equivalents in the lung lining might inhibit pro-oxidant reaction with Fe on LA surface and thus, ROS generation.

The development of ferruginous bodies has been shown to occur years after fiber exposures in humans (Pooley, 1972, Treffry *et al.*, 1987). No evidence exists to show that in animals the toxicity of asbestos is due to ferruginous bodies and not the fiber core, however, it has been shown that upon isolation of these bodies from a patient lung the production of ROS, as measured by DNA strand breaks *in vitro*, was increased relative to fibers without ferruginous bodies (Lund *et al.*, 1994). From our study one can postulate that since in an acellular system Fe can rapidly bind LA fibers, it is likely that the inhibition of the acute

inflammatory response *in vivo* might relate to the availability p of Fe in its catalytically active form in cells and on the surface of the fibers. In a chronic condition, the presence of fibers with open Fe binding sites in the lung might lead to a new Fe equilibrium between proteins and the surface of the fibers causing bioactive Fe to be associated with fibers and possibly results in a decreased inflammatory response.

The intratracheal instillation produces an acute bolus response characterized by inflammation, however, if conducted at relatively less toxic levels of exposure, it can provide mechanistic insights and allow interventional strategies. Similar to the response from intratracheal instillation in our study, short-term inhalation of asbestos materials has been shown to induce acute inflammation (Dostert et al., 2008). As with instillation, *in vitro* exposures, although not realistic when conducted in relevant cell types allow one to examine the acute mechanisms involved in inflammogenic responses at a cellular level. Because the fiber length in the LA mix used in this study is relatively shorter than other asbestos materials such as amosite and crocidolite, it is likely that over time the intracellular and extracellular processes that control the Fe binding might be different with longer fibers. It has been shown that significant quantities of fibers are internalized by BEAS-2B cells during 24hr incubation with LA collected in 2000 (Duncan et al., 2010). Because the LA sample used in the present study is similar to the LA sample of 2000, it is likely that the shorter fiber fractions are readily phagotytosed by alveolar macrophages. Uptake by alveolar macrophages of the LA sample *in vivo* may be responsible for mediating the inflammatory responses not airway epithelial cells such as used in our *in vitro* study. Long-term retention of fibers in the lung will likely depend on the size range of different fractions of LA.

In conclusion we determined that LA fibers contain surface silicon, can readily bind exogenous Fe in an acellular system and this binding can increase ROS production. However, loading of LA with Fe decreased the inflammatory response of LA both *in vitro* and *in vivo*. By chelating LA-bound and endogenous host associated Fe, the toxicity of LA was increased suggesting that Fe in moderate concentrations inhibits the inflammatory response induced by fibers. Our data suggests that the deficiency of Fe in cells or on the surface of fibers might increase the acute inflammatory response of LA.

CHAPTER 4. INFLAMMASOME ACTIVATION BY LIBBY AMPHIBOLE AND THE ROLE OF IRON

4.1 Introduction

The inflammasome is a multiprotein complex which initiates the inflammatory cascade resulting in the innate immune response evident after exposures to a variety of pathogens (Pang and Iwasaki, 2011, Conforti-Andreoni *et al.*, 2011, Martinon *et al.*, 2002). The inflammasomes primarily functions through the cleavage and activation of caspases. These caspases once activated cleave and activate pro-inflammatory cytokines such as interleukin-1β (IL-1β) and interleukin-18 (IL-18). IL-1β is known to not only mediate inflammatory response but also cellular apoptosis, proliferation, and differentiation. IL-18 is known to be involved with activating cellular immunity after microbial exposure to LPS (Mojtahedi and Ghaderi, 2005).

Depending on the activating signal the proteins that complex to form the inflammasome and the caspases that cleave IL-1β are different. It has been shown that asbestos and silica can activate the NALP3 inflammasome after exposure (Cassel *et al.*, 2008, Dostert and Petrilli, 2008). Furthermore NALP3 -/- mice have been shown to be protected from the development of fibrosis after silica exposure compared to wild type mice (Dostert and Petrilli, 2008, Cruz *et al.*, 2007). This has led researchers to postulate that the activation of the inflammasome may have a role in the development of asbestosis after asbestos exposure. Asbestos exposure is also known to cause an up-regulation of IL-1β

which is known to be vital to both the inflammation and fibrosis that occurs after asbestos exposure (Lindroos *et al.*, 1997, Wang *et al.*, 2004).

Previously our lab has demonstrated that through modifications of surface available iron (Fe) on Libby amphibole (LA) the inflammatory response can be altered both *in vitro* and *in vivo* (Shannahan et al. 2011b). Specifically, we showed that the acute inflammatory response was dampened when LA was loaded with Fe while inflammation was enhanced when LA was treated with an Fe chelator. These findings along with new research regarding the inflammasome led us to hypothesize that the availability of Fe on the surface of LA modifies the activation of the inflammasome. In order to address this hypothesis we examined 1) LA's ability to induce the inflammasome, and 2) the role of Fe in inflammasome induction. Activation of the inflammasome pathway was assessed through analyzing mRNA expression changes after exposure to LA in the lungs of rats (Figure 4.1).

Figure 4.1.

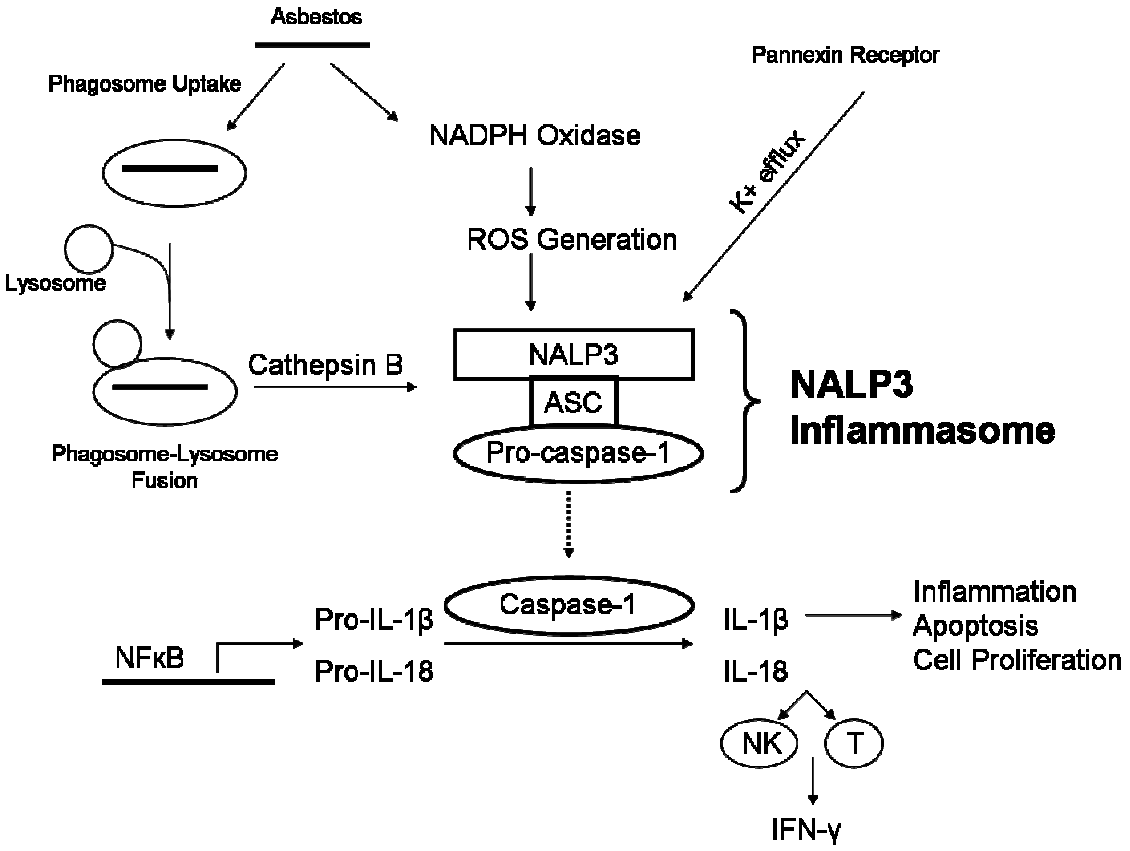

Figure 4.1. A schematic of the inflammasome signaling pathway. The SA Bioscience's PCR array included all components of inflammasome pathway. Capthesin-B is a known activator of the inflammasome that has been shown to be induced by other asbestos materials. Genes encoding inflammasome complex proteins of included a variety of NALPs and ASC. ASC is an adaptor protein containing a CARD domain that cleaves and activates caspase-1. NALP proteins are known to bind and activate ASC. Specifically NALP3 has been shown to be activated by asbestos exposure. The inflammasome activation causes the activation and release of caspase-1 which cleaves pro-IL-1 β and pro-IL-18 to their active IL-1β, and IL-18

forms. Activation of IL-18 is known to lead to the induction interferon-γ by activating natural killer (NK) and T cells.

4.2 Materials and Methods

Animals. Male, 11-12 week old SH rats were purchased from Charles River Laboratories, Raleigh, NC. All rats were maintained in an isolated animal room within an Association for Assessment and Accreditation of Laboratory Animal Care (AALAC) approved animal facility at 21 ± 1°C, 50 ± 5% relative humidity, and 12 h light/dark cycle. Rats were housed (2/cage) in polycarbonate cages containing beta chip bedding. Animals received standard (5001) Purina rat chow (Brentwood, MO) and water *ad libitum*. The U.S. EPA NHEERL Institutional Animal Care and Use Committee (IACUC) approved the protocol.

Preparation of Fe loaded of LA. LA was suspended in saline at a concentration of 5 mg/ml, sonicated for 15 min and vortexed. The LA suspension was then mixed with an equal volume of ferric chloride ($FeCl_3$) (Sigma Aldrich, St. Louis MO) at either 215 μg/ml. Samples were incubated at room temperature for 1 hr on a rotator before being centrifuged for 15 min at 14,000 rpm. The pellet was washed 3 times with double distilled water to remove non bound Fe before being re-suspended in saline. Based on previous experimentation the amount of Fe associated with the fiber is approximately 16 μg/mg of fiber (Shannahan et al. 2011b).

Intratracheal Instillation of Libby Amphibole. LA fibers were suspended in saline, sonicated for 15 minutes in a water bath, and vortex mixed in order to obtain uniform suspension of fibers for instillation. To assure that fibers did not settle at the bottom when removing suspension for instillation, the suspension was mixed prior to each instillation. Rats (n=8/time point) were anesthetized with isoflurane and intratracheally instilled as described

previously (Wallenborn *et al.*, 2009) with 300 μl saline only or containing 1 mg deferoxamine, 21 μg $FeCl_3$, 0.5 mg of LA, 0.5 mg LA loaded with Fe (FeLA), or 0.5 mg LA + 1 mg deferoxamine (LA + DEF).

Necropsy, Sample Collection, and Analysis. Four hours or 1 day following instillation rats weighed 309 ± 1.46g (Values mean weight ± S.E.) and were anesthetized with an overdose of sodium pentobarbital (Virbac AH, Inc., Fort Worth, TX; 50-100 mg/kg, ip). Animals were exsanguinated via the abdominal aorta. The trachea was then cannulated and the whole lung was lavaged with Ca^{2+}/Mg^{2+} free PBS (pH 7.4, at 37°C) equal to 35 ml/kg body weight (representing total lung capacity). The lung lobes were lavaged three times with the same PBS aliquot. The right lung lobes were then removed, placed in liquid nitrogen, and stored at -80°C for later RNA isolation.

RNA Isolation and Real-Time Quantitative PCR. Total RNA was isolated from cells using RNeasy micro kits (Qiagen, Valencia, CA), and from caudal lung lobes frozen in liquid nitrogen using RNeasy mini kit (Qiagen). An inflammasome rat specific PCR array was used to analyze changes in mRNA expression due to LA exposure via manufacturer's instructions (SA Biosciences, Frederick, MD). Data were normalized to β –actin as the control gene. Relative fold mRNA expression was calculated considering saline exposed SH rats as controls.

Statistical Analysis. Data are expressed as mean ± S.E. (SH rats, n = 6/ group). Sigma Stat version 3.5 (Systat Software, Inc., Point Richmond, C.A.) was used to determine statistical

comparisons via a one-way analysis of variance with exposure as the factor followed by a post-hoc comparison using the Holm-Sidak method. Statistical significance was determined when p was found to be less than or equal to 0.05 between treatment groups.

4.3 Results

4.3.1 Activation of genes related to inflammasome

In order to examine the ability to LA to induce the inflammasome as well as the role of Fe, gene expression of inflammasome specific markers were analyzed using SA Biosciences rat inflammasome arrays in lungs of rats 4 h post-exposure. mRNA expression of cathepsin B, a known activator of the inflammasome, was induced after LA exposure in rats (Figure 4.2). Furthermore, cathepsin B expression was at control levels when rats were exposed to Fe loaded LA and LA + Def. ASC mRNA expression was also induced following LA exposure in rats while exposure to Fe loaded LA and LA+ Def did not induce its expression above control levels (Figure 4.2). Importantly NALP3 mRNA was also elevated following LA exposure but remained unchanged due to Fe loading of LA or exposure to LA + Def (Figure 4.2). All LA exposures induced interleukin-1β (IL-1β) mRNA expression (Figure 4.2). As observed with other genes Fe loaded LA however significantly reduced this IL-1 β mRNA expression. Surprisingly this trend existed also with animals exposed to LA + Def. NfκB mRNA expression was increased following LA and LA + Def exposure. Fe loading of LA however did not induce NfκB mRNA expression. All treatments with LA were able to induce mRNA expression of IL-6 compared to controls (Figure 4.2). Fe loading of LA however significantly dampened the induction of IL-6 while LA + Def significantly enhanced the induction of IL-6 compared to LA.

4.3.2 Gene expression of immune and inflammatory cytokines

Exposure to LA, Fe loaded LA or LA + Def did not alter pulmonary interferon-γ or interleukin-18 (IL-8) mRNA expression (Figure 4.3). mRNA expression of the eosinophilic

chemokine CCL-11 was only up-regulated in rats exposed to LA + Def while expression was unchanged in other exposure groups (Figure 4.3). Even though mRNA expression of CCL-11 was increased at 4 h eosinophils were not noticeably present in the lavage at 4 or 24 h post exposure (data not shown). mRNA expression of the macrophage cytokines CCL-7, CCL-12, and CXCL3 were increased after LA exposure (Figure 4.3). Exposure to Fe loaded of LA also increased these cytokines but to a lesser extent compared to LA exposed rats. In general, LA + Def exposure resulted in an exacerbated induction of mRNA expression of these cytokines compared to LA. Pulmonary Cox-2 mRNA expression was increased following exposure to Def, LA, Fe loaded LA, and LA +Def compared to controls (Figure 4.3). Animals exposed to LA + Def demonstrated significantly enhanced induction of Cox-2 compared to LA.

Figure 4.2

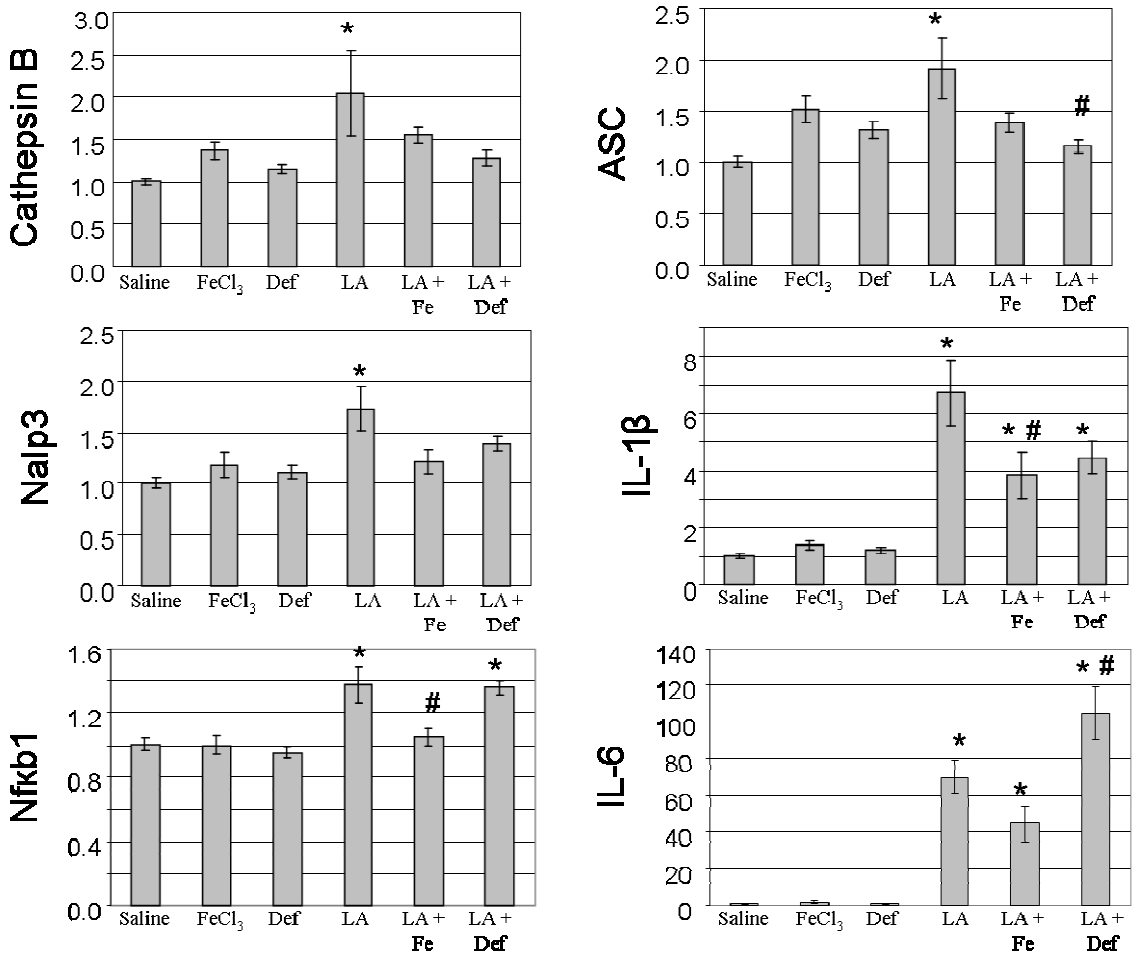

Figure 4.2. Alterations in mRNA expression of genes related to activation of the inflammasome pathway 4 h after exposure to LA, Fe loaded LA, or LA + Def. * Indicates significant difference from saline controls ($p<0.05$). # Indicates significant difference from LA exposed rats ($p<0.05$).

Figure 4.3.

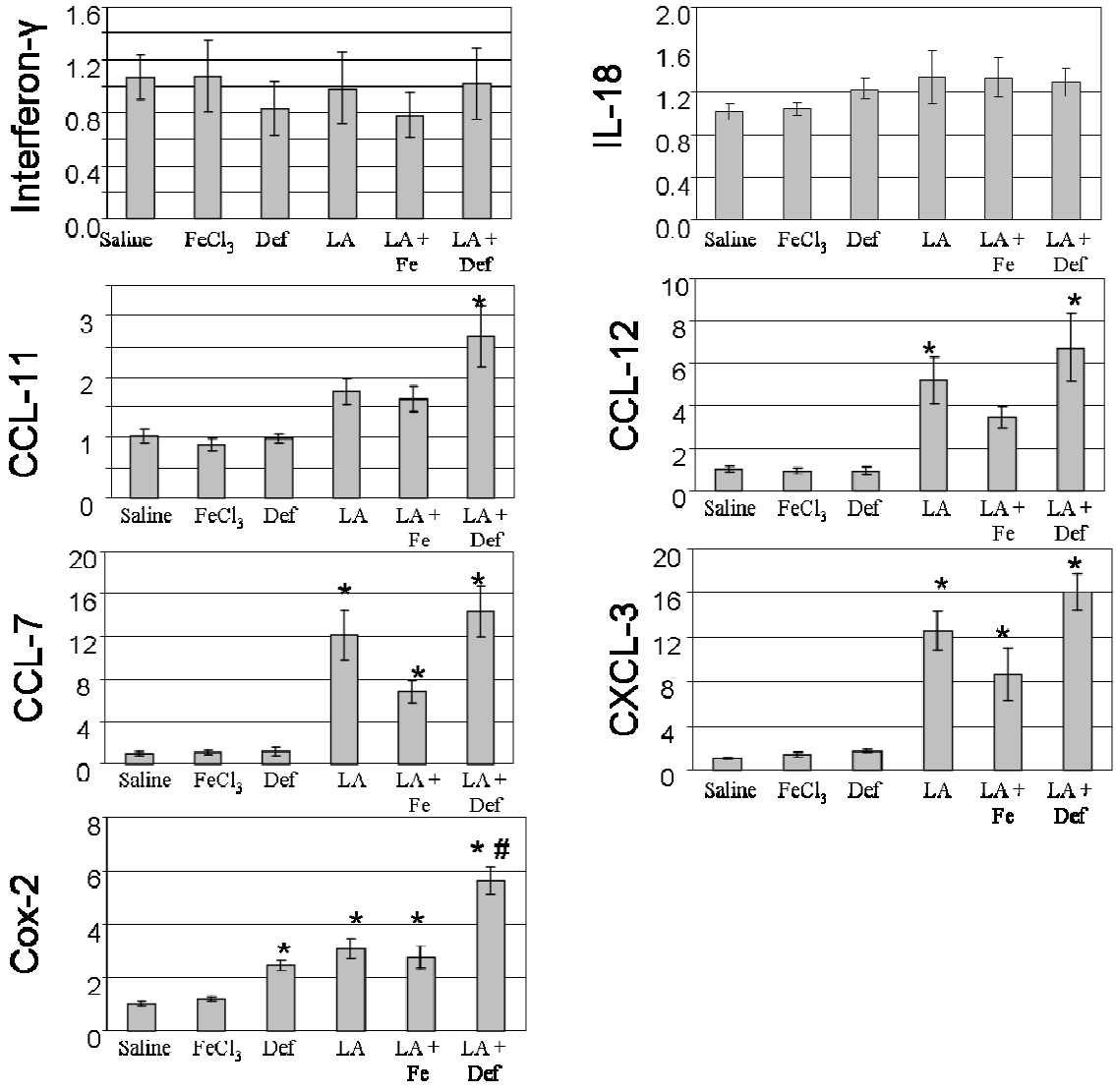

Figure 4.3. Immune and inflammatory cytokine mRNA expression 4 h after exposure to LA, Fe loaded LA, or LA + Def. * Indicates significant difference from saline controls ($p<0.05$). # Indicates significant difference from LA exposed rats ($p<0.05$).

4.4 Discussion

Chrysotile asbestos and silica exposures have been shown to activate the NALP3 inflammasome in mice and its activation has been found necessary to the development of fibrosis after silica exposure (Dostert *et al.*, 2008). It is not known if physicochemically distinct asbestos materials, such as LA might induce inflammation through activation of inflammasome complex. LA exposures have been associated with dose dependent increases in asbestosis among Libby, Montana residents (Sullivan, 2007, Moolgavkar *et al.*, 2010). In this study we examined the ability of LA to induce the inflammasome and the role of surface available Fe in rats. Our data show that, like other asbestos materials, LA exposure is associated with increases in expression of genes related to the inflammasome pathway that that is associated with inflammatory response. Furthermore, Fe loading of LA diminished the induction of many of these inflammasome associated genes and the related inflammatory response compared to LA suggesting that surface complexed Fe inhibits LA-induced inflammatory response through diminishing inflammasome activity. Removal of cellular and LA-bound Fe by Def increased the inflammatory response induced by LA in the absence of increased expression of key inflammasome genes and therefore may enhance inflammation through an inflammasome independent mechanism. Previous studies have demonstrated that the activation of the NALP3 inflammasome was dependent on two modes of activation 1) internalization of fibers into a phagolysome complex and increases in cathepsin B and 2) the production of reactive oxygen species by NADPH oxidase (Dostert *et al.*, 2008). Our data supports these studies, because LA was able to induce cathepsin B mRNA expression and our other studies have demonstrated an internalization of LA in alveolar macrophages.

Further analysis is required to demonstrate the activation of NADPH oxidase and its possible contribution to inflammasome activity.

The inflammasome once activated controls the inflammatory cascade through directing cleavage of pro-IL-1 β and pro-IL-18. LA however only was shown to induce IL-1 β but did not alter IL-18 expression. IL-18 is known to activate natural killer cells and T cells causing a release of interferon-γ thereby initiating an immune response to pathogens. Specifically, IL-1β has demonstrated a role in the fibrosis response to asbestos exposure and is a well known inflammatory cytokine (Lindroos *et al.*, 1997, Zhang *et al.*, 1993, Kline *et al.*, 1993). This study does not examine the mechanism regulating IL-1β and IL-18 transcription; however transcriptional activation of IL-1β is postulated to be mediated via activation of NADPH oxidase-mediated ROS generation and activation of NFκB signaling. LA specifically increased only in IL-1 β leading to an inflammatory response not genes related to a specific immune response such as IL-18 or interferon-γ.

Interestingly loading LA with Fe significantly diminished gene expression of many inflammasome markers. This leads us to postulate that catalytically available cellular Fe inhibits inflammasome activation. Thus, it is likely that in the absence of readily available catalytically active Fe, the Fe binding sites on LA might promote the removal of tightly bound Fe from endogenous proteins rendering them more active leading to further activation of the inflammasome. Since fibers are readily internalized by alveolar macrophages *in vivo* we do not believe the loading of Fe decreases the ability of fibers to be engulfed by macrophage but decreases its ability to signal once engulfed through complexing endogenous Fe. Treatment of LA with Def further induced the expression of many macrophage cytokines compared to LA and Fe loaded LA. These findings support the conclusion that Def treatment

of LA enhances inflammation via an inflammasome independent pathway. This inflammasome independent pathway may be related to increased recruitment and activation of alveolar macrophages to the site of exposure. The increased removal of Fe from protein coordination sites by Def treatment may signal for this enhanced inflammatory cell influx. Further study into exactly how removal of Fe from LA by Def increases inflammatory cell recruitment required.

Due to the LA sample being a mixture of winchite, richerite, and tremolite one can not determine which fiber type is causing inflammasome activation. Further study would require assessing each individual fiber's ability to induce the inflammasome. Another deficiency in this study is that the whole tissue potion of the lungs were homogenized and assessed for inflammasome mRNA expression changes. This could be diluting the signal as epithelial cells have yet to demonstrate inflammasome activity as seen in macrophages (Cruz *et al.*, 2007, Hornung *et al.*, 2008). The next step to this study would be to isolate primary alveolar macrophages and analyze gene expression changes in response to fiber exposure and the role of surface available Fe. It is necessary to substantiate gene expression analysis by assessing inflammasome specific protein levels after LA exposure and the role of Fe in modulating their activity. Our previous study (Chapter 3) determined that bronchiolar epithelial cells exposed to LA exhibited similar modulations in inflammatory response as seen in our current analysis of the inflammasome. This supports the ability of Fe to alter the inflammatory response in both cell types however the mechanism governing these effects is not clearly understood. The ability of epithelial cells to possibly activate the inflammasome as well as other general mechanisms by which cells activate an inflammatory response requires further study.

Overall our data supports the conclusion that LA like other asbestos fibers is able to induce the NALP3 inflammasome and cause a specific induction of IL-1 β. This increase in IL-1 β may contribute to the inflammation after exposure and may influence asbestosis development. Fe loading of LA was found to diminish the activity of the inflammasome. Def enhancement of LA-induced inflammation may be through an inflammasome independent mechanism or through the regulation of a different set of inflammasome genes since LA plus Def did not further enhance the transcription of NALP3 genes. Due to the relatively short length of the LA sample it is possible that these fibers are more readily engulfed and therefore activate the inflammasome more readily while other longer fibers may activate the inflammasome primarily through ROS generation not mediated macrophage fiber uptake.

CHAPTER 5. THE ROLE OF CARDIOVASCULAR DISEASE-ASSOCIATED IRON OVERLOAD IN LIBBY AMPHIBOLE-INDUCED PULMONARY INJURY AND INFLAMMATION

5.1 Introduction

Asbestos exposure in general is known to cause pulmonary toxicity leading to a variety of diseases including asbestosis, mesothelioma, and lung cancer. Miners and residents in the town of Libby, Montana have increased incidences of asbestos-related diseases, such as asbestosis and mesothelioma, associated with occupational and/or environmental exposure to amphibole contamination from a major vermiculite mine (Peipins *et al*. 2003, Sullivan 2007). The Libby amphiboles (LA) are a mixture of winchite, richterite, tremolite, and other minerals in prismatic, acicular, and asbestiform morphologies (Meeker *et al.* 2003). Because physicochemically diverse fibers can induce various diseases with varying potencies, toxicological studies have begun focusing on how the LA fiber mix might cause toxicity differently than fibers that have been studied for decades (Putnam *et al*., 2008; (Duncan *et al.* 2010).

Toxicity due to inhalation of asbestos fibers has been linked to the production of reactive oxygen species (ROS) both directly by the fibers and indirectly by activation of inflammatory cells (Sanchez *et al*. 2009). ROS cause cellular damage through oxidation of lipids, proteins, and DNA. This damage leads to activation of cell signaling pathways and transcription factors that can cause a variety of alterations in gene expression related to antioxidants, apoptosis, cytokines, growth factors, and stress response (Kamp, Weitzman

1999). The inability to clear fibers, such as amphiboles, resulting in their biopersistence causes the lung to exist in a state of chronic oxidative stress and inflammation due to the prolonged activation of inflammatory cells and the generation of ROS.

Fe has a considerable role in the production of ROS by asbestos fibers. It has been postulated that Fe associated with the surface of fibers has the ability to support Fenton reactions using reducing equivalents, such as airway lining ascorbate, thereby generating ROS (Ghio *et al*. 2008). Furthermore, modulation of the amount of Fe on the surface of the fiber alters ROS production and consequently the toxicity of fibers (Gazzano *et al.* 2007a). Chelation of Fe reduces the generation of ROS upon exposure to asbestos *in vitro (Kamp et al.* 1995a) and *in vivo* (Kamp *et al.* 1995b). Asbestos binds endogenous chelatable Fe *in vivo* upon deposition into the airways (Ghio, Churg & Roggli 2004). Once associated with the fiber, this additional Fe from the host may augment toxicity by potentiating ROS production (Ghio *et al.* 2006). Thus, it is likely that bioavailable host Fe can modify the toxicity of asbestos fibers.

Under oxidative stress, cellular Fe is generated by HO-1 catalyzed degradation of heme (Raval, Lee 2010). This process is known to transcriptionally activate production of ferritin, an intracellular Fe binding protein which is highly critical in regulating cellular oxidative stress and a number of cellular processes catalyzed by Fe, such as the activity of mitochondrial aconitase (Gozzelino, Jeney & Soares 2010). Systemically Fe homeostasis is maintained by a high abundant extracellular Fe transport protein, transferrin (Kibel, Belovari & Drenjancevic-Peric 2008). A number of cell membrane Fe and metal transporters are involved in tightly regulating levels of chelatable non-heme Fe (Anderson, Vulpe 2009). In many chronic diseases the regulation of Fe homeostasis is disrupted, especially in

cardiovascular (CVD), where hemoglobin is vulnerable to degradation by constant sheer stress on peripheral vessels (Yasuda, Funakubo & Fukui 2002). In chronic conditions, individuals with CVD exhibit systemic tissue Fe-overload, including the lung (Kruszewski 2004, Ellervik *et al*. 2010, Xie *et al*. 2008). Underlying oxidative stress and a dysregulation of Fe homeostasis lead to increased systemic non-heme Fe levels (Kruszewski 2004). Due to the essential role of Fe in catalytic activity of a many proteins it is possible that the disruption of Fe homeostasis by its binding to asbestos fibers over time increases the pulmonary toxicity more readily in those having Fe-overload.

We have recently characterized dysregulation of pulmonary Fe homeostasis in two rat models of human cardiovascular diseases; the spontaneously hypertensive (SH) and the spontaneously hypertensive heart failure (SHHF) (Shannanan *et al.*, 2010). As with human CVD, these rat models, (SHHF>SH) have greater transcriptional activation of lung ferritin at mRNA and protein level together with increased HO-1 relative to healthy rats. Also associated with these complications SH and SHHF exhibit an increase in chronic inflammation, lower antioxidant levels and oxidative stress in their lungs at baseline when compared to healthy Wistar Kyoto (WKY) rats (Shannahan *et al*. 2010). Attributable to the ability of asbestos to complex host-tissue Fe, we believe that SH and SHHF, with inherent Fe-overload are appropriate for investigating the role of Fe in pulmonary injury caused by fibers. We hypothesized that SH and SHHF rats will exhibit greater and prolonged lung injury and inflammation upon exposure to LA, relative to healthy WKY rats, due to their preexistent dysregulation of Fe homeostasis. To address this hypothesis, we exposed WKY, SH, SHHF to LA and examined changes in biomarkers associated with Fe homeostasis, inflammation, and oxidative stress.

5.2 Materials and Methods

Libby Amphibole. The Libby amphibole (LA) sample was collected from the Rainy Creek Complex near Libby, Montana in 2007 by the United States Geological Survey and was processed to produce inhalable material by Meeker *et al*., as indicated earlier (Meeker et al. 2003). The sample was further size fractionated by water elutriation as described previously (Webber *et al.* 2008) in order to isolate a rat respirable fraction ($PM_{2.5}$) using a settling velocity of 3.4×10^{-4} cm s^{-1}. Transmission Electron Microscopy showed 97.8% (135/138) of elutriated fibers had aspect ratios ≥ 5 consistent with the composition of LA obtained from the 2000 sample (Meeker *et al.* 2003,Webber *et al.* 2008) and with the composition of LA obtained from the $PM_{2.5}$ elutriated fraction of the 2000 collection (Lowers and Bern, 2009). Fiber dimensions, as determined using transmission microscopy of the elutriated LA 2007 sample were: mean length 4.99μm ± 4.53 and width 0.28μm ± 0.19; median length = 3.59μm, width = 0.23μm with upper and lower values of length being 0.52μm – 27.30μm and width 0.07μm – 1.15μm. The estimated fiber count for 1 mg LA sample was 218×10^6. In comparison to the elutriated LA 2007 sample used in the present study air samples from Libby Montana have been shown to contain fibers having a mean length of 7.64μm ± 8.40 and width 0.51μm ± 0.46, and median length 5.2μm and width 0.39μm with upper and lower values of length being 0.5μm – 195μm and width 0.01μm – 10μm; with an aspect ratio of ≥ 5 (U.S. EPA 2010). The median fiber length being smaller than the mean length suggests that there are likely a larger proportion of fibers that are smaller than the mean length.

Animals. Male, 11-12 week old, healthy WKY, and SH and obese SHHF rats were purchased from Charles River Laboratories, Raleigh, NC. All rats were maintained in an

isolated animal room in an Association for Assessment and Accreditation of Laboratory Animal Care (AALAC) approved animal facility at 21 +/- 1°C, 50 +/- 5% relative humidity, and 12 h light/dark cycle. Rats were housed (2/cage) in polycarbonate cages containing beta chip bedding. Animals received standard (5001) Purina rat chow (Brentwood, MO) and water *ad libitum*. The U.S. EPA NHEERL Institutional Animal Care and Use Committee (IACUC) approved the protocol.

Intratracheal Instillation of Libby Amphibole. Since the rat respirable sample of LA was prepared using the water elutriation method, a uniform saline suspension of LA for intratracheal instillation was achieved by vortexing followed by water bath sonication for 15 min. The suspension was vortexed prior to each instillation to ensure that fibers did not settle at the bottom of the tube. In order to ensure the fibers did not interact with any biological molecules or chemical dispersants of the media prior to landing on the airway surface, we decided not to use a biological dispersion media or any other chemicals for preparing the instillate. Rats (WKY n=12/time point; SH n=6/time point; SHHF n=6/time point) were anesthetized with isoflurane and intratracheally instilled with 300 μl saline containing either 0, 0.25, or 1.0 mg of LA as described previously (Wallenborn *et al*. 2009). The concentrations selected although high were, in general, consistent with instillation studies using other fiber types (Adamson, Bakowska 2001, Hirano, Ono & Aimoto 1988). Doses were chosen to assure a response in the lung upon instillation allowing for a comparative analysis between strains. Theoretically, a rat will deposit 0.07 mg of fibers during 6 hour inhalation at 10mg/m^3 based on the assumption that minute volume is 200ml and the deposition fraction to pulmonary region is 0.10. Intratracheal instillation ensured the

delivery of exact concentrations of LA into the lung and allowed us to control for likely strain-related deposition differences due to their variation in breathing parameters (Shannahan *et al.*, 2010). In our previous study approximately 30% of WKY presented with non-pathogenic cardiac hypertrophy (Shannahan *et al*. 2010). Therefore WKY group size was increased (n=12) to eliminate the data from those with hypertrophic hearts (heart weight > 1.3g; normal heart weight ~1g) and still maintain appropriate group sizes for statistical comparisons.

Necropsy, Sample Collection, and Analysis. Rats were weighed (WKY 280 ± 3.46g, SH 283 ± 3.43g, and SHHF 432 ± 4.94g (Values mean weight ± S.E.)) and anesthetized with an overdose of sodium pentobarbital (Virbac AH, Inc., Fort Worth, TX; 50-100 mg/kg, ip) 1 day, 1 week, or 1 month following instillation of LA. Blood was collected though the abdominal aorta into blood collection tubes, which were used for a different study. Blood was then removed from the vasculature of the lung by perfusion of Ca^{2+}/Mg^{2+} free phosphate buffered saline (PBS) via the pulmonary artery to avoid interference in data analysis involving Fe-binding proteins and capacities.

The trachea was then cannulated and the left lung lobe tied off. The right lung lobes were lavaged with Ca^{2+}/Mg^{2+} free PBS (pH 7.4, at 37°C) equal to 35 ml/kg body weight (representing total lung capacity) x 0.6 (right lung capacity being 60% of total lung capacity). The lavage volume was normalized for SHHF to WKY rats based on the assumption that the lung growth and thus, volumes remained similar at a given age despite the obesity-induced increase in body mass of SHHF rats. The lung lobes were lavaged three times with the same PBS aliquot. The right lung lobes were then removed, placed in liquid nitrogen, and stored at

-80°C for later analysis. The left lung was fixed at 40% of its total capacity by instillation of 10% neutral buffered formalin through the trachea and stored in 10% formalin at 4°C until processed for histopathology.

Cell Differential and Bronchoalveolar Lavage Fluid (BALF) Analysis. Aliquots of BALF were taken for total cell counts (Coulter Inc., Miami, FL, USA), cell differentials, and analyses of lung injury markers. Cell differentials were conducted by Cytospin preparation (Shandon, Pittsburgh, PA), and slides were stained with LeukoStat (Fisher Scientific Co., Pittsburgh, PA). Macrophages and neutrophils were counted under light microscopy and quantified based on total cell count. The remaining cell free BALF was evaluated for the following: total protein (Coomassie plus Protein Assay Kit, Pierce, Rockford, IL), albumin (DiaSorin, Stillwater, MN), lactate dehydrogenase (LDH) activity (Thermo Fischer Diagnostics, Middletown, VA), N-acetyl-β-D-glucosaminidase (NAG) activity (Roche Diagnostics, Indianapolis IN), γ-glutamyl transferase (GGT) activity (Thermo Fischer Diagnostics), and the Fe-binding proteins, ferritin (Kamiya Biomedical Company, Seattle, WA) and transferrin (Trf) (DiaSorin, Stillwater, MN). Total Fe-binding capacity (TIBC) was calculated by adding the unsaturated Fe-binding capacity (UIBC) (UIBC Assay, Genzyme Diagnostics, Charlottetown, Prince Edward Island, Canada) and the non-heme Fe (Serum Fe-SL Assay, Genzyme Diagnostics). All assays were adapted for BALF analysis and ran using the Konelab Arena 30 clinical analyzer (Thermo Chemical Lab Systems, Espoo Finland). Data were normalized to volume of BALF.

One aliquot of BALF was mixed with an equal volume of 6% perchloric acid and ascorbate was measured by HPLC (C-18 Bondpack column, Millipore Waters

Chromatography, Milford, MA) using amperometric electrochemical detection (Bioanalytical Systems, W. Layfayette, IN). Total glutathione levels were measured using 5,5,9-dithiobis(2-nitro-benzoic) acid-glutathione disulfide reductase recycling assay via the Konelab clinical analyzer (Anderson 1985).

Lung Tissue Analysis. Ascorbate and glutathione levels were measured in the caudal lung lobes. Individual samples were homogenized in 3% perchloric acid, and supernatants were analyzed for ascorbate and glutathione as described above. Caudal lung lobes were homogenized in Tris-HCl buffer (pH 7.4) with protease inhibitors present. The individual samples were then centrifuged (14000 g) for 20 min (4°C) and the supernatant stored at -80°C. The supernatant was used to determine total protein content, ferritin, Trf, non-heme Fe, total Fe binding capacity (TIBC), and unsaturated Fe-binding capacity (UIBC) as stated above. Data were normalized to total protein content of tissues.

RNA Isolation and Real-Time Quntitative PCR. Total RNA was isolated from caudal lung lobes frozen in liquid nitrogen using RNeasy mini kit (Qiagen, Valencia, CA). One-step RT-PCR was carried out using Platinum Quantitative RT-PCR ThermoScript One-Step System (Invitrogen, Carlsbad, CA) according to manufacturer's instructions (Shannahan *et al.* 2010). PCR was performed for 18S ribosomal RNA (Control), macrophage inflammatory protein (MIP-2), heme-oxygenase-1 (HO-1), transferrin (Trf), ferritin light chain (FLC), ferritin heavy chain (FHC), and divalent metal transporter-1 (DMT-1). Primers for these mRNA were purchased from Applied Biosystems, Inc. (Foster City, CA). Relative fold mRNA

expression was calculated for SH and SHHF rats considering the saline exposed WKY values as control.

Lung Histopathology. The right lung lobe was trimmed, embedded in paraffin, sectioned to a thickness of approximately 3 microns (transverse), and stained with hematoxylin and eosin (H&E). The lung lesions were evaluated with particular attention to the lesion location (i.e, bronchi, terminal bronchi, alveolar duct, alveoli, interstiteum, centriacinar regions, pleura). The morphological evaluation took into consideration the characteristics of each inflammatory cellular component, i.e., polymorphonuclear cells, macrophages, fibrosis, microgranulomas, as well as changes in the alveolar epithelium. Histopathological changes were scored using semiquantitative grading at five levels (0 = normal; 1 = minimal; 2 = mild; 3 = moderate; 4 = severe) taking into consideration the degree of severity and the type of lesion (Shackelford *et al*. 2002, Nyska *et al.* 2005).

Statistical Analysis. Data are expressed as mean ± S.E. (WKY, n = 8-12/ treatment group; SH, n = 6/ treatment group; SHHF, n = 6/ treatment group). Sigma Stat version 3.5 (Systat Software, Inc., Point Richmond, C.A.) was used to determine statistical comparisons via a two-way analysis of variance with strain and exposure as factors followed by a post-hoc comparison using the Holm-Sidak method. Statistical significance was determined when p was found to be less than or equal to 0.05 between treatment groups and strains.

5.3 Results

5.3.1 Pulmonary Inflammation, and Injury

In order to quantify inflammation and injury response following LA exposure and to determine the baseline strain differences, BALF samples were analyzed for various biomarkers. Baseline levels (saline control) of BALF protein were significantly higher in SH and SHHF when compared to WKY (SHHF>SH>WKY) (Figure 5.1), consistent with our previous study (Shannahan *et al*. 2010). Surprisingly, at 1 day post-exposure no increases in BALF protein occurred in WKY or SH while SHHF rats exposed to LA demonstrated marked variability and decreases compared to strain matched control. By 1 week, only SH rats (with moderate baseline increase in protein relative to WKY) exposed to LA showed concentration-dependent increases in total protein which persisted to 1 month. Because of the already very high levels at baseline, the LA-induced changes in BALF protein for 1 week and one month were not distinguishable in SHHF rats. Albumin levels were consistent with the trends demonstrated by total protein at all time points. GGT activity was significantly increased in a concentration-dependent manner and regardless of protein levels in BALF in all strains at 1 day; however, the changes in LA-exposed WKY were significantly greater when compared to LA-exposed SH and SHHF rats at 1 day and 1 week (Figure 5.1). At 1 week through 1 month, GGT activity still remained significantly elevated after 1 mg LA exposure in all strains, but the magnitude of effect decreased in a time-dependent manner. Concentration-dependent increases in LDH activity were observed at the same level in all strains at 1 day (Figure 5.1). At 1 week and continuing to 1 month, LDH activity remained elevated in all strains; however, the increase was more pronounced in SHHF when compared WKY. NAG activity, a marker of phagocyte activation increased in a concentration-

dependent manner after LA exposure in all three strains at 1 day and 1 week with no remarkable strain differences and had returned to baseline by 1 month (Figure 5.1). Despite markedly higher baseline BALF protein in SH and SHHF, the baseline levels of these enzyme markers in most instances were comparable between strains.

All strains exhibited robust neutrophilic influx in response to LA exposure at 1 day (Figure 5.2). Interestingly, SHHF exposed to 1 mg LA had a significantly greater number of neutrophils in their BALF compared to WKY receiving the same dose (SHHF>SH>WKY). Although to a lesser extent than the 1 day time point, neutrophil increases persisted in SH and SHHF rats at 1 week and 1 month (SH>SHHF). However, in the case of WKY, the initial robust increase in neutrophils at 1 day was largely reversed by 1 week. In WKY, numbers of lavageable macrophages decreased at 1 day and 1 month in response to LA. BALF macrophages also decreased in SH and SHHF at 1 day, but this effect was less remarkable than the effect in WKY. SH and SHHF exposed to 1 mg LA at 1 week had greater numbers of macrophages than controls when compared to dose-matched WKY. This increase in macrophages persisted only in SH through 1 month. The value of total cells in each of the three strains reflected changes in macrophages and neutrophils together.

5.3.2 Fe-Binding Proteins and Capacities in BALF

One of the objectives of this study was to evaluate potential strain-related differences in non-heme Fe pool in response to acute LA exposure. Therefore, BALF and also lung tissue levels of ferritin and transferrin (Trf) at both the protein and transcriptional level, and Fe-binding capacities were analyzed. As we have noted in our previous study, the baseline (controls) BALF levels of ferritin and Trf were highly elevated in SH and SHHF when compared to WKY. BALF ferritin protein levels were found to be significantly elevated only

in SH and SHHF exposed to LA in a concentration-dependent manner through 1 month (Figure 5.3). At 1 week and 1 month, SH, but not WKY or SHHF exposed to 1 mg LA, showed increases in BALF Trf relative to strain matched controls. The increases in Trf might reflect greater vascular protein leakage, as demonstrated by BALF protein leakage, since circulating levels of Trf, unlike ferritin, are high as it serves as a major systemic Fe transporter protein (Anderson, Vulpe 2009, Ghio *et al*. 1998).

The BALF levels of non-heme Fe, as in the case of ferritin and Trf, were also significantly elevated at baseline (saline controls) in both SH and SHHF when compared to WKY. Non-heme Fe increased only in SH, but not in WKY or SHHF rats, in a concentration-dependent manner at 1 day and 1 week time points (Figure 5.3) which is associated with increases in vascular protein leakage. The non-heme Fe data at 1 month was highly variable within and between groups and inconsistent with other time points. We presumed that determination of airway lining Fe-binding capacity might allow one to understand the role of Fe movement between BALF Fe-binding proteins and inhaled fibers. We determined unsaturated and saturated (total) Fe-binding capacities (UIBC and TIBC) in BALF. Although the levels appeared to be high in SH and SHHF, no significant baseline strain differences existed in UIBC in the present study (Figure 5.3). This is unlike our previous study where SH and SHHF rats had increased unsaturated Fe-binding capacities in BALF (Shannahan *et al*. 2010). The changes in BALF UIBC due to LA exposure were small and showed an increase which was significant only in WKY at one month when compared to WKY saline control. In general, TIBC was found to be elevated in control SHHF compared to control WKY (Figure 5.3). LA exposure did not alter TIBC at any time point in any strain.

5.3.3 Lung Expression of mRNA Markers of Fe Homeostasis, Oxidative Stress, and Inflammation

To understand the relationship between LA-induced pulmonary injury/inflammation and Fe homeostasis, we determined transcriptional levels of genes that regulate heme catabolism, Fe transport, Fe storage, oxidative stress and inflammation in rats exposed to saline or LA. As expected, the baseline expression of MIP-2 (a potent neutrophil chemoattractant), and HO-1 (a marker of oxidative stress) were markedly elevated in SH and SHHF relative to WKY, which supports the baseline differences in neutrophilic inflammation between the three strains. Surprisingly, only WKY increased MIP-2 in a concentration-dependent manner at 1 day in response to LA, despite neutrophilic inflammation being similar in all three strains at 1 day and persistent in SH and SHHF up to 1 month (Figure 5.4). No exposure-related induction of HO-1 expression was noted at 1 day in any of the strains; on the contrary, its expression was decreased from already high baseline by LA-exposure in SHHF (Figure 5.4). At 1 week after 1 mg LA exposure, HO-1 expression was increased only in the SH rats. Because ferritin protein is made of a ferritin light chain (FLC) and a ferritin heavy chain (FHC), each possessing different kinetic property for binding Fe, we determined transcriptional activation of both these subunits. FHC at all time points and FLC mRNA at 1 day and 1 week demonstrated no consistent strain-related baseline differences (saline controls), however, at 1 month the expression of FLC in SH and SHHF was greatly enhanced at baseline relative to WKY. These baseline alterations suggest a disease associated progression in FLC expression. FLC mRNA was not induced after LA exposure in any strains at 1 day or 1 week, except for a small but significant rise in SHHF at 0.25 mg LA dose. However at 1 month its expression increased in WKY as well as SH at

high concentration of LA. Surprisingly, SHHF showed a significant decline in its expression from already increased baseline, suggesting that less compromised SH retained the capacity to sustain LA-induced FLC expression while highly compromised SHHF, lost this ability. FHC mRNA expression was elevated in a concentration-dependent manner in only in SHHF at 1 day but not at later time points. No consistent strain or exposure-related differences were noted in Trf or divalent metal transporter-1 (DMT-1).

5.3.4 Fe-Binding Proteins and Capacities in Lung Tissue

Lung ferritin protein also exhibited strain related differences at baseline (SHHF>SH>WKY), which were unchanged 1 day after exposure to LA. At 1 week, however, only SH rats exposed to 1 mg LA had increased ferritin protein in lung tissue compared to saline controls (Figure 5.5). At 1 month no changes in ferritin levels were observed due to exposure in any strain. Lung Trf protein levels were generally higher at baseline in SH and SHHF rats. LA exposure did not affect Trf protein in the lung at any time in WKY and SHHF but resulted in a concentration-dependent increase at 1 day in SH rats (Figure 5.5). No major alterations were seen in lung tissue levels of non-Heme Fe, unsaturated Fe-binding capacity (UIBC), or total Fe-binding capacity (TIBC) (data not shown).

5.3.5 Antioxidant Levels in BALF and Lung Tissue

Alveolar Fe homeostasis and oxidative stress will likely be influenced by antioxidants such as ascorbate and glutathione in BALF and lung tissue. Baseline ascorbate levels in BALF were generally lower in SH and SHHF when compared to WKY (Figure 5.6). SH, and to some extent WKY and SHHF, exposed to 0.25 mg of LA at all time points exhibited a

general decrease in BALF ascorbate when compared to their saline controls; however, most of these changes were insignificant except in SH at 1 day. There were marked variations in the baseline levels of lung tissue ascorbate between all three strains at each time point. Ascorbate in the lung tissue of SH was decreased due to exposure at 1 day, while WKY and SHHF demonstrate no marked changes. At 1 week lung tissue ascorbate levels were elevated in WKY in response to 0.25 mg LA exposure but unchanged in both SH and SHHF. WKY lung tissue ascorbate levels returned to baseline by 1 month while SH still demonstrated decreases after exposure. BALF glutathione levels were undetectable in all strains, while lung levels of glutathione were not found to be different between strains at baseline and remained unaltered due to LA exposure in all animal models (Figure 5.6).

5.3.6 Lung Histopathology

Although the strain related differences in specific biomarkers in lung and BALF were apparent, pathologically the LA-induced lesion severity differences could not distinguished between strains. Marked histological alterations were noted in all three strains in time- and concentration-related manner following LA exposure (Table 5.1). At 1 day the types of lesion characterized by acute alveolar neutrophilic inflammation and cell injury were LA concentration-dependent. The distribution of inflammatory foci in the lungs at 1 day was centriacinar but multifocal, and generally consisted of neutrophilic influx, associated with macrophages present within the lumen of the terminal bronchiole, alveolar duct, and adjacent alveoli (Figure 5.7 A, B and C). These changes were associated with minimal alveolar hyperplasia, in which the lining alveolar epithelium tended to be cuboidal instead of flattened. No incidences of interstitial fibrosis were observed at 1 day in any strain at either dose. However, at 1 week and at 1 month as shown in Figure 5.7 E and F, all animals

developed multifocal interstitial fibrosis and alveolar hyperplasia in a concentration-dependent manner (Table 5.1 and Figure 5.7 D, E and F). By 1 month neutrophil-like cells were not readily apparent while macrophages persisted within alveoli and interstitium (Figure 5.7). In few rats receiving 1 mg of LA focal granuloma-like formation was noted at this time. The severity scores and incidence for each of these pathological indices are given in Table 5.1.

Figure 5.1

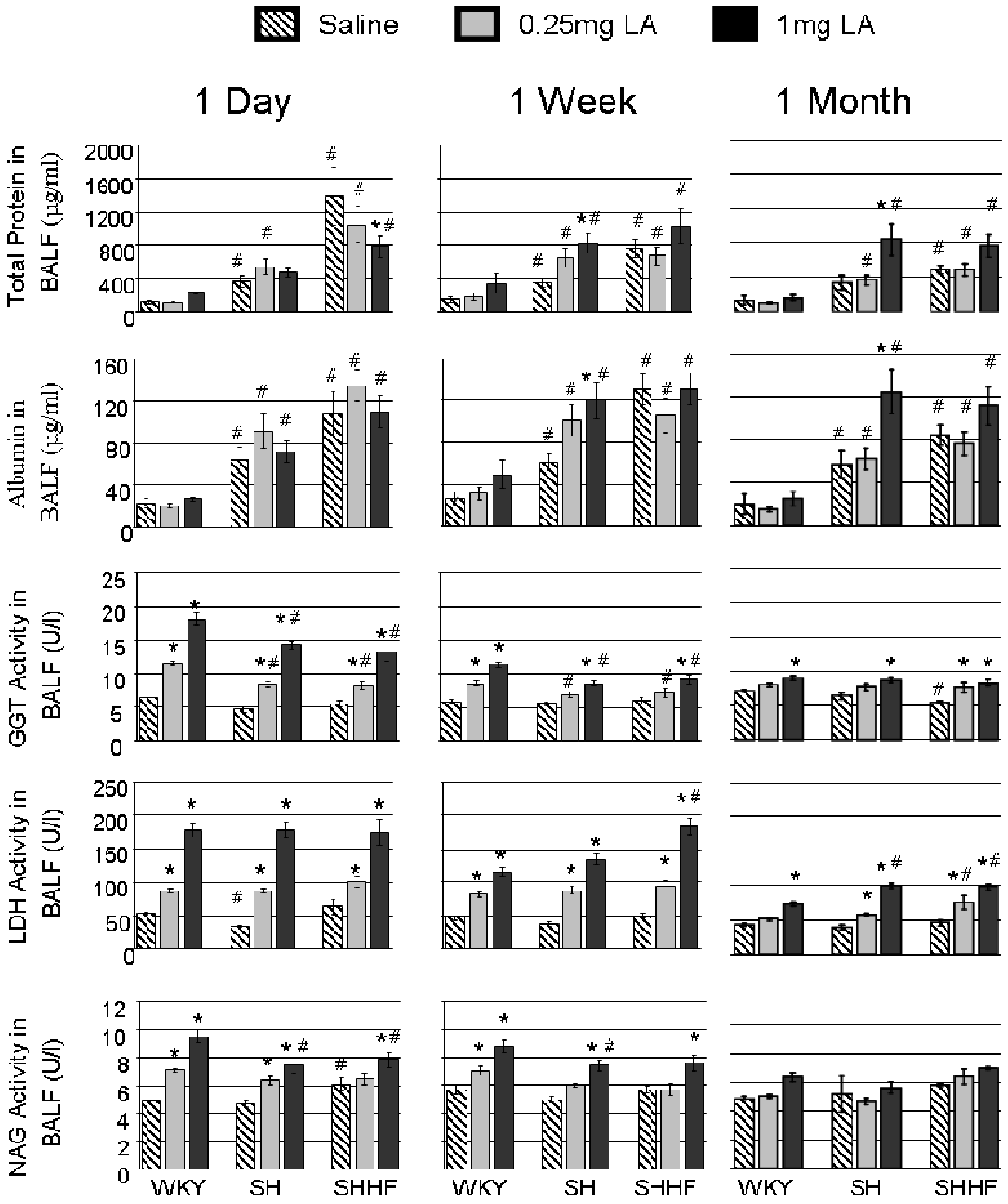

Figure 5.1. Temporal changes in BALF protein, albumin, and LDH, NAG and GGT activities in WKY, SH and SHHF rats following intratracheal instialltion of saline (control), 0.25 mg LA, or 1 mg LA. Values are mean ± SE (WKY, n =8-12/group; SH and SHHF, n = 6/group). * Indicates significant difference within strain in respect to saline controls

($p<0.05$). # Indicates significant difference from WKY at the same exposure concentration ($p<0.05$).

Figure 5.2

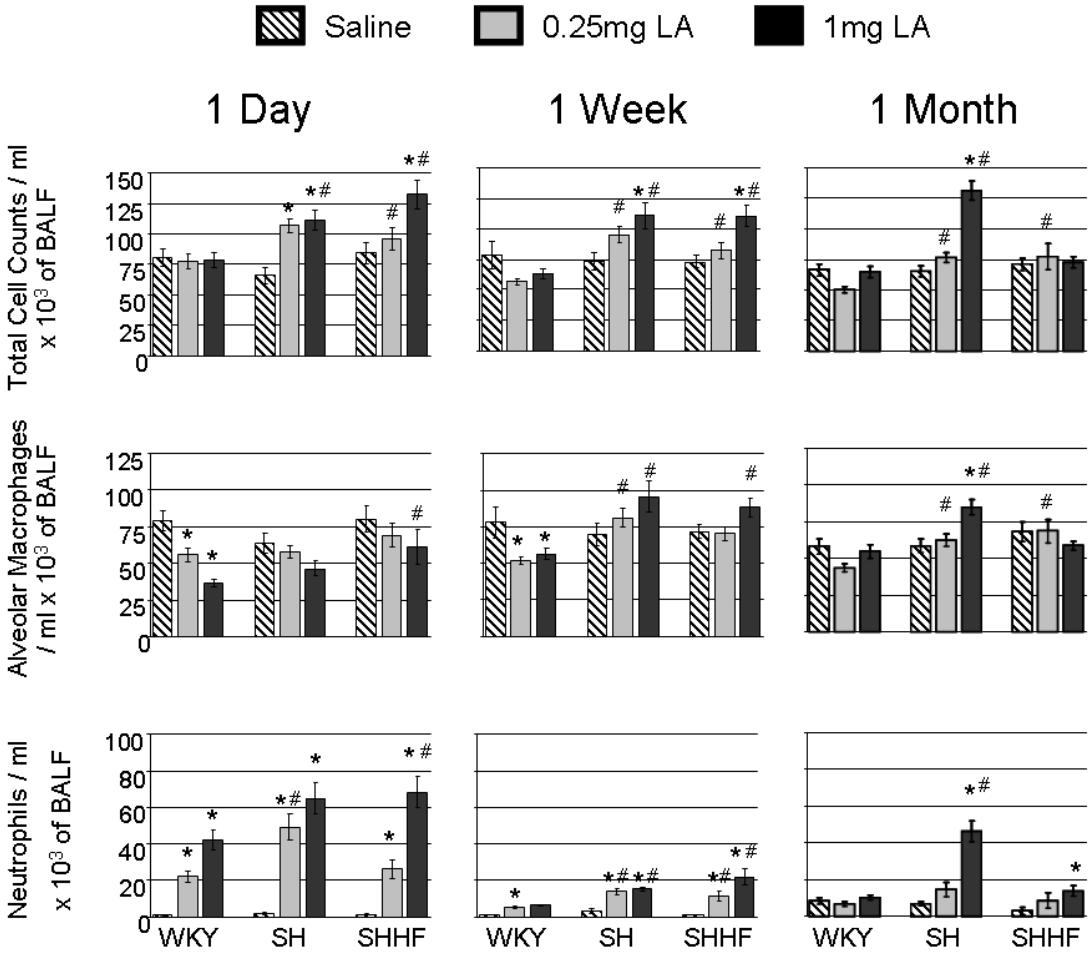

Figure 5.2. Alterations in inflammatory cells (total cells, macrophages and neutrophils) in BALF of WKY, SH, and SHHF instilled with saline (control), 0.25 mg LA, or 1 mg LA. Values are mean ± SE (WKY, n =8-12/group; SH and SHHF, n = 6/group). * Indicates significant difference within strain in respect to saline controls ($p<0.05$). # Indicates significant difference from WKY at the same exposure concentration ($p<0.05$).

Figure 5.3

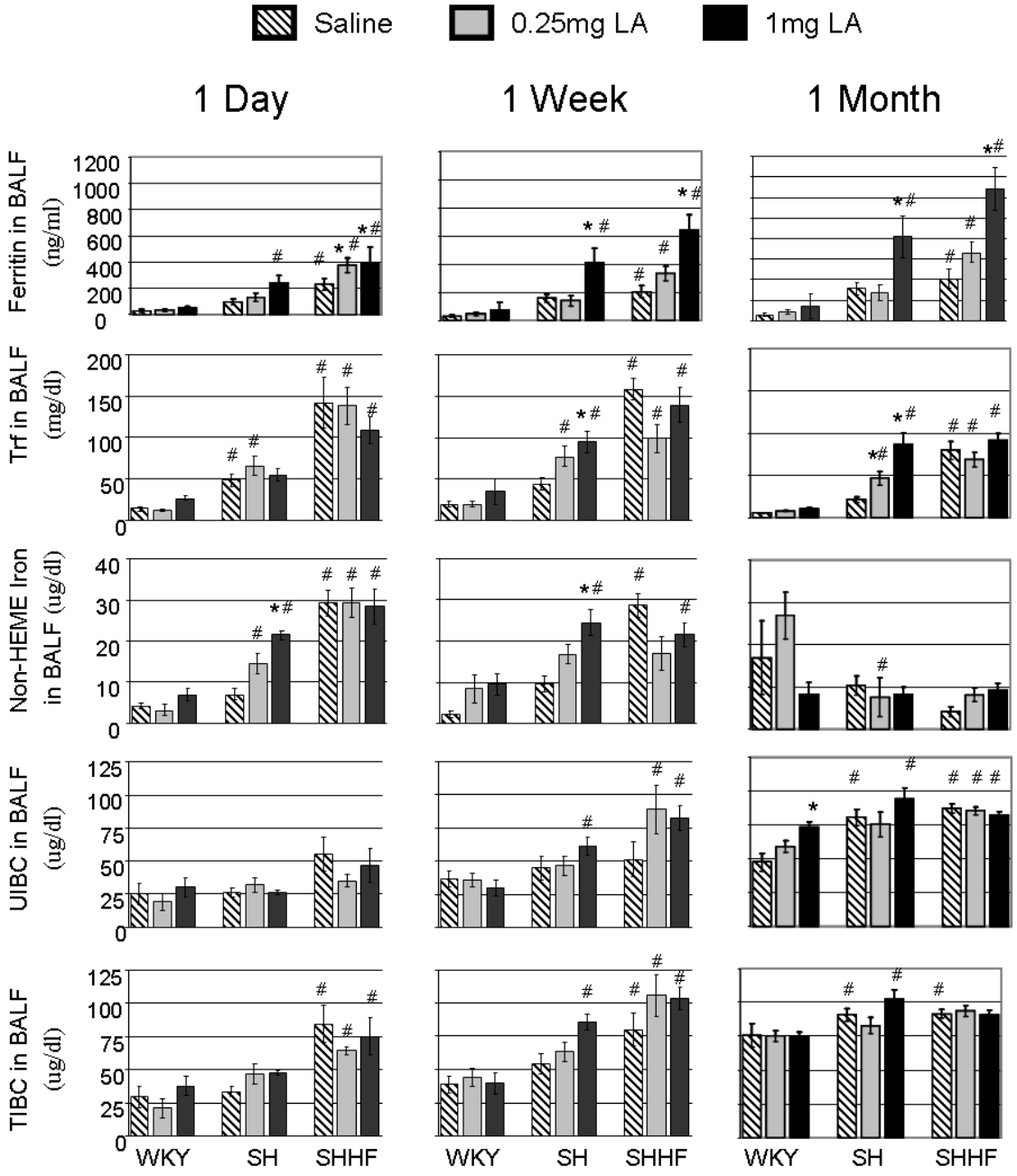

Figure 5.3. Time-related changes in markers of Fe homeostasis in the BALF of WKY, SH, and SHHF intratracheally exposed to saline (control), 0.25 mg LA, or 1 mg LA. Unsaturated Fe-binding capacity (UIBC) is a measurement of the capacity of BALF components to bind

catalytically active Fe. TIBC (total Fe-binding capacity), a calculated value (UIBC + non-heme Fe), is a measurement of all the Fe currently bound to BALF components. Values are mean ± SE (WKY, n =8-12/group; SH and SHHF, n = 6/group). *Indicates significant difference within strain in respect to saline controls ($p<0.05$). # Indicates significant difference from WKY at the same exposure concentration ($p<0.05$).

Figure 5.4

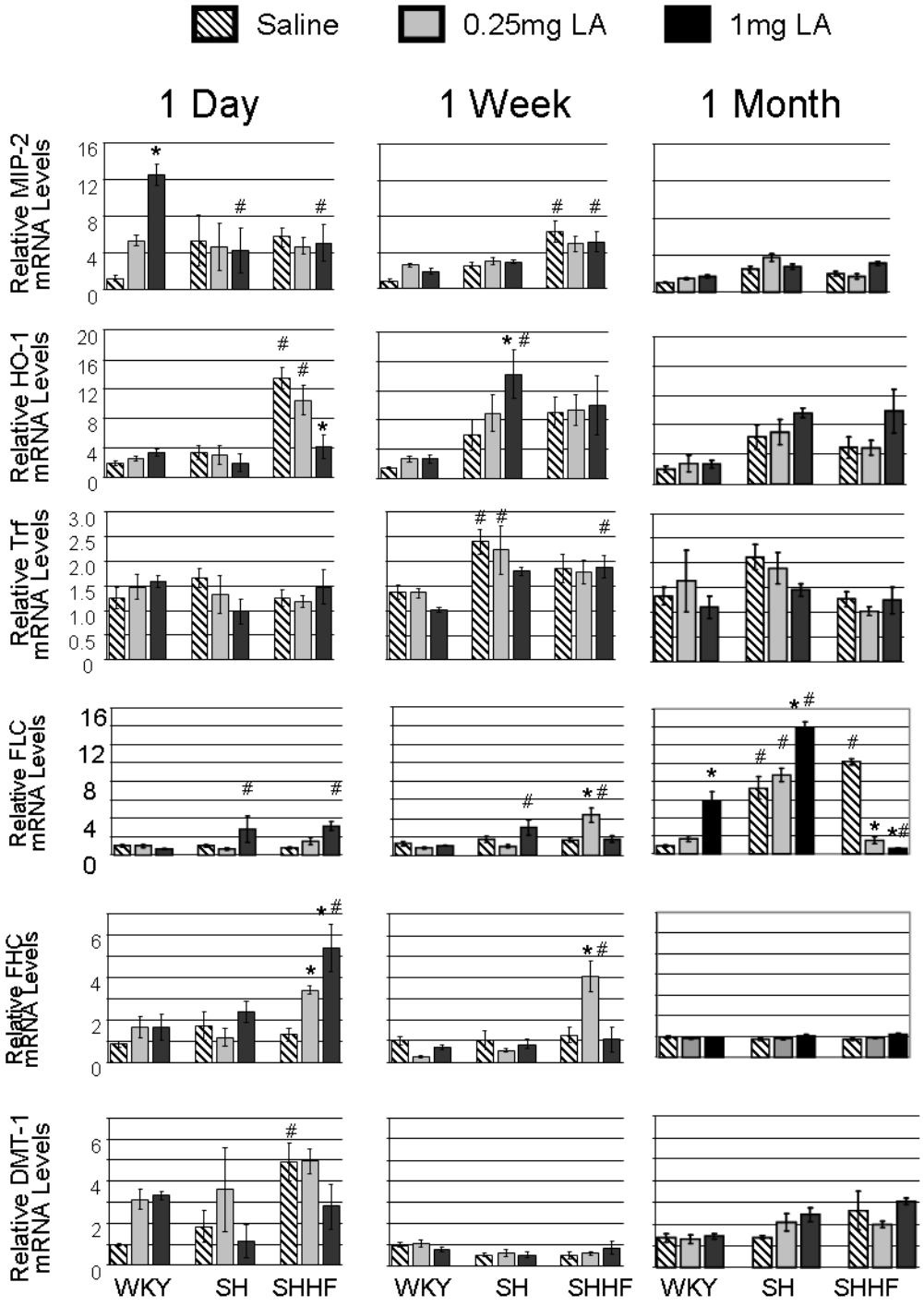

Figure 5.4. Relative mRNA expressions for markers of inflammation, Fe homeostasis and oxidative stress in the lungs of WKY, SH, and SHHF rats exposed to saline (control), 0.25

mg LA, or 1 mg LA. Real-time reverse transcriptase PCR was used for analysis. MIP-2 (Macrophage Inflammatory Protein-2), HO-1 (Heme Oxygenase-1), Trf (Transferrin), FLC (Ferritin Light Chain), FHC (Ferritin Heavy Chain), and DMT1 (Divalent Metal Transporter 1). Values are mean ± SE (n = 6/group). * Indicates significant difference within strain in respect to saline controls ($p<0.05$). # Indicates significant difference from WKY at the same exposure concentration ($p<0.05$).

Figure 5.5

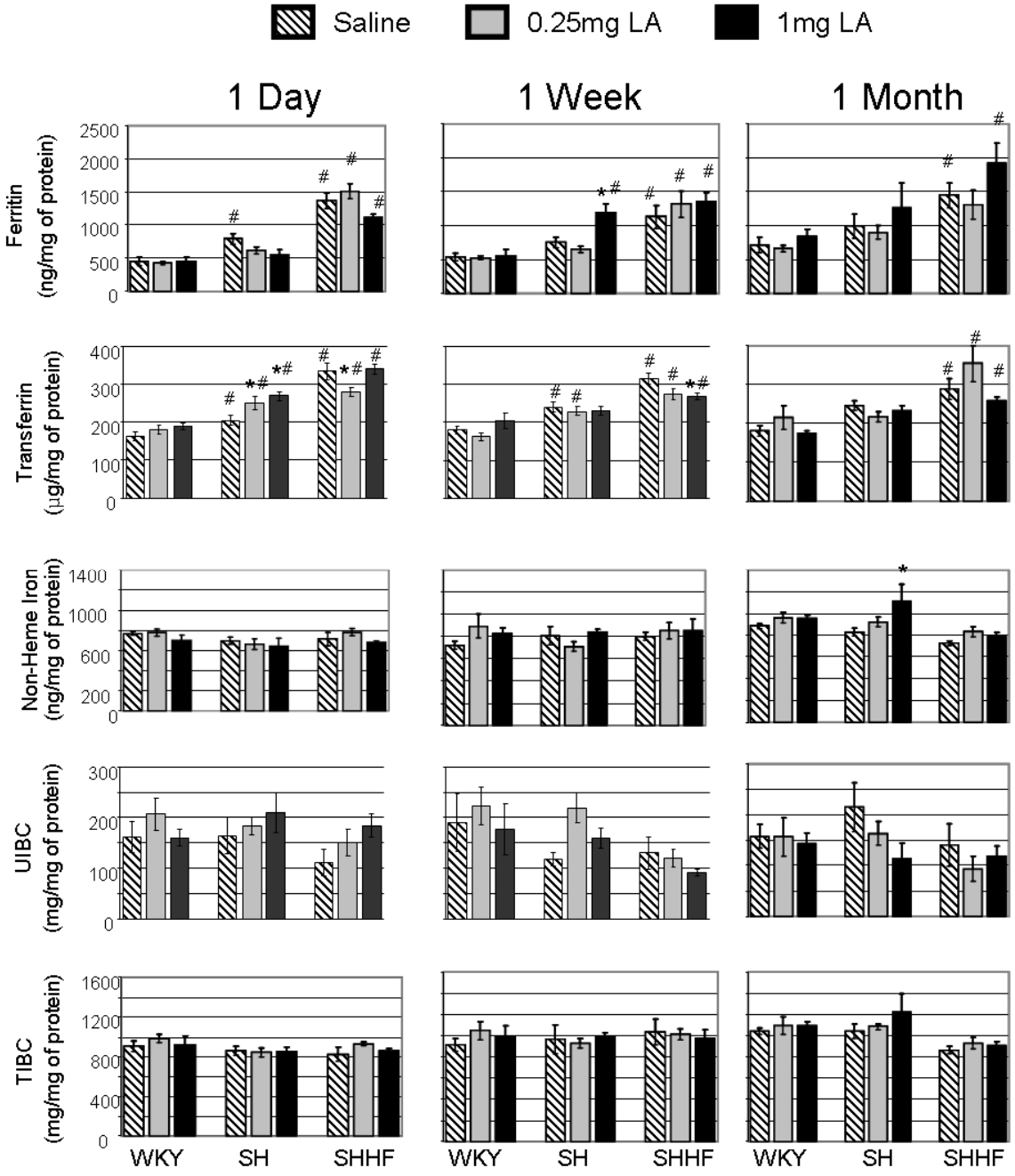

Figure 5.5. Temporal changes in ferritin and transferrin in the lung tissue of WKY, SH, and SHHF rats following single intratracheal instillation of saline (control), 0.25 mg LA, or 1 mg LA. (WKY, n =8-12/group; SH and SHHF, n = 6/group). * Indicates significant difference

within strain in respect to saline controls ($p<0.05$). # Indicates significant difference from WKY at the same exposure concentration ($p<0.05$).

Figure 5.6

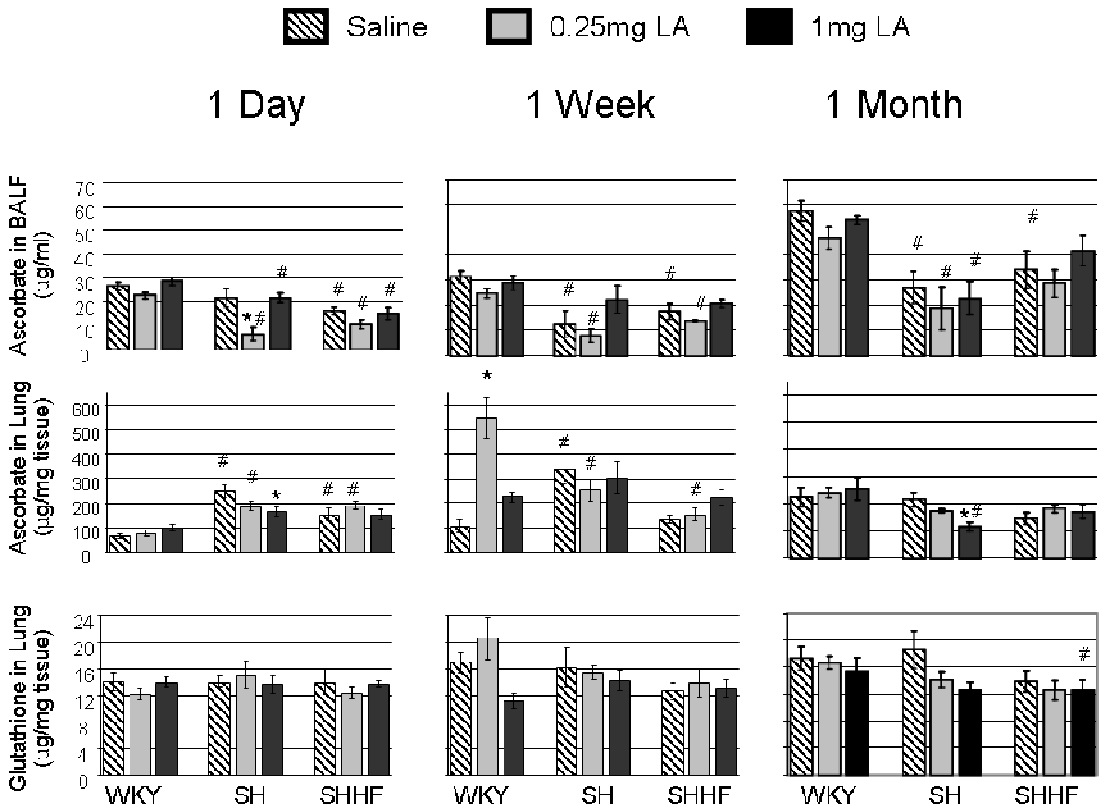

Figure 5.6. BALF and Lung tissue glutathione and ascrobate in WKY, SH, and SHHF rats exposed intratracheally to saline (control), 0.25 mg LA, or 1 mg LA. Values are mean ± S.E (WKY, n =8-12/group; SH and SHHF, n = 6/group). *Indicates significant difference within strain in respect to saline controls ($p<0.05$). # Indicates significant difference from WKY at the same exposure concentration ($p<0.05$).

Table 5.1. Histological evaluation showing the mean severity of lesions after exposure to LA in WKY, SH, and SHHF rats.

				Average Score of Pathology Severity (Number of Animals Affected by Exposure)				
Time Point	Rat Strain	LA Conc. (mg/rat)	Animals/ group	Neutrophils	Macrophages	Epithelial Hyperplasia	Interstitial Fibrosis	Granuloma Formation
1 Day	WKY	0.0	10	0.1 (1)	0.1 (1)	0.1 (1)	0.0	0.0
		0.25	10	0.5 (4)	0.7 (6)	0.2 (2)	0.0	0.0
		1.0	11	2.0 (10)	1.6 (10)	0.9 (9)	0.0	0.0
	SH	0.0	6	0.0	0.0	0.0	0.0	0.0
		0.25	6	1.0 (6)	1.0 (6)	1.0 (6)	0.0	0.0
		1.0	6	2.0 (6)	2.0 (6)	1.0 (6)	0.0	0.0
	SHHF	0.0	6	0.0	0.0	0.0	0.0	0.0
		0.25	6	1.0 (6)	1.0 (6)	0.0	0.0	0.0
		1.0	6	2.0 (6)	2.0 (6)	1.0 (6)	0.0	0.0
1 Week	WKY	0.0	11	0.0	0.0	0.0	0.0	0.0
		0.25	10	0.0	1.0 (10)	1.0 (10)	0.0	0.0
		1.0	11	1.0 (11)	2.0 (11)	2.0 (11)	1.0 (11)	0.0
	SH	0.0	6	0.2 (1)	0.2 (1)	0.2 (1)	0.0	0.0
		0.25	6	0.0	1.0 (6)	1.0 (6)	0.0	0.0
		1.0	6	1.0 (6)	2.0 (6)	2.0 (6)	1.0 (6)	0.0
	SHHF	0.0	6	0.0	0.0	0.0	0.0	0.0
		0.25	6	0.0	1.0 (6)	1.0 (6)	0.0	0.0
		1.0	6	1.0 (6)	2.0 (6)	2.0 (6)	1.0 (6)	0.0
1 Month	WKY	0.0	8	0.0	0.3 (2)	0.0	0.0	0.0
		0.25	8	0.0	1.0 (2)	0.0	0.0	0.0
		1.0	12	0.0	2.0 (12)	1.0 (12)	1.0 (11)	0.2 (2)
	SH	0.0	6	0.0	0.0	0.0	0.0	0.0
		0.25	6	0.0	1.0 (6)	0.0	0.0	0.0
		1.0	6	0.0	2.0 (6)	1.0 (6)	1.0 (6)	0.3 (2)
	SHHF	0.0	6	0.0	0.0	0.0	0.0	0.0
		0.25	6	0.0	0.0	0.0	0.0	0.0
		1.0	6	0.0	2.0 (6)	1.0 (6)	1.0 (6)	0.2 (1)

WKY, SH, and SHHF rats exposed to saline (control) or LA (0.25 or 1.0 mg/rat) were examined for pulmonary lesion types and the location. The number within bracket shows the number of rats that are affected per total number of rats examined per group. These lesions were classified to reflect alveolar infiltration of neutrophils and macrophages, alveolar epithelial hyperplasia, and interstitial fibrosis. Note that within the time points studied in the

present experiment, no pleural thickening, inflammation or fibrosis were noted. Lesions were graded on a scale of increasing severity from 1-4 and the mean severity of lesions reflect the average score per animal.

Figure 5.7

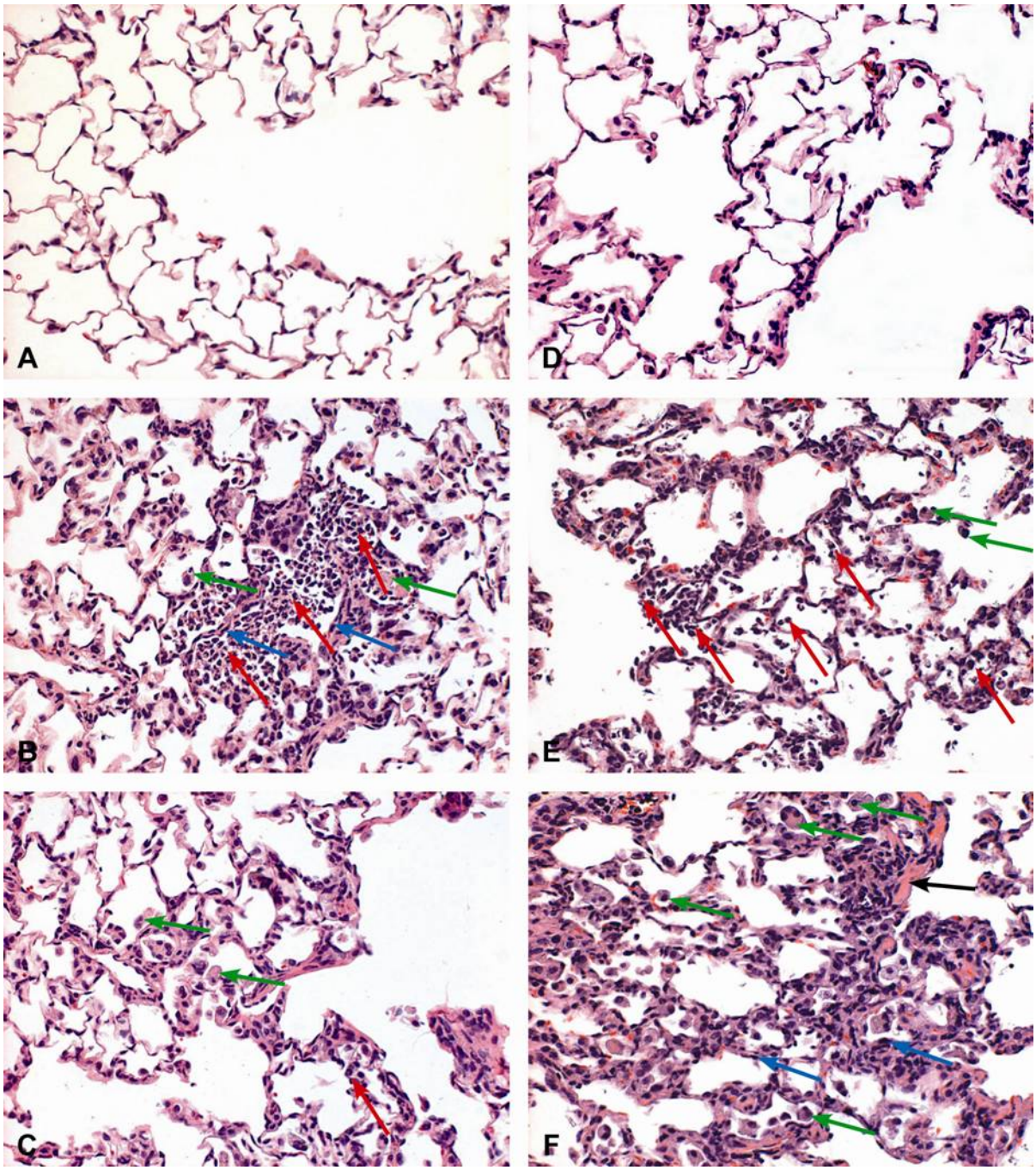

Figure 5.7. Time related histological alterations in the lung following a single intratracheal instillation of LA in WKY rats demonstrated after H & E staining. The photomicrographs for WKY rats 1 day and 1 month post-exposure to saline, 0.25, and 1.0 mg LA are shown. A and

D**:** Representative histological sections of lungs from WKY rats exposed to saline at 1 day and 1 month, respectively. B and E**:** Histological sections of lungs from WKY rats exposed to 0.25 mg LA at 1 day and 1 month, respectively. C and F**:** Histological sections of lungs from WKY rats exposed to 1.0 mg LA at 1 day and 1 month, respectively. Red arrows denote alveolar neutrophilic influx, green arrows show intra alveolar macrophage accumulation, blue arrows indicate alveolar hyperplasia, and black arrows interstitial fibrosis. All images are at X 20 magnification.

5.4 Discussion

The ROS generation and toxicity of asbestos fibers has been shown to be increased by surface-complexed Fe and also by binding of tissue-associated Fe (Kamp *et al*. 1995b, Governa *et al*. 1999, Gazzano *et al*. 2007b). In this study, we postulated that genetically-predisposed rat models with CVD-associated pulmonary Fe-overload would show greater pulmonary injury and inflammation following LA exposure when compared to healthy WKY rats due to increased availability of endogenous Fe to complex with LA. While initial inflammatory response to LA was only slightly exacerbated in SHHF, we found that there was a greater persistency of inflammation in SH and SHHF relative to WKY. This was associated with changes in Fe homeostasis biomarkers with a general increase in Fe binding proteins only in SH and SHHF rats suggesting that more readily available endogenous protein-complexed Fe might be released over time to bind LA fibers thus, causing persistency in inflammation. The formation of ferruginous-bodies over asbestos fibers is known to occur with persistent inflammation over a long period of time in humans (Ghio *et al*., 2003).

MIP-2, which is a major neutrophil chemotectic factor in rats (Smartt *et al*. 2010), has been shown to be increased in epithelial and mesothelial cells *in vitro,* and in the pleural lavage of F344 rats following asbestos exposure (Hill *et al*., 2003; Driscoll *et al*., 1998). WKY were able to mount an acute and largely reversible inflammatory response (neutrophilic influx) with the reversible induction of MIP-2 mRNA, which was associated with activation of alveolar macrophages (increased NAG activity in BALF). However, SH and SHHF, despite their initial robust neutrophilic inflammation at 1 day, did not transiently increase expression of MIP-2. Antioxidant deficiency in alveolar lining might result in earlier

MIP-2 induction in SH and SHHF rats. Ascorbate, a key antioxidant of airway lining and the first line of defense, was lower at baseline in SH and SHHF and not increased following LA exposure when compared to WKY. Early initial oxidant stress might have triggered MIP-2 expression prior to 1-day in SH and SHHF while it was delayed in WKY due to availability of sufficient ascorbate in the airway lining. Our subsequent studies have shown induction of MIP-2 at 4 hours in SH rats following LA exposure (Shannahan *et al*., 2011a).

Exposure to asbestos has been shown to cause acute pulmonary inflammation following intratracheal instillation and inhalation exposure in animals and has been postulated to contribute to chronic diseases (Dostert *et al*. 2008, Fattman *et al*. 2006). The predominance of neutrophilic inflammation acutely after LA exposure is expected based on the physicochemical nature of inhaled fibers as observed in earlier studies (Putnam *et al*. 2008, Dorger *et al*. 2002). In the present study however, the mechanisms mediating this inflammatory response was likely different between healthy and Fe-overloaded CVD models because only WKY transiently increased MIP-2 mRNA in response to LA exposure at 1 day while only SH and SHHF demonstrated changes in Fe regulatory proteins. The observation that neutrophilic influx was more persistent in SH and SHHF compared to WKY exposed to LA suggests that they may be more sensitive to developing chronic active inflammation associated with lung disease.

Biomarkers of Fe homeostasis were significantly elevated at baseline and also changed in response to LA in only in SH and SHHF relative to WKY. Specifically, the expression of FHC, which is considered important in sequestering Fe during acute inflammation/injury (Koorts and Viljoen 2007) was induced only acutely and only in SHHF rats in an LA concentration-dependent manner which was accompanied by increases in

BALF ferritin. FLC, which is known to be induced with chronic Fe-overload, was increased later in SH and SHHF at baseline consistent with its role in long-term baseline inflammation. However, unlike SH and WKY, the inability of SHHF to transcribe FLC in response to LA at 1 month when baseline expression is already very high, suggests that more severe Fe-overload might impair their ability to further increase ferritin which can lead to increases in the availability of catalytically active Fe and thus, might contribute to chronic inflammation and injury following LA exposure. Increases in BALF ferritin were associated with an increased non-heme Fe and Trf in SHHF at baseline and also following LA exposure. These data further support the hypothesis that increased mobility of endogenous Fe from its protein-bound form in rat models of CVD-associated Fe-overload and their inability to maintain normal Fe homeostasis likely contribute to persistent inflammation and exacerbated pulmonary disease.

Heme oxygenase-1 (HO-1) is an inducible enzyme which catabolizes heme into labile Fe, carbon monoxide, and biliverdin (Driscoll et al. 1998, Gozzelino, Jeney & Soares 2010). The labile Fe released from HO-1 induces ferritin production, which binds and stores Fe, thereby reducing oxidative stress and thus plays an important role in the antioxidant response to Fe-mediated ROS generation. The regulation of HO-1 as well as its other downstream effects lacks sufficient study. However, it is thought that induction of HO-1 may be biphasic, peaking rapidly initially after exposure and then again induced months after. In our study, only SH rats exposed to LA were able to induce HO-1 mRNA expression at 1 week which accompanied elevations in BALF and lung ferritin protein but not mRNA suggesting that transcriptional activation might have occurred in the course of 1 week. The increased baseline expression of HO-1 coincided with high baseline levels of ferritin protein and

mRNA in SHHF rats. Interestingly, SHHF, already high in baseline expression, showed an inhibition of HO-1 expression at 1 day due to LA exposure. Since mice lacking the ability to induce HO-1 are more susceptible to the cytotoxic effects of ROS and inflammation (Kapturczak *et al.* 2004, Poss, Tonegawa 1997), it is possible that the SHHF might be more vulnerable to injury and chronic exacerbation due to inhibition of HO-1 after LA exposure. However, acute transcriptional activation of FHC despite inhibition HO-1 due to LA exposure suggests a complex mechanism of regulating oxidative stress and Fe homeostasis in the SHHF. The availability of Fe in the CVD models may cause an inhibition of HO-1 transcription through poorly understood mecahanisms of negative feedback regulation.

Asbestos fibers are known to cause acute oxidative stress and inflammation which persists over time and contributes to chronic fibrosis, granuloma and lung cancer. We show the presence of inflammation at all times and fibrosis at 1 week and 1 month following a single dose of LA in all rat strains which leads to focal granuloma formation in few animals at 1 month. Although it is believed that environmentally relevant low-level exposures over a long period of time are not associated with lung inflammation, and fibrosis following asbestos exposure in humans, it has not been experimentally demonstrated. In animals, inflammation develops as soon as 3 days following inhalation of asbestos at occupationally-relevant concentrations (earliest determined) leading to pulmonary fibrosis over longer duration (Sabo-Attwood *et al*. 2005, Dostert *et al*. 2008). The persistence of inflammation as evidenced by increases in BALF cellularity and histological alterations suggests a persistent immune cell response, critical in chronic pulmonary disease, especially in rats with underlying Fe-overload.

There are limitations in generalizing the role of Fe-overload in LA-induced lung injury. The genetic rat models of CVD-associated Fe-overload may not exactly mimic the mechanisms of Fe-overload in humans. While intratracheal instillation allows us to precisely control the exposure dose, it will produce a one time bolus effect which may not be apparent with inhalation, where exposure continues with concurrent compensatory response. Because the fiber length in the LA mix used in this study is relatively shorter than other asbestos materials such as amosite and crocidolite, it is likely that the major portion of LA would have been phagocytosed by alveolar macrophages. Thus, the pattern of lung injury caused by LA could be very different from other fibers that are not phagocytosed. However, we have noted that, as in case of other fiber types, LA can bind exogenous Fe (Shannahan *et al*., 2011). Due to the difference in fiber characteristics, the kinetics of clearance of LA fibers might be different from other long fibers. The clearance of LA is also likely different in different rat models and can influence the degree of lung response.

Conclusions

In conclusion, SH and especially SHHF demonstrated changes at baseline in markers of Fe homeostasis, oxidative stress, and inflammation relative to WKY. Acute exposure to LA induced transient pulmonary inflammation and MIP-2 expression in WKY without increases in markers of Fe homeostasis (ferritin) and oxidative stress (HO-1). However, in SHHF, and to some extent in SH, LA exposure caused more persistent inflammation over 1 week and 1 month, which was associated with marked changes in biomarkers of iron homeostasis with a generalized increases in ferritin. These findings suggest the involvement of endogenous Fe metabolism in more persistent pulmonary inflammation seen in SH and SHHF, which may be critical in their susceptibility to chronic asbestos-related disease.

CHAPTER 6. SUB-CHRONIC PULMONARY PATHOLOGY, IRON-OVERLOAD AND TRANSCRIPTIONAL ACTIVITY AFTER LIBBY AMPHIBOLE EXPOSURE IN RAT MODELS OF CARDIOVASCULAR DISEASE

6.1 Introduction

Residents and miners in Libby, Montana were exposed to a mixture of amphibole type asbestos fibers containing winchite, richerite, tremolite, and other minerals in prismatic, acicular, and asbestiform morphologies during the town's extensive vermiculite mining (Sullivan, 2007, Meeker *et al.*, 2003, Whitehouse *et al.*, 2008, Moolgavkar *et al.*, 2010). Epidemiological studies have shown a dose-dependent correlation between Libby amphibole (LA) exposure and the incidences of asbestos-induced diseases such as asbestosis, lung cancer, and mesothelioma in this population (Sullivan, 2007, Moolgavkar *et al.*, 2010, Putnam *et al.*, 2008). Exposure to LA has also been associated with increased autoimmune disease in residents (Noonan *et al.*, 2006). These diseases are known to develop years to decades after exposure to asbestos and are possibly due to the bio-persistency of amphibole fibers within the lung causing prolonged inflammation and oxidative stress resulting in diverse pulmonary diseases based upon genetic differences (Bernstein *et al.*, 2003, Bernstein *et al.*, 2005).

Asbestos is able to produce reactive oxygen species (ROS) through Fenton reactions facilitated by surface available metals such as iron (Fe). Interestingly asbestos and silica can associate endogenous Fe after inhalation exposure forming Fe-rich asbestos bodies on the surface of the fibers (Ghio *et al.*, 2004). This Fe once bound to the surface of asbestos

maintains the capability to redox cycle enhancing the fiber's ability to produce ROS when incubated with the appropriate reducing equivalents (Ghio *et al.*, 2006). It has been postulated that this Fe once bound would enhance the ability of asbestos to produce ROS and thereby exacerbate toxicity (Gazzano *et al.*, 2007, Gazzano *et al.*, 2007, Ghio *et al.*, 1992, Hardy and Aust, 1995). Our previous studies have established that LA can bind Fe and that this Fe is redox active in an acellular environment (Shannahan et al. 2011a). However we also have demonstrated that Fe loading of LA inhibits the acute inflammatory response *in vitro* in cells and *in vivo* in rats. Furthermore by increasing the cellular catalytically active Fe pool *in vitro* the acute inflammatory response after LA exposure was also reduced. The role of Fe in the progression of the chronic diseases induced by LA and other asbestos materials however is unknown.

Increased tissue Fe-overload may increase bioactive and protein bound Fe levels and affect the inflammatory response necessary for compensatory mechanisms to be induced following an environmental insult. Individuals with chronic diseases such as thalassemia, diabetes, arthritis, cancer, and cardiovascular disease (CVD) have been shown to exist in a state of systemic Fe-overload (Abdalla *et al.*, 2011, Sen *et al.*, 2011, Allen, 2010, Toyokuni, 2011). Humans with CVD are known to exist in a state of systemic Fe-overload, inflammation, and oxidative stress (Kruszewski, 2004, Ellervik *et al.*, 2010), which may influence their susceptibility to asbestos-induced diseases. We have previously characterized the underlying pulmonary disease present in two accepted rat models of human CVD the spontaneously hypertensive (SH) rat and the spontaneously hypertensive heart failure (SHHF) rat (Shannahan *et al.*, 2010). We determined that both the SH and SHHF existed in

a state of pulmonary Fe-overload, inflammation and oxidative stress compared to control normotensive Wistar Kyoto (WKY).

Recently, we have shown that an acute exposure to LA in rat models of CVD-associated Fe-overload (SH and SHHF) resulted in the lack of exacerbation of inflammation despite increases in Fe binding proteins and their transcription (Shannahan et al., 2011b). Already high baseline inflammation together with dysregulated Fe homeostasis might diminish the acute inflammogenic response to additional insults. In this continuing study, we hypothesized that prolonged presence of LA in the lungs of SH and SHHF rats will cause further accumulation of fiber-associated Fe, and aberrant tissue repair leading to diversified pathological alterations. Furthermore we postulated that examining the transcriptional activity of the whole lung genome might allow additional insights into the role of Fe in the progression of lung disease in these models. Because CVD, diabetes and cancer are prevalent in humans and are associated with the highest mortality and global health burden, understanding the role of Fe-overload becomes significant in environmental exposures such as the one experienced by residents of Libby, Montana.

6.3 Materials and Methods

Libby Amphibole. The Libby amphibole (LA) sample was collected from the Rainy Creek Complex near Libby, Montana in 2007 by the United States Geological Survey and was processed to produce inhalable material by Meeker et al., as indicated earlier (Meeker *et al.*, 2003). The sample was further size fractionated by water elutriation as described previously (Webber *et al.*, 2008) in order to isolate a rat respirable fraction ($PM_{2.5}$) using a settling velocity of 3.4×10^{-4} cm s^{-1}.

Animals. Male, 11-12 week old, healthy WKY, and SH and obese SHHF rats were purchased from Charles River Laboratories, Raleigh, NC. All rats were maintained in an isolated animal room in an Association for Assessment and Accreditation of Laboratory Animal Care (AALAC) approved animal facility at 21 +/- 1°C, 50 +/- 5% relative humidity, and 12 h light/dark cycle. Rats were housed (2/cage) in polycarbonate cages containing beta chip bedding. Animals received standard (5001) Purina rat chow (Brentwood, MO) and water *ad libitum*. The U.S. EPA NHEERL Institutional Animal Care and Use Committee (IACUC) approved the protocol.

Intratracheal Instillation of Libby Amphibole. Since the rat respirable sample of LA was prepared using the water elutriation method, a uniform saline suspension of LA for intratracheal instillation was achieved by vortexing followed by water bath sonication for 15 min. The suspension was vortexed prior to each instillation to ensure that fibers did not settle at the bottom of the tube. In order to ensure the fibers did not interact with any biological molecules or chemical dispersants of the media prior to landing on the airway surface, we

decided not to use a biological dispersion media or any other chemicals for preparing the instillate. Rats (WKY n=12/time point; SH n=6/time point; SHHF n=6/time point) were anesthetized with isoflurane and intratracheally instilled with 300 μl saline containing either 0.0, 0.25, or 1.0 mg of LA as described previously (Wallenborn *et al.*, 2009). The concentrations selected although high were, in general, consistent with instillation studies using other fiber types (Adamson and Bakowska, 2001, Hirano *et al.*, 1988). Doses were chosen to assure a response in the lung upon instillation allowing for a comparative analysis between strains. Theoretically, a rat will deposit 0.07 mg of fibers during 6 hour inhalation at $10mg/m^3$ based on the assumption that minute volume is 200ml and the deposition fraction to pulmonary region is 0.10. Intratracheal instillation ensured the delivery of exact concentrations of LA into the lung and allowed us to control for likely strain-related deposition differences due to their variation in breathing parameters (Shannahan *et al.*, 2010). In our previous study approximately 30% of WKY presented with non-pathogenic cardiac hypertrophy (Shannahan *et al.*, 2010). Therefore WKY group size was increased (n=12) to eliminate the data from those with hypertrophic hearts (heart weight > 1.3g; normal heart weight ~1g) and still maintain appropriate group sizes for statistical comparisons.

Necropsy, Sample Collection, and Analysis. Rats were weighed and anesthetized with an overdose of sodium pentobarbital (Virbac AH, Inc., Fort Worth, TX; 50-100 mg/kg, ip) 1 day, 1 week, 1 month, or 3 months following instillation of LA. Blood was collected through the abdominal aorta into blood collection tubes, which were used for a different study. Blood was then removed from the vasculature of the lung by perfusion of Ca^{2+}/Mg^{2+} free phosphate

buffered saline (PBS) via the pulmonary artery to avoid interference in data analysis involving Fe-binding proteins and capacities.

The trachea was then cannulated and the left lung lobe tied off. The right lung lobes were lavaged with Ca^{2+}/Mg^{2+} free PBS (pH 7.4, at 37°C) equal to 35 ml/kg body weight (representing total lung capacity) x 0.6 (right lung capacity being 60% of total lung capacity). The lavage volume for SHHF despite their increased body weight was kept same as the mean volume of WKY rats based on the assumption that the lung growth will remain similar at a given age in both strains despite the obesity-induced increase in body mass of SHHF rats. The lung lobes were lavaged three times with the same PBS aliquot. The right lung lobes were then removed, placed in liquid nitrogen, and stored at -80°C for later analysis. The left lung was fixed at 40% of its total capacity by instillation of 10% neutral buffered formalin through the trachea and stored in 10% formalin at 4°C until processed for histopathology.

Cell Differential and Bronchoalveolar Lavage Fluid (BALF) Analysis. Aliquots of BALF were taken for total cell counts (Coulter Inc., Miami, FL, USA), cell differentials, and analyses of lung injury markers. Cell differentials were conducted by Cytospin preparation (Shandon, Pittsburgh, PA), and slides were stained with LeukoStat (Fisher Scientific Co., Pittsburgh, PA). Macrophages and neutrophils were counted under light microscopy and quantified based on total cell count. The remaining cell free BALF was evaluated for the following: total protein (Coomassie plus Protein Assay Kit, Pierce, Rockford, IL), albumin (DiaSorin, Stillwater, MN), and the Fe-binding proteins, ferritin (Kamiya Biomedical Company, Seattle, WA) and transferrin (Trf) (DiaSorin, Stillwater, MN). All assays were

adapted for BALF analysis and ran using the Konelab Arena 30 clinical analyzer (Thermo Chemical Lab Systems, Espoo Finland). Data were normalized to volume of BALF.

Statistical Analysis of BALF Data. Data are expressed as mean ± S.E. (WKY, n = 8-12/ treatment group; SH, n = 6/ treatment group; SHHF, n = 6/ treatment group). Sigma Stat version 3.5 (Systat Software, Inc., Point Richmond, C.A.) was used to determine statistical comparisons via a two-way analysis of variance with strain and exposure as factors followed by a post-hoc comparison using the Holm-Sidak method. Statistical significance was determined when p was found to be less than or equal to 0.05 between treatment groups and strains.

Lung Histopathology. The right lung lobe from each animal was trimmed, embedded in paraffin, sectioned to a thickness of approximately 3 microns (transverse), and stained with hematoxylin and eosin (H&E), Perls Prussian blue, or Masson's trichrome. The lung lesions were evaluated with particular attention to the lesion location (i.e, bronchi, terminal bronchi, alveolar duct, alveoli, interstiteum, centriacinar regions, pleura). The morphological evaluation took into consideration the characteristics of each inflammatory cellular component, i.e., polymorphonuclear cells, macrophages, fibrosis, microgranulomas, as well as changes in the alveolar epithelium. Lesions were also evaluated for Perls Prussian blue staining for ferric Fe content and Masson's Trichrome for collagen in order to understand modulation of pulmonary Fe content and progression of fibrosis. Histopathological changes were scored using semiquantitative grading at five levels (0 = normal; 1 = minimal; 2 = mild; 3 = moderate; 4 = severe) taking into consideration the degree of severity and the type of

lesion (Shackelford *et al.*, 2002), (Nyska *et al.*, 2005). In order to verify pathological changes and possible chronic progression of lesion development after LA exposure the study was repeated in 36 SHHF rats examining lung pathology 3 months and 6 months post-exposure. SHHF rats were instilled with saline containing 0.0, 0.25, or 1.0 mg of LA and necropsies were performed 3 or 6 months later for detailed pathological evaluation. This additional study substantiated the findings of the 3 month study and demonstrated the presence but not progression of fibrotic and proliferative lesions after LA exposure (Data not shown).

Immunohistochemistry. Due to the presence of focal hyperplasic changes in SHHF rats, 5-micron lung sections were cut from parrifin embedded lung blocks from these rats exposed to 0.0, 0.25 and 0.5 mg LA and were were immunohistochemically stained for epithelial cell markers in order to determine the origin of the hyperplastic changes within LA-induced lung lesions. The hydrated lung sections were first incubated with 3% hydrogen peroxide to block endogenous peroxidase. These sections were blocked with the appropriate blocking reagents and then incubated with primary antibodies specific for Surfactant Protein-A (sc-7699), Clara Cell Protein-10 (sc-9772), and the Cytokeratins 10 (sc-58720), and 14 (sc-53253) Santa Cruz Biotechnology Inc., Santa Cruz CA.), and Cytokeratin 19 (CRC946) (Cell Marque Corporation, Rocklin, CA). Biotinylated secondary antibodies were used with peroxidase-conjugated streptavidin to detect cellular localization of proteins of interest. Positive control slides using known reactive tissues and negative control slides in which the primary antibody was omitted were also prepared. A board certified pathologist then evaluated the slides.

Gene Array. Total RNA was isolated from caudal lung lobes frozen in liquid nitrogen using RNeasy mini kit (Qiagen, Valencia, CA). RNA integrity was assessed by the RNA 6000 LabChip® kit using a 2100 Bioanalyzer (Agilent Technologies, Palo Alto, CA). We examined global gene expression changes in rat lung tissue using the Affymetrix platform (Rat Genome 230 2.0 Array). Gene expression changes were assessed after exposure to LA (1.0 mg/rat & 0.0 mg/rat) at 3 months post-exposure in each strain.

There were 6 samples per group and gene expression in each sample was assayed on separate chips. Biotin-labeled cRNA was produced from 15 μg total RNA using an Affymetrix "IVT-express labeling kit (cat# 901228). Total cRNA was then quantified using a Nano-Drop ND-1000 spectrophotometer (NanoDrop Technologies, Wilmington, DE) and evaluated for quality after fragmentation on a 2100 Bioanalyzer. Following overnight hybridization at 45^{o}C to Affymetrix 430_2 GeneChips in an Affymetrix Model 640 GeneChip hybridization oven, the arrays were washed and stained using an Affymetrix 450 fluidics station as recommended by the manufacturer and scanned on an Affymetrix Model 3000 (7G) scanner. After scanning, raw data (Affymetrix .cel files) were obtained using Affymetrix Command Console Operating Software (version 3.0). This software also provided summary reports by which array QA metrics were evaluated including average background, average signal, and 3'/5' expression ratios for spike-in controls, β-actin, and GAPDH.

Gene Array Data Analysis. The resulting CEL files were loaded into Rosetta Resolver and normalized with the Rosetta error-model. Differentially expressed probesets were determined within Rosetta Resolver using a one-way ANOVA with a Benjamini-Hochberg

multiple test correction (false discovery rate set at 0.05). Each of the five treatments (including SHR saline and SHHF saline) was contrasted to WKY- saline as the control. The resulting five lists of DEGs were combined to generate a master list. Venn diagrams were generated from this master list of DEGs for LA induced changes relative to each strain's control using Rosetta Resolver.

Functional Analysis. For a global assessment of impacted Kyoto Encyclopedia of Genes and Genomes (KEGG) pathways, the master list was submitted to the Database for Annotation, Visualization and Integrated Discovery (DAVID) (Huang da *et al.*, 2009) for analysis. P-values from this analysis were used to generate a heatmap of KEGG pathways.

All genes were filtered to meet the criteria of intensity greater than or equal to 30 and had a fold change greater than 1.5 or less than or equal to -1.5. Functional lists of genes were constructed from KEGG pathway genes: inflammation, and cell cycle control. Inflammation genes were assembled from KEGG pathways: 4060, 4062, 4070, 4310, 4510, 4514, 4520, 4620, 4621, and 4670. Cell cycle control genes were assembled from KEGG pathways: 4115, 5200, 5215, 5217, 5222, and 5223. For each of the functional lists, genes that were on the pathway-specific list and on the master list were submitted to Eisen's Cluster (Eisen *et al.*, 1998) for hierarchical clustering. The genes were median centered with average linkage. The resulting cluster was displayed using Treeview (Eisen *et al.*, 1998). Two other functional lists, growth and fibrosis, were obtained from NetAffx (http://www.affymetrix.com/estore/analysis/index.affx). The lists were combined and the genes that were on both the growth and fibrosis and were clustered with Eisen's Cluster and displayed with Treeview.

6.3 Results

6.3.1 Libby Amphibole Characterization

Fiber characterization parameters were recently published (Shannahan et al. 2011b). In brief, based on transmission electron microscopy, fiber dimensions, of the elutriated LA 2007 sample were: mean length 4.99μm ± 4.53 and width 0.28μm ± 0.19; median length = 3.59μm, width = 0.23μm with upper and lower values of length being 0.52μm – 27.30μm and width 0.07μm – 1.15μm. The estimated fiber count for 1 mg LA sample was 218 x 10^6. In comparison to the elutriated LA 2007 sample used in the present study air samples from Libby Montana have been shown to contain fibers having a mean length of 7.64μm ± 8.40 and width 0.51μm ± 0.46, and median length 5.2μm and width 0.39μm with upper and lower values of length being 0.5μm – 195μm and width 0.01μm – 10μm; and an aspect ratio of ≥ 5 (U.S. EPA 2010). The median fiber length being smaller than the mean length suggests that a larger proportion of fibers are likely smaller than the mean length. Transmission Electron Microscopy of LA obtained from the 2000 sample similar to one used in the present study showed that 97.8% (135/138) of elutriated fibers had aspect ratios ≥ 5 (Meeker *et al.*, 2003, Webber *et al.*, 2008), Lowers and Bern, 2009).

6.3.2 Pulmonary Inflammation, and Injury as Determined using BALF

In order to quantify inflammation and injury response following LA exposure, BALF samples were analyzed for various biomarkers. It was anticipated that some of the BALF cell parameters might not actually reflect the long-term inflammatory changes in the lung and

therefore, extensive pathological analysis was done (see below) for all three strains. Baseline levels (saline control) of BALF protein and albumin were significantly higher in SH and SHHF when compared to WKY (SHHF>SH>WKY) (Figure 6.1), based on our previous study (Shannahan *et al.*, 2010). Only SHHF exposed to 1 mg LA demonstrated elevated BALF protein at 3 months, however, because of the variable and high levels at baseline, it was difficult to ascertain if this increase was related to LA exposure. The recovery of alveolar macrophages in BALF was unchanged after LA exposure in all strains despite increased cellularity and presence of fiber-laden macrophages. As seen at earlier time points, neutrophils were significantly increased at baseline in SHHF compared to SH and WKY while LA-induced increases in neutrophils were noted during1day through 1 month (Shannahan et al., 2011) time points and were largely reversed by the 3 months in all strains. Baseline levels (saline control) of BALF ferritin and transferrin were significantly higher in SHHF when compared to WKY (SHHF>SH>WKY) (Figure 6.1) suggesting an underlying state of CVD associated Fe-overload. However, at 3 months after LA exposure the increases noted during earlier time points (Shannahan et al., 2010) were largely reversed.

6.3.3 Histological Evaluation for H&E, Collagen, and Ferric Fe Staining

Histological analysis of H&E stained lung tissue sections for the 1 day, 1 week and 1 month time points have been recently reported (Shannahan et al., 2011b). In this paper we examined pathological lesions from 3 month H&E slides and also performed trichrome staining for collagen and Perls blue staining for ferric Fe from lung tissue sections obtained at 1 week, 1 month and 3 month time points to understand the time course of the development of fibrosis and accumulation of ferric Fe in all three strains. All strains demonstrated interstitial fibrosis after exposure to LA shown by trichrome staining for

collagen (Table 6.1 and Figure 6.2). More intense fibrotic foci were apparent in terminal bronchiolar areas where fibers likely accumulate. Pathology scoring of the staining intensity showed concentration- and time-related increases over 1 week to 3 month time points suggesting progression of fibrotic lesions. However, no strain-related differences could be ascertained from comparative analysis of trichrome staining. Control WKY and SH did not stain for ferric Fe while a few spontaneous alveolar macrophages stained positive in SHHF (Table 6.1). No discernible changes in Perls blue staining were apparent between control and exposed rats at 1 week time point. At 3 months only a few macrophages stained positive for ferric Fe in WKY and SH rats exposed to high concentration of LA. However, the SHHF had a greatly exacerbated number macrophages stain positive for Fe compared to WKY and SH (SHHF>SH>WKY) (Table 6.1 and Figure 6.2). These Fe positive macrophages could be noticed around the lesion areas. Interestingly alveolar macrophages appeared to internalize LA at 1 week post-exposure and fibers remained visible in macrophages 3 months post-exposure (Figure 6.2).

6.3.4 Immunohistochemical Evaluation

One important observation made in 3 month H&E stained slides of SHHF was the presence of atypical hyperplastic lesions (Figure 6.3). These hyperplastic lesions were only present in LA-exposed SHHF rats and were highly focal. These lesions appeared to be dose dependent (saline 0/0 lesion incidence; 0.25 mg LA 2/6 lesion incidence; 1 mg LA 4/6 lesion incidence). The lesions were located at or near terminal bronchioles and consisted of atypical stacking of cells with the appearance of interstitial cellular aggregation. The experiment was repeated for verification by additional 5 step sections from each animal. In order to determine the cellular origin of these hyperplastic cells and determine the possible

presence of squamation, several cytokeratin and epithelial cell markers were examined immunohistochemically. These lesions were negative for the squamous epithelial markers cytokeratin 10 and 14 (Figure 6.3). Lesions however stained positive for 1) the bronchiolar epithelial cell markers, cytokeratin 19, a clara cell and 2) the alveolar type II cell marker surfactant protein A, and 3) the clara cell specific marker, clara cell 10 (Figure 6.3). Based on the evaluation of these markers we designated these atypical hyperplastic lesions to be of bronchiolar epithelial cell origin. To determine the further progression of hyperplastic changes over time additional animals instilled at the same dose levels were held out to 3 and 6 months post-exposure to LA. This experiment verified the presence of atypical hyperplastic lesions in SHHF at 3 months. At 6 months post-exposure to LA atypical hyperplastic lesions were present but did not progress in severity from what was observed at 3 months (Data not shown). Unlike the 3 month time point, one focal spontaneous lesion showing typical hyperplastic epithelium was found in a control SHHF at 6 months, however LA exposed SHHF demonstrated a clear increase in the incidences of hyperplastic lesions that were atypical.

6.3.5 Gene Expression Analysis

We compared the gene expression profiles in all strains exposed to 1.0 mg of LA compared to controls in order to determine genes and pathways that still remained altered at 3 months post-exposure to LA. We presumed that a snapshot of expression analysis later in the course of lung injury but prior to progression of lung disease might allow us to identify signature patterns that will provide insight into the relationship between acute injury and chronic asbestos-related disease. Further we anticipated that this would allow determination of potential mechanistic differences between healthy and cardiovascular compromised Fe-

overload animals. Baseline strain differences were remarkable and primarily involved genes related to immune regulation, inflammation and disease condition. Surprisingly, a large number of genes were still differentially expressed at 3 months especially in WKY and SH rats after a single intratracheal instillation of LA when compared to saline controls; however major strain differences were noted. It was apparent from the Venn diagram of LA-induced changes in each strain that WKY and SH had thousands genes changed due to LA at 3 month while SHHF showed minimum changes (only 180 genes significantly altered after LA exposure) (Figure 6.4). The Venn diagram demonstrated only 15 genes that were modified in common between all three strains in response to LA exposure at 3 months (Figure 6.4). The SH rats demonstrated the highest number total of genes changed after LA exposure (SH>WKY>SHHF) with more down regulated compared to the WKY and SHHF (Figure 6.4).

In order to understand relative strain differences and LA effect in parallel, we compared the mean expression values of WKY-saline control to the mean expression values of WKY-LA, SH-saline, SH-LA, SHHF-saline, SHHF-LA and determined relative fold differences. Although with marked intensity differences, most of the baseline gene changes seen in SH and SHHF relative to WKY are in the same direction (up or down) as those seen in WKY after LA exposure. It is difficult to ascertain specific mechanistic insight from this, however one can speculate that LA exposure over a long period of time in WKY is associated with an effect on the trancriptome activity of the lung likely reflective of underlying pathology at baseline in SH and SHHF. Based on the list of DEGs for each contrast, the pathways significantly altered due to baseline strain differences or LA exposure are depicted in the heat map shown in Figure 6.5. The green and black colors show no effect

while the red color show pathways with genes significantly altered. The review of KEGG pathways identified processes involving lipid and steroid metabolism, glycolysis, inflammation, leukocyte migration, cell cycle control, oxidative phosphorylation, diabetes and many more to be altered due to baseline strain differences and after LA exposure (Figure 6.5). The glutathione metabolism pathway was significantly changed only in WKY exposed to LA. Similarly, only WKY exposed to LA demonstrated an effect on pathways related to oxidative phosphorylation and tumor suppression signaling (Figure 6.5). SH rats exposed to LA demonstrated an effect on pathways assigned to cancer after exposure while SHHF had this pathway affected significantly at baseline as well as after LA exposure (Figure 6.5). SHHF exposed to LA also had other pathways related to cell proliferation altered including basal cell carcinoma while the p53 signaling pathway was affected only in WKY (Figure 6.5).

Cluster analysis of DEGs that changed in the same direction in all three strains with LA exposure and those that did not, revealed insights into specific genes within processes that were still affected by LA exposure and how each strain responded differently. Hierarchical clustering of genes identified within selected KEGG pathways was performed to understand the strain-related directional changes in gene expression belonging to specific processes. As indicated in Figure 6.6, many genes related to inflammation were induced markedly at baseline in SH and to some degree in SHHF relative to WKY. The expression levels of the same genes were increased more readily after LA exposure in WKY, and to a lesser extent in SHHF but had a tendency to be inhibited in SH. (Figure 6.6, cluster 1). Notable examples of genes within this cluster included NfκB, tumor necrosis factor, and a variety of interleukins. Figure 6.6, cluster 2 shows genes that are expressed at high levels in

WKY at baseline relative to baseline expression in SH and SHHF. These genes remained unchanged in WKY but tended to be inhibited from their already low baseline in SH and SHHF after LA exposure (Figure 6.6). Many of these genes involved chemokines such as Cxcl-14, and CCl-5, suggesting that some genes that regulate inflammatory response to LA tended to be inhibited in SH and SHHF but not WKY. A third cluster within Figure 6.6, cluster 3 contained genes involved in neutrophil chemotaxis that are expressed at high levels in SH and SHHF at baseline compared to WKY (Figure 6.6). Since this analysis was done at 3-months post-exposure, this data together with the return of neutrophils to baseline in all respective strains suggests that no active neutrophilic influx is occurring in the lung at this time and that baseline neutrophil inflammation associated with underlying CVD is still persisting in SH and SHHF.

The other differential expression pattern that was apparent from the clustering involved cell cycle control genes. We noted remarkable strain difference at baseline and following LA exposure in the expression of genes involved in cell cycle control (Figure 6.7). Genes expressed at high levels in the lungs of SH and SHHF at baseline including matrix metalloproteinase-9 and some oncogenes are separated in cluster 1 of Figure 6.7. These genes in cluster 1 seem to be induced in WKY after LA but are inhibited in SH and SHHF rats (Figure 6.7). A few cell cycle control and growth arrest genes are expressed at lower levels at baseline in SH and SHHF when compared to WKY-saline (Figure 6.7, cluster 2). These genes in cluster 2 are inhibited only in SH and SHHF after LA exposure while remaining unchanged in WKY (Figure 6.7). Figure 6.7, cluster 3 includes genes such as tumor suppressor genes and growth receptors that are induced only in WKY 3 months following LA exposure (Figure 6.7).

Since the process of fibrosis has been shown to progressively occur after asbestos exposure, we postulated that this process would still be active at 3 months post-exposure to LA based on the persistency of amohibole-type fibers in the lung. We thus examined differentially expressed genes in order to gain further insight into fibrotic and proliferative changes seen after LA exposure. There were strain related differences in expression of genes involved in cell growth and fibrosis at baseline and in response to LA exposure. Figure 6.8, cluster 1 identifies genes that are expressed at high levels in WKY and SH at baseline (WKY>SH) and are reduced in SH following LA exposure. These genes include transforming growth factor-α, and endoglin, a receptor involved in transforming growth factor signaling (Figure 6.8). Figure 6.8, cluster 2 shows genes that are expressed at high levels at baseline in SH and are induced in WKY but inhibited in SH following LA exposure. These genes include platelet derived growth factor receptor-α, pim-1 an inflammatory cytokine, and TIMP-1 an inhibitor of matrix metalloproteinases (Figure 6.8). Figure 6.8, cluster 3 contains genes that are induced primarily in WKY and SHHF following exposure to LA. Genes in this cluster include inducible transforming growth factor-β, and cytochrome B-245 β otherwise known as NOX-2 (Figure 6.8).

Figure 6.1

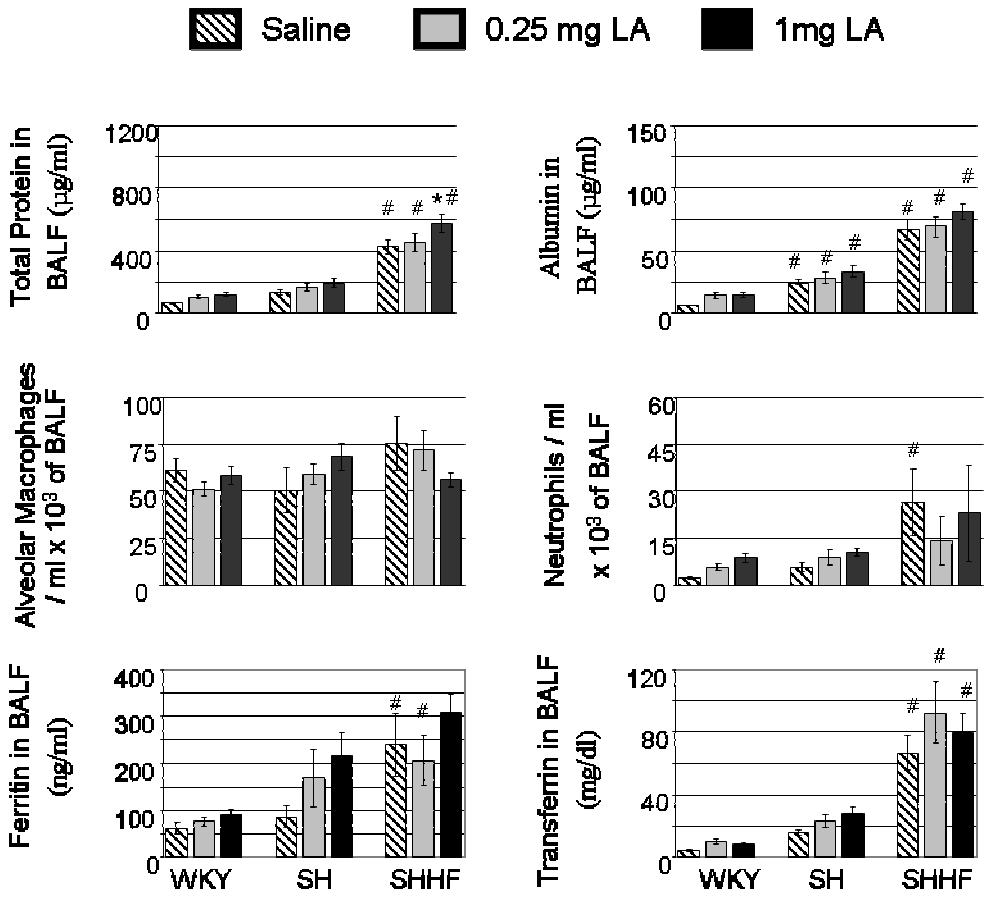

Figure 6.1. Alterations in BALF protein, albumin, macrophages, neutrophils, ferritin, and transferrin in WKY, SH and SHHF rats following intratracheal instillation of saline (control), 0.25 mg LA, or 1 mg LA. Values are mean ± SE (WKY, n =8-12/group; SH and SHHF, n = 6/group). * Indicates significant difference within strain in respect to saline controls ($p<0.05$). # Indicates significant difference from WKY at the same exposure concentration ($p<0.05$).

Table 6.1 Histological evaluation showing the staining of lesions for ferric Fe and collagen after exposure to LA in WKY, SH, and SHHF rats.

				Average Score (Number of Animals Affected by Exposure)	
Time Point	Rat Strain	LA Concentration (mg/rat)	Animals/ group	Perls Blue Staining for Ferric Iron	Trichrome Staining for Collagen
1 Week	WKY	0.0	5	0.0	0.0
		0.25	6	0.0	1.0 (6)
		1.0	6	0.3 (2)	1.0 (6)
	SH	0.0	6	0.0	0.2 (1)
		0.25	6	0.0	1.0 (6)
		1.0	6	0.3 (2)	1.0 (6)
	SHHF	0.0	6	0.0	0.0
		0.25	6	0.8 (4)	1.0 (6)
		1.0	6	0.8 (4)	1.2 (6)
1 Month	WKY	0.0	5	0.0	0.0
		0.25	5	0.0	1.0 (5)
		1.0	5	0.0	0.8 (4)
	SH	0.0	6	0.0	0.0
		0.25	6	0.0	0.8 (5)
		1.0	5	1.0 (4)	1.0 (6)
	SHHF	0.0	6	0.3 (2)	0.0
		0.25	6	1.5 (6)	1.0 (6)
		1.0	6	1.7 (6)	1.2 (6)
3 Month	WKY	0.0	5	0.0	0.0
		0.25	6	0.0	1.0 (6)
		1.0	5	0.4 (2)	1.7 (5)
	SH	0.0	6	0.0	0.0
		0.25	6	0.5 (2)	0.8 (5)
		1.0	6	0.8 (3)	1.5 (6)
	SHHF	0.0	6	0.3 (2)	0.0
		0.25	5	0.6 (2)	0.8 (5)
		1.0	6	1.7 (6)	2.0 (6)

WKY, SH, and SHHF rats exposed to saline (control) or LA (0.25 or 1.0 mg/rat) were examined for pulmonary collagen deposition and ferric iron (Fe) accumulation using Masson's trichrome and Perls Blue staining respectively. The number within bracket shows the number of rats that are affected per total number of rats examined per group. Collagen

deposition and ferric Fe accumulation were graded on a scale of increasing severity from 1-4 and the mean severity of lesions reflect the average score per animal.

Figure 6.2

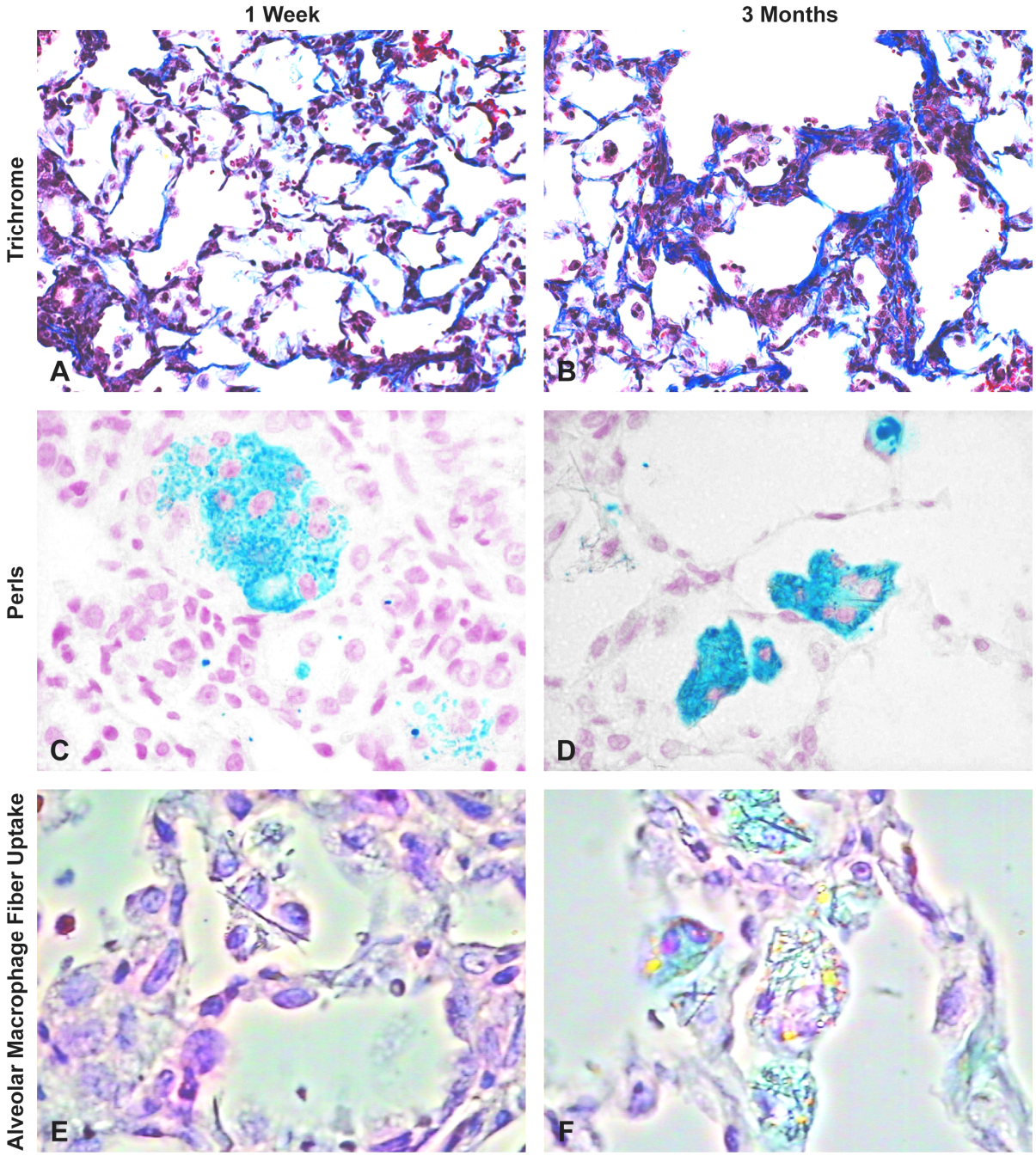

Figure 6.2. Time-related collagen deposition, ferric iron (Fe) alterations and alveolar macrophage fiber uptake in the lung following a single intratracheal instillation of LA in SHHF rats. The photomicrographs of lung tissue sections of SHHF rats 1 week, 1 month, and

3 months post-exposure to 1.0 mg LA are shown. A and B: Representative sections of lung stained for collagen using Masson's Trichrome stain from SHHF rats exposed to 1.0 mg LA at 1 week, and 3 months, respectively. Images are at X 20 magnification. C and D: Representative sections of lung stained for ferric Fe using Perls Blue stain from SHHF rats exposed to 1.0 mg LA at 1 week, and 3 months, respectively. Images are at X 60 magnification. E and F: Representative sections of lung using phase contrast microscopy to focus on alveolar macrophage uptake of LA in SHHF rat exposed to 1.0 mg LA at 1 week and 3 months, respectively. Images are at X 40.

Figure 6.3

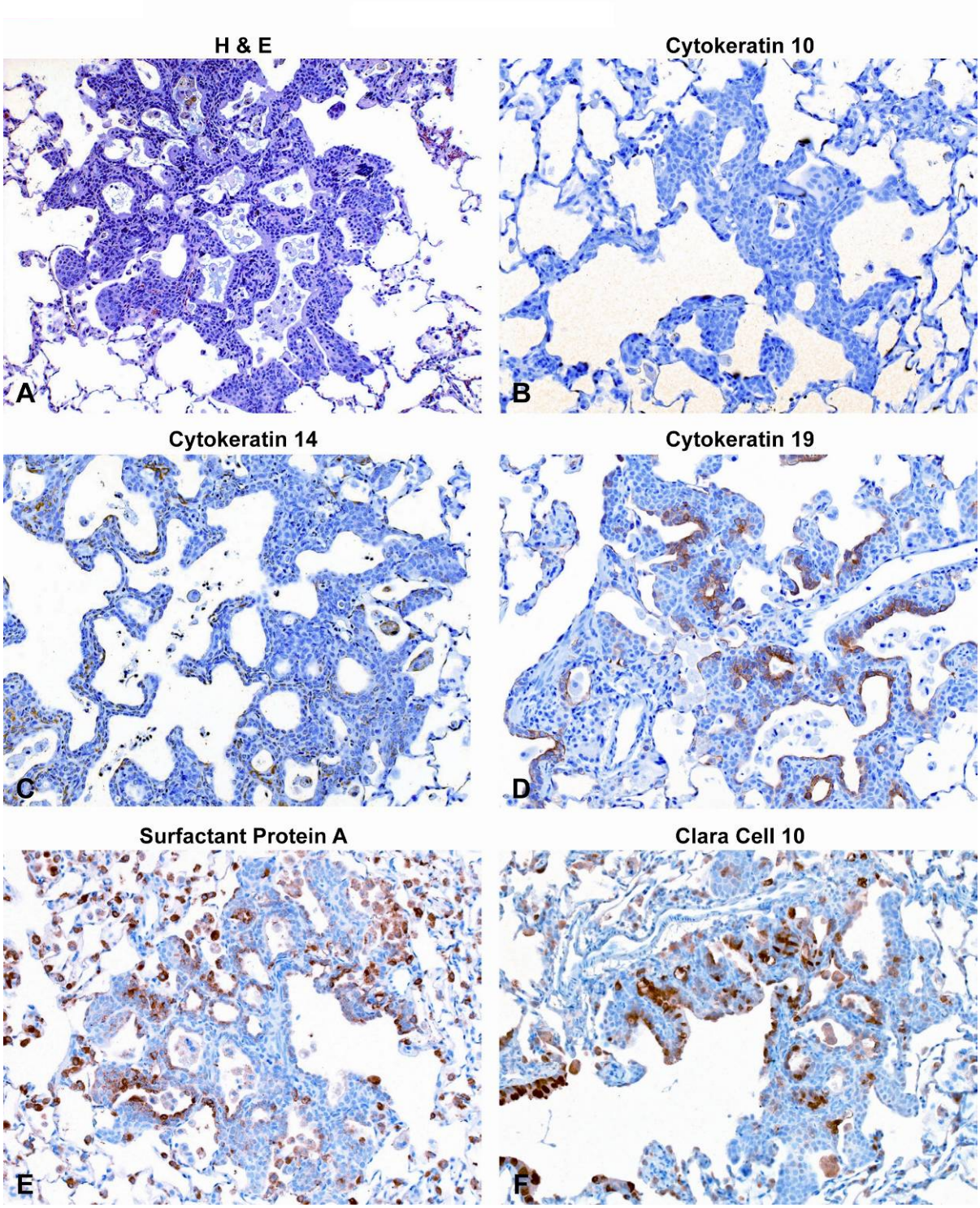
H & E
A
Cytokeratin 10
B
Cytokeratin 14
C
Cytokeratin 19
D
Surfactant Protein A
E
Clara Cell 10
F

Figure 6.3. Immunohistochemical characterization of atypical hyperplastic lesions in SHHF at 3 months after a single instillation of 1.0 mg LA. A: Representative image of H & E stained lung section from SHHF exposed to 1.0 mg LA 3 month post-exposure demonstrating the presence of an atypical hyperplastic lesion. B and C: Lung sections immunohistochemically stained for the squamous cell markers cytokeratins 10 and 14 respectively from SHHF exposed to 1.0 mg LA 3 months post-exposure. D: Lung sections immunohistochemically stained for the bronchiolar cell marker cytokeratins 19 from SHHF exposed to 1.0 mg LA 3 months post-exposure. E: Lung sections immunohistochemically stained for surfactant protein-A, a marker of alveolar type II and clara cells from SHHF exposed to 1.0 mg LA 3 months post-exposure. F: Lung sections immunohistochemically stained for the clara cell marker, clara cell 10 from SHHF exposed to 1.0 mg LA 3 months post-exposure. All images are at X 20 magnification.

Figure 6.4

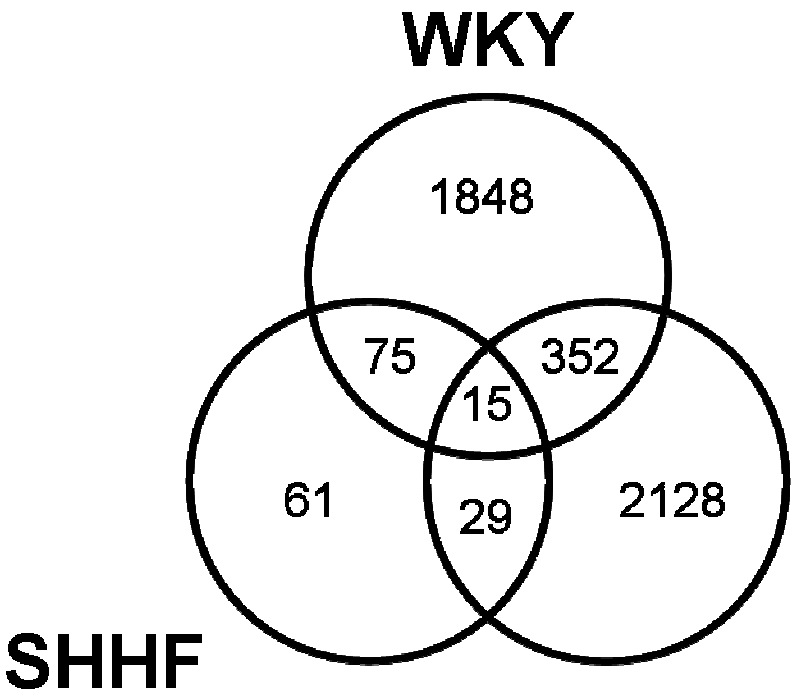

Strain	Total Genes	Up-Regulated	Down-Regulated
WKY	2290	89%	11%
SH	2524	42%	58%
SHHF	180	72%	28%

Figure 6.4. A Venn diagram of differentially expressed genes (DEGs) comparing WKY, SH, and SHHF rats 3 months following intratracheal instillation exposure to 1.0 mg LA compared to strain matched saline controls. The table shows the direction of changes in differentially expressed genes for each strain.

Figure 6.5

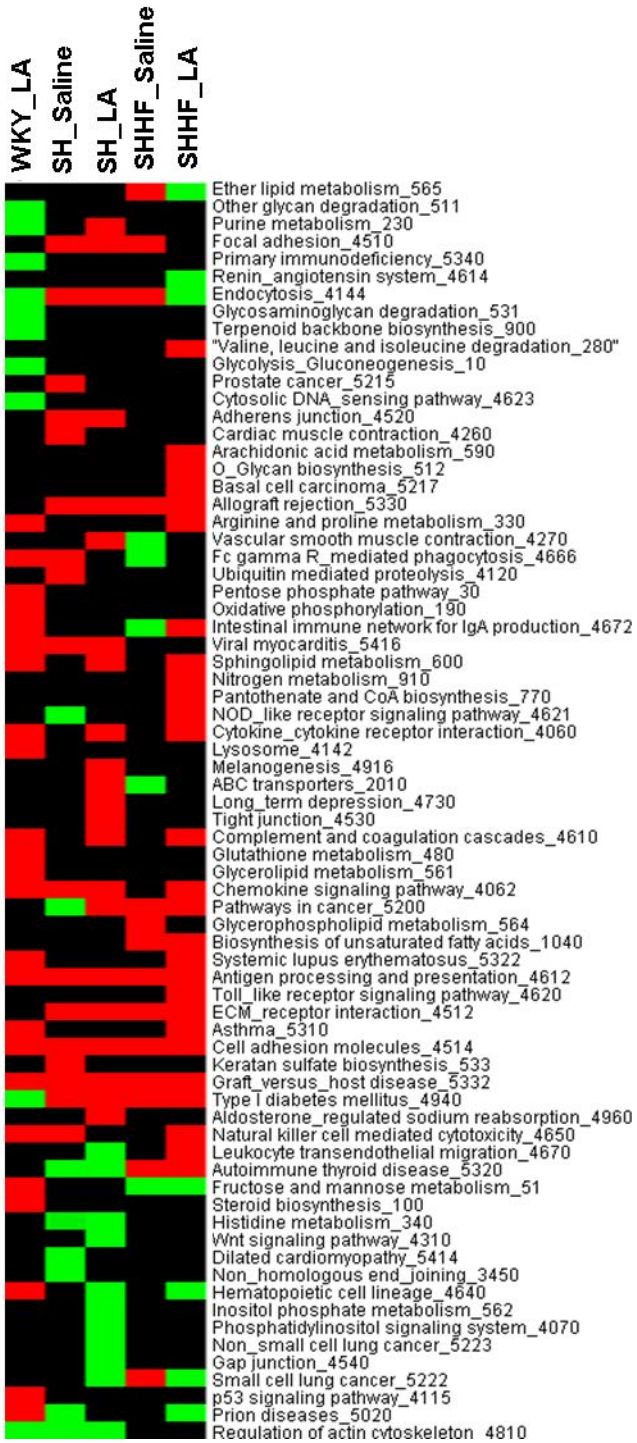

Figure 6.5. DAVID KEGG pathway specific pulmonary gene expression heat map analyzing global expression changes comparing WKY, SH, and SHHF rats 3 months following

intratreacheal instillation exposure to 1.0 mg LA normalized to control WKY exposed to saline. Black indicates a similar number of genes are activated and the pathway is not altered compared to control (WKY saline). Green indicates that the pathway lacks activation of many genes compared to control (WKY saline). Red indicates the pathway was significantly altered ($p \leq 0.05$) and contains genes that were activated within the pathway compared to control (WKY saline). This is based on the list of differentially expressed genes (DEGs) for each contrast.

Figure 6.6

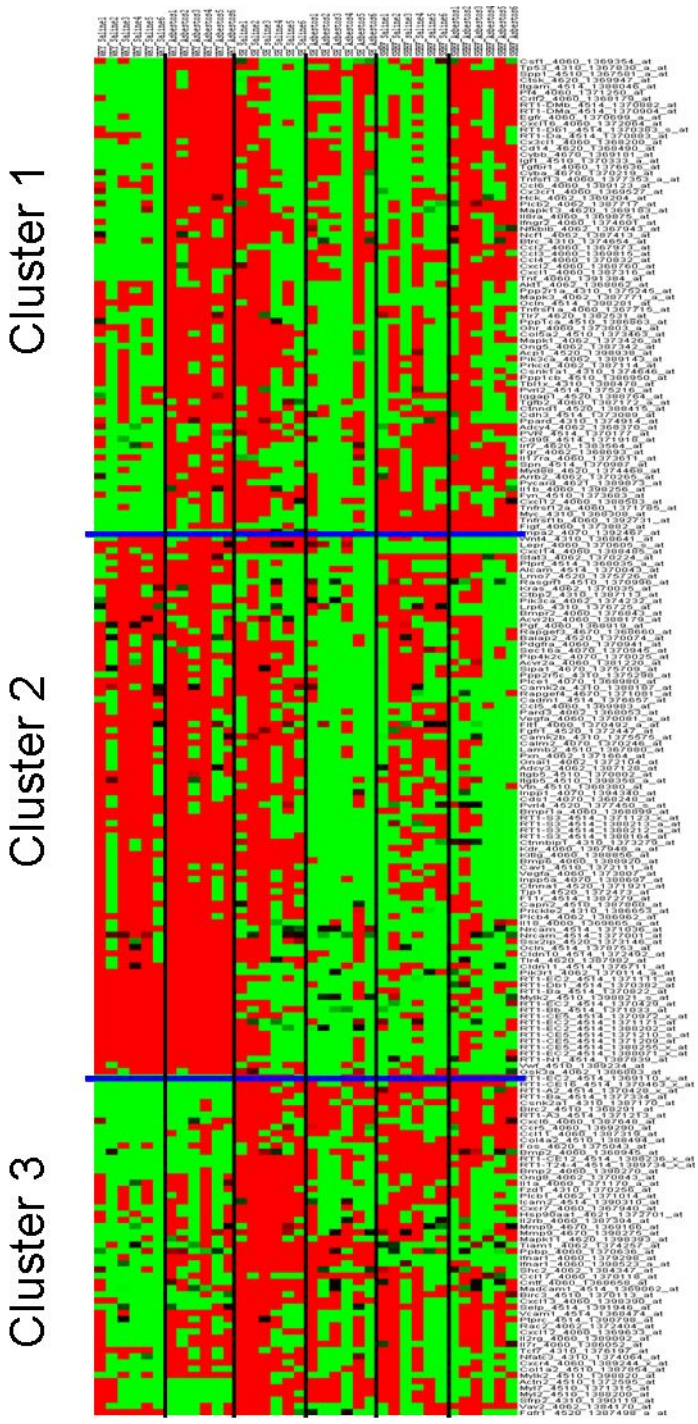

Figure 6.6. Clustering of inflammation specific pulmonary genes comparing WKY, SH and SHHF rats 3 months after intratracheal instillation exposure of 1.0 mg LA. Differentially

expressed genes (DEGs) related to inflammation were assembled from KEGG pathways: 4060, 4062, 4070, 4310, 4510, 4514, 4520, 4620, 4621, and 4670. All genes were filtered to meet the criteria of intensity greater than or equal to 30 and had a fold change greater than 1.5 or less than or equal to -1.5. Genes were then hierarchically clustered using Eisen's Cluster Analysis, were median centered with average linkage, and viewed using Treeview.

Figure 6.7

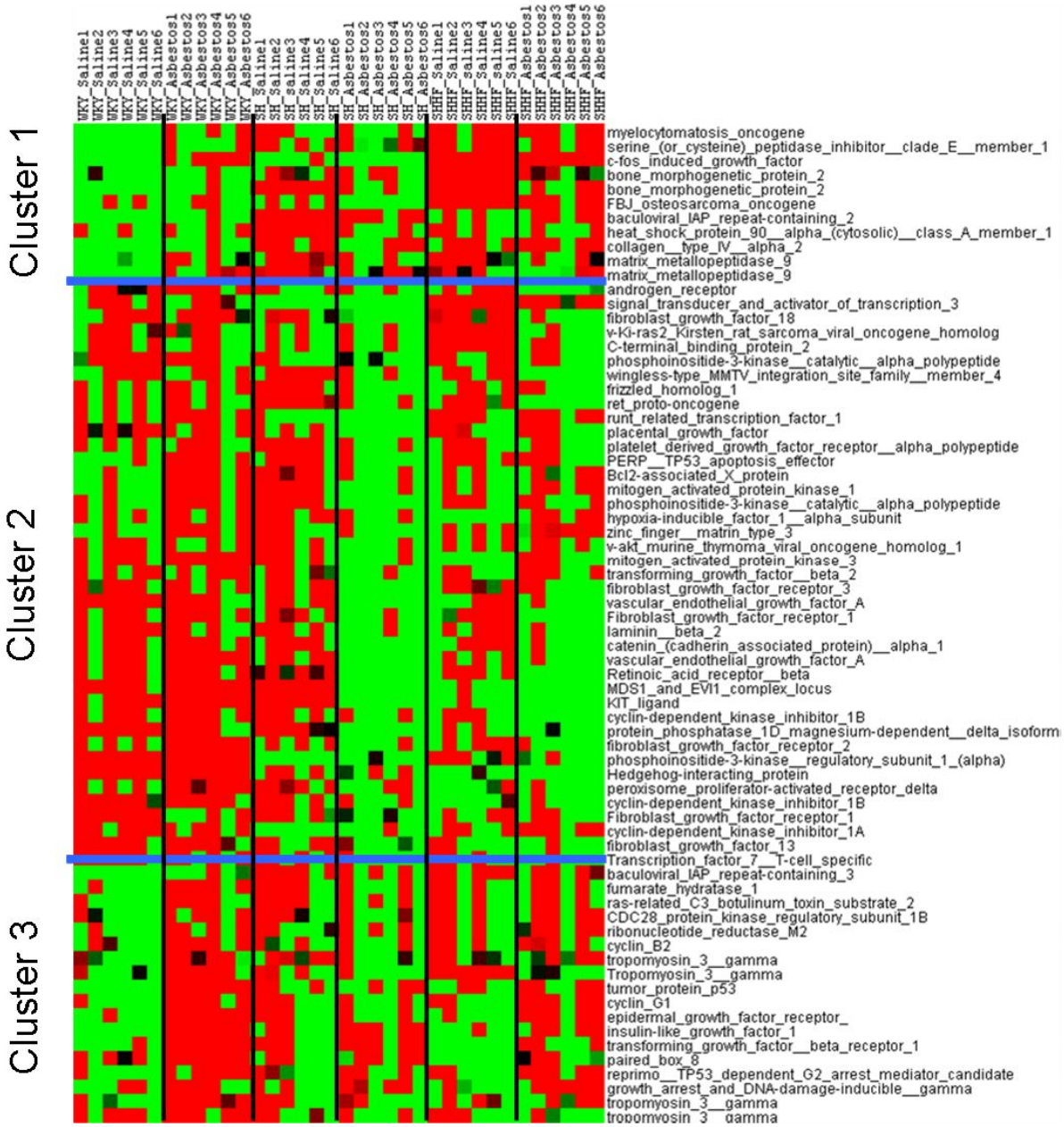

Figure 6.7. Clustering of cell cycle control specific pulmonary genes comparing WKY, SH and SHHF rats 3 months after intratracheal instillation exposure of 1.0 mg LA. Differentially expressed genes (DEFs) related to cell cycle control were assembled from KEGG pathways: 4115, 5200, 5215, 5217, 5222, and 5223. All genes were filtered to meet the criteria of

intensity greater than or equal to 30 and had a fold change greater than 1.5 or less than or equal to -1.5. Genes were then hierarchically clustered using Eisen's Cluster Analysis, were median centered with average linkage, and viewed using Treeview.

Figure 6.8

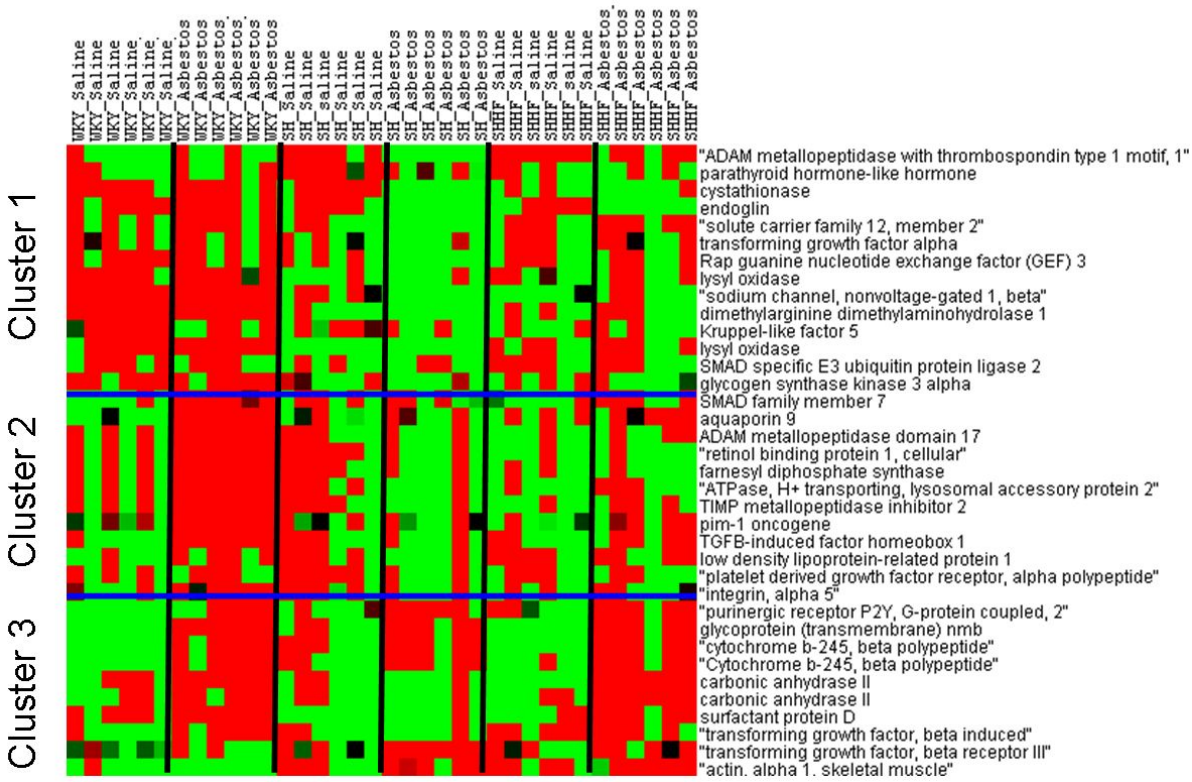

Figure 6.8. Clustering of growth factor and fibrosis specific pulmonary gene expression comparing WKY, SH and SHHF rats 3 months after intratracheal instillation exposure of 1.0 mg LA. Functional lists for genes related to growth and fibrosis, were obtained from NetAffx (http://www.affymetrix.com/estore/analysis/index.affx). All genes were filtered to meet the criteria of intensity greater than or equal to 30 and had a fold change greater than 1.5 or less than or equal to -1.5. Genes were then hierarchically clustered using Eisen's Cluster Analysis, were median centered with average linkage, and viewed using Treeview.

6.4 Discussion

The molecular mechanisms of acute inflammation that lead to chronic fibrosis or lung cancer after asbestos exposure remains elusive despite decades of research. Fiber-associated Fe has been postulated to play a role in the inflammatory process; however, its influence on chronic pathological outcome is unknown. The literature is controversial regarding the role of Fe overload and chronic disease susceptibility. Studies have demonstrated that the accumulation of Fe at tumor sites is a consequence due to tumor-associated inflammation and oxidative stress (Kukulj *et al.*, 2010). Other studies however have shown that Fe is causal in tumor progression postulating that the availability of Fe promotes ROS generation, which leads to cancer through oxidation and damage of DNA (Hu *et al.*, 2010, Toyokuni, 2011). We have recently have shown that rat models of CVD-associated Fe-overload do not show an exacerbation of acute LA-induced inflammation and that this acute inflammatory response induced by LA is reduced by Fe despite its ability to generate ROS (Shannahan et al. 2011a, Shannahan et al. 2011b). In this study we postulated that exposure of SH and SHHF rats to LA due to their underlying CVD and associated pulmonary Fe-overload would result in further accumulation of Fe in the lung and differential pathological outcomes over a longer period of time (3 and 6 months). We further hypothesized that a snapshot analysis of lung gene expression signatures in control and LA-exposed rats, 3 months post-exposure, would allow us to delineate the relationship between acute injury and long-term occurrence of pathology, and the role of CVD-associated Fe-overload.

Here we show that pulmonary fibrosis progresses to a similar degree in all three strains over 3 months after LA exposure despite differences in expression of genes related to

fibrosis in all three strains. Fe accumulation was also found in fiber-laden alveolar macrophages and was highly exacerbated in SHHF. Surprisingly, only SHHF developed atypical hyperplastic lesions of bronchiolar origin in response to LA. The overall transcriptional activity supports the development of hyperplastic lesions in SHHF and underlying chronic inflammation. However, the role of key genes in given processes is difficult to ascertain from expression analysis.

Persistent systemic inflammation and Fe-overload are the hallmark features of chronic diseases in humans and in animals, however it is not known if they are consequence of the disease or causal (Yao and Rahman, 2011, O'Byrne, 1996). We have shown that SH and SHHF due to their genetic predisposition to CVD have increased baseline inflammation as characterized by increased presence of neutrophils, and Fe-overload that relates to the severity of of disease (SHHF>SH) (Shanahan et al. 2010). In this study we hypothesized that pulmonary gene expression patterns might be different in SH and SHHF rats having increased presence of neutrophils at baseline and may relate to inflammation and pathology induced by LA. Genes involved in inflammatory processes mediated by NFkB and other signaling pathways were generally up-regulated at baseline in both SH and SHHF relative to WKY, along with several metabolic and pathological processes.

Gene expression analysis revealed that the LA effect on inflammatory genes that regulate innate immunity is still evident at 3 months post-exposure in WKY but less so in SHHF and SH with suppressed acquired immunity genes at baseline (Figure 6.6 cluster 1). This pattern of response suggests that SH and SHHF 3 months after LA exposure are unable to sustain increased inflammatory gene expression despite their elevated baseline lung neutrophils. This may be related to their already high baseline expression and an inability to

further up-regulate inflammatory genes or temporal differences in gene expression between strains.

Persistent inflammatory response in the case of asbestos exposure leads to pulmonary fibrosis at the terminal bronchiolar region of the lung, coinciding with the site of fiber deposition (Brody *et al.*, 1981). Despite gene expression pattern differences between strains our study demonstrates similar degrees of fibrotic lesions in the lung. Even though the LA-induced neutrophilic influx had subsided in all three strains at 3 months, the inflammatory gene expression still remained induced in WKY compared to SH and SHHF who express these genes at high level at baseline. We speculate that the increased inflammatory gene expression was necessary for progressing to fibrosis in all strains regardless of how the gene expression is increased (LA exposure in WKY and high baseline in SH and SHHF). We further postulate that LA-induced inflammation and fibrosis-related gene expression might have been dampened because of the Fe that accumulated within fiber-laden macrophages in Fe-overloaded SHHF. Underlying genetic differences may also be involved in differential regulation of inflammation and fibrosis.

Unlike long thin fibers that remain intercalated at the terminal bronchiolar region, the shorter fibers are likely to be readily phagocytozed by alveolar macrophages (Bernstein *et al.*, 2010). *In vitro* studies have shown that epithelial cells can take up relatively short LA fibers (Duncan *et al.*, 2010). Light microscopy examinations with phase contrast revealed the presence of LA fibers within alveolar macrophages at 3 months suggesting that these fibers are taken up by alveolar macrophages and are not cleared from the lung. Amosite fibers of a similar length to LA have been shown to be engulfed by alveolar macrophages *in vivo* (Bernstein *et al.*, 2010). Furthermore, the half life of these fibers have been shown to be

greater than 90 days suggesting that some of these fibers within macrophages will remain in the lung for the lifetime of the animal. The ability of alveolar macrophages to engulf but not clear the LA fibers may result in chronic inflammation within the lung affecting disease progression.

The enhanced progressive accumulation of Fe within fiber laden alveolar macrophages in the SHHF supports the hypothesis that the increased availability of cellular Fe increases the accumulation of Fe at the site of fiber deposition within the lung. Coating of endogenous Fe on the surface of fibers has been shown in mice and in humans after exposure (Ghio *et al.*, 2006, Ghio *et al.*, 2009). We have shown that LA binds Fe in an acellular system in minutes (Shannahan et al. 2011a). Here we show that, as in humans and mice, LA likely associates cellular Fe in rats and that this process is rapid in rats with underlying Fe-overload. Furthermore, our previous study with LA (Shannahan et al., 2011a) and another study with quartz (Ghiazza *et al.*, 2011) have shown that the bio-availability of catalytically active Fe may reduce the inflammatory response following fiber exposure. This supports the conclusion that possibly the Fe-overload conditions seen in SH and SHHF might reduce the inflammatory gene induction caused by LA due to accumulation of Fe at the site of fiber deposition.

Surprisingly, only the SHHF developed atypical hyperplastic lesions at 3 months and 6 months post-exposure to LA. These proliferative lesions likely originated form bronchiolar epithelial cells and did not involve squamation based on immunohostochemical detection of a series of cell specific markers. Unlike the typical hyperplastic changes seen in the bronchiolar epithelial and alveolar type II cells after asbestos induced lung fibrosis (Robledo *et al.*, 2000, Crouch, 1990), the hyperplastic changes seen in LA-exposed SHHF were

classified as atypical based on the stacking of hyperplastic cells; but were not classified as adenomatous. Such atypical lesions have been noted in bronchoalveolar neoplasia and atypical adenomatous hyperplasia of the lung in humans and have been associated with genetic changes in the EGF receptor (Kitamura and Okudela, 2010, McIntire *et al.*, 2010). Case studies with asbestos exposure have shown the coexistence of atypical adenomatous hyperplasia, primary lung adenocarcinoma and pleural mesothelioma (Thomas *et al.*, 2004, Tsuzuki *et al.*, 2008). Because these lesions in SHHF rats at 3 months did not progress over 6 months, it is difficult to ascertain their significance. However, these findings allow us to speculate that SHHF might have genetic traits that predispose them earlier to asbestos-induced lung cancer development.

We presumed that analysis of expression of inflammatory cytokines, growth factors and cell cycle control genes would allow for insights into the proliferative lesions seen only the in SHHF rat model. We noted that the cellular processes involving cell cycle control, and growth were differentially affected in all three strains. TP53 a key tumor suppressor gene was induced only in WKY exposed to LA. The loss of function of the tumor suppressor gene, TP53 has been implicated in the development of lung cancer and cellular proliferation following asbestos exposure (Morris *et al.*, 2004). C-Fos, a member of AP-1 oncogene family, which is implicated in cell motility and invasion (Han et al., 2010) and the FBJ oncogene were upregualted only in LA-exposed SHHF. The EGF receptor has been implicated in adenomatus hyperplastic cell growth (Adiseshaiah *et al.*, 2008) and was also increased in SHHF. A number of cellular processes as determined based on pathway analysis using KEGG indicated significant changes in pathways in cancer, and basal cell carcinoma development, especially in SHHF. This may facilitate the proliferative phenotype

seen in the SHHF after LA exposure. Baseline high levels of oxidative stress and inflammation demonstrated by SHHF also may influence their increased sensitivity to develop proliferative lesions compared to other animal strains. Thus, the SHHF may be an appropriate model to study proliferative changes following asbestos exposure due to the high number of incidences seen in this study.

There are limitations of the study that concern the interpretation of findings: 1) Animal models have genetic CVD which may influence their susceptibility to LA more so than Fe-overload. 2) The use of intratracheal instillation, while allowing precise control for pulmonary dose, might produce a one time high response relative to inhalation where injury and compensatory processes occur simultaneously. 3) The temporality of gene expression patterns was not considered. 4) The analysis of whole lung tissue expression might reduce actual changes seen at the site of lesion. 5) Due to LA being shorter than other well studied fibers, the kinetics of retention and the effect on the pulmonary cells might be different.

In conclusion, we report that LA exposure is associated with progressive fibrosis and increased gene expression for inflammatory markers and fibrosis in all three strains, however the accumulation of Fe within fiber-laden macrophages is primarily seen in SHHF. The SHHF was found to develop atypical hyperplastic lesions that presented with cellular stacking and were of bronchiolar cell origin. Transcriptional analysis of lung tissue revealed LA-induced changes in inflammation, immune regulation and number of pathological and metabolic processes, however, with remarkable strain-related differences. Genes involved in Fe homeostasis did not remain altered at 3 months following LA exposure. Key regulatory genes of cell cycle control and growth were differentially affected in all three strains, however; specific cancer-related processes were significantly altered only in SHHF. Thus,

disease associated Fe-overload might result in increased accumulation of Fe at the site of fiber deposition, however, this might not be causal in susceptibility to induce proliferative changes.

CHAPTER 7. OVERALL CONCLUSIONS AND SIGNIFICANCE

These studies taken together demonstrate the role of iron (Fe) in Libby amphibole (LA) asbestos-induced lung inflammation in healthy and cardiovascular disease (CVD) compromised rats with Fe-overload. It has been postulated that increased amounts of Fe on the surface of asbestos would potentiate the production of reactive oxygen species (ROS) by fibers and thereby enhance inflammation and toxicity. The link between the ability of Fe to generate ROS and the enhancement of the toxicity of a variety of pollutants has been proposed. No systematic approaches, however, have been taken to understand if the injury and inflammatory responses are exacerbated when Fe levels are increased. The literature provides conflicting evidence of the role of Fe due to differences in the experimental approaches. Fe can be catalytically active and is ubiquitously present in the ambient air, our diet, and tissues. Thus, the understanding of its role in toxicity after environmental exposures to particles and fibers is fundamental and necessary. In order to make our research questions and experiments more relevant to humans and applicable to diseases associated with environmental exposures, we systematically evaluated the role of Fe in fiber-induced lung inflammation in healthy and CVD compromised rat models with Fe-overload.

To understand the role of Fe in asbestos toxicity and the progression of lung diseases, it is necessary to integrate findings from epidemiology, human, animal, *in vitro*, and acellular chemical studies. Often, integration of results from various types of studies is difficult. Human and animal studies have demonstrated an ability of asbestos to bind Fe after exposure

(Shen *et al.*, 2000, Gibbs *et al.*, 1994, Ghio *et al.*, 2004, Pascolo *et al.*, 2011). Furthermore, fibers coated with Fe have been shown to generate increased ROS compared to fibers without additional Fe in acellular systems. Based on these independent studies, it was postulated that endogenous Fe on the surface of fibers could enhance ROS production and toxicity (Governa *et al.*, 1999, Ghio *et al.*, 2006, Lund *et al.*, 1994, Ghio *et al.*, 1992). Further studies examining fibers with different Fe contents also showed this trend (Gazzano *et al.*, 2007, Srivastava *et al.*, 2010).

Our research supports the conclusion that LA fibers bind exogenous Fe, and with increased levels of Fe, the fibers become more redox active in an acelllular system. This increased redox activity due to associated Fe, however, does not seem to be the mechanism responsible for the acute inflammatory response demonstrated after fiber exposure in cells and *in vivo*. Rather, the increased bioavailability of cellular Fe to bind fibers and also the fiber-associated Fe are responsible for inhibiting the acute inflammatory response to fibers. These findings were confirmed in animal models with CVD-associated Fe-overload (SH and SHHF rats) that demonstrated reduced inflammatory gene expression compared to a healthy model (WKY). Furthermore, the ability of LA to associate endogenous Fe *in vivo* was validated by the prominent accumulation of Fe in fiber-laden macrophages in Fe-overloaded SHHF rats.

Fe is the most abundant metal in the environment and is an essential metal for living organisms. Fe is required for basic biological functions such as transporting and releasing oxygen in our tissues, electron transport, energy metabolism, and DNA synthesis and repair. Although it is likely that other essential metals can bind fibers *in vivo* and modulate biological processes, Fe is of the most biological interest. The importance of Fe is due to

high endogenous levels and the stability constant for its complexation with the fiber is higher than any other cation found within the body. Furthermore, Fe is abundant within our environment and is a key component of many air pollutants. The ability of Fe to facilitate Fenton reactions *in vivo* can make it a promoter of oxidative stress. As Fe is highly redox active, its endogenous levels are tightly regulated within the body by the Fe transporters and binding proteins such as lactoferrin, transferrin, and ferritin. Lactoferrin and transferrin are Fe transport proteins responsible for the binding of free Fe and its transport into cells.

In contrast to transferrin and lactoferrin's role in Fe transport, ferritin is the body's primary Fe storage protein and is useful in determining an organism's Fe status. Ferritin consists of a combination of two subunits: ferritin heavy chain and ferritin light chain. Ferritin heavy chain is responsible for sequestration of Fe by oxidation, while the light chain is responsible for the storage of Fe. According to where it is in the body and its function, the proportion of each subunit is different. Light chain rich ferritins are associated with conditions of Fe-overload and are known to release Fe very slowly. Heavy chain rich ferritins are known to be associated with inflammatory responses as the body prepares to quickly bind Fe that is released due to oxidative damage to heme-containing proteins and catabolism of heme groups by HO-1

In environmental exposures, Fe has been postulated to play a key role in the inflammatory response induced by inhaled fibers and silicates including asbestos. Human exposure to asbestos has been shown to cause the development of lung cancer, the fibrotic condition asbestosis, and mesothelioma. Individuals in the town of Libby, Montana who were exposed for years both occupationally and environmentally to an amphibole mixture (winchite, richerite, and tremolite) during mining of asbestos-contaminated vermiculite

(Meeker *et al.*, 2003), have recently shown increased incidences of asbestos-related diseases (Peipins *et al.*, 2003, Sullivan, 2007). Similar to other asbestos fiber-types, the chemical formula of fibers in the LA sample contains Fe which can redox cycle and produce ROS, as well as silicon which has been shown with other fibers to facilitate the association of endogenous Fe.

Our acellular studies support these findings in that LA could bind Fe and this additional Fe rendered them more redox active. However, our *in vitro* and *in vivo* studies demonstrated that having additional Fe bound on the surface of the fibers inhibited the inflammatory response compared to unmodified fibers. Recently, this mechanism has also been shown to be true for quartz-induced inflammation (Ghiazza *et al.*, 2011). We believe the reason for this disconnect between the acellular studies and the cell and animal toxicity studies is the high concentration of Fe and reducing equivalents present in the acellular experiments to promote Fenton chemistry. However, this is unlikely in a live cell where mechanisms exist to inhibit abbarent ROS production.

We postulated that Fe might reduce the inflammatory response by inhibiting the activity of the inflammasome as other asbestos fibers have recently been shown to induce inflammation through this pathway. The inflammasome is a multiprotein complex known to initiate the inflammatory cascade following exposure to a variety of stimuli. Asbestos fibers have shown an ability to specifically induce the NALP3 inflammasome (Dostert and Petrilli, 2008, Dostert *et al.*, 2008) while NALP3 knockout mouse models have been shown to be protected from the development of silicosis following exposure to silica (Cassel *et al.*, 2008). For the first time, our study demonstrates the activation of the inflammasome after LA exposure and the ability of Fe to transcriptionally inhibit signaling targets of this pathway

involved in acute inflammation (Chapter 4). Furthermore, at 3 months post-LA exposure, expression of genes involved in the inflammasome pathway, while still up-regulated in healthy rats seem unaltered in rats with Fe-overload. Our findings support the role of Fe in activation of inflammasome-mediated signaling in rat models of Fe-overload. This altered activation of the inflammasome in Fe-overload models may contribute to the differential inflammatory response seen after exposure and may cause variations in susceptibility to asbestos exposure.

Importantly, in Chapter 3 we use IL-8 as a marker of inflammagenic response to LA in a bronchiolar epithelial cell line, while in Chapter 4 we use IL-1β, an inflammatory response marker produced by alveolar macrophages following inflammasome activation. We find that Fe similarly alters the inflammatory response in both cell types as demonstrated by altered induction of IL-8 and IL-1β. Induction of IL-8 has currently not been found to be due to activation of the inflammasome. These findings support the conclusion that there may be a general mechanism by which Fe alters the inflammatory response such as differential activation or expression of transcription factors such as Nf-κB. The ability of Fe to modulate inflammation in different cell types via unique or similar mechanisms requires further study.

Although inflammation orchestrated by integration of a variety of signaling pathways is needed by the body, it can also be detrimental if not properly regulated. Our studies demonstrate modifications in the acute inflammation induced by asbestos due to the bioavailability of Fe. A robust inflammatory response may be needed to stimulate appropriate repair mechanisms. On the other hand, if this inflammatory response does not resolve or is too intense, there could be non-reversible damage to the lung and lead to the progression of diseases. SHHF had persistent high baseline inflammation but did not

demonstrate an ability to further induce inflammatory gene expression comparable to WKY. Historical evidence suggests that the inflammatory response is a delicate balance. During the flu pandemic of 1918, younger healthy individuals were curiously more susceptible to the morbidity and mortality caused by the flu (Hsieh *et al.*, 2006). This was later found to be related to their robust inflammatory response after contracting the flu. Older individuals who commonly were at risk for mortality from the flu were found to survive due to their reduced/weakened inflammatory response. Because older people are likely to have Fe-overload, one can postulate that this Fe reduces the inflammatory response to inhalable pathogens and air pollutants.

Many chronic diseases including diabetes, thalasemmia, cancer, and CVD are associated with not only inflammation and oxidative stress, but also systemic Fe-overload (Galanello *et al.*, 2010, Allen, 2010, Kruszewski, 2004, Ellervik *et al.*, 2010). The examination of rat models of CVD in Chapter 1 demonstrates pulmonary inflammation, oxidative stress, and Fe-overload. Therefore, we believe that these models were appropriate for the study of CVD-associated Fe-overload and its consequences in air pollution exposures. The sheer stress caused by elevated blood pressure in these models is thought to contribute to the release of Fe from hemoglobin resulting in systemic Fe-overload. It is not known if these increases in tissue Fe levels are causal or a consequence of the underlying disease. This increased systemic Fe is thought to contribute to the systemic oxidative stress and inflammation seen in these individuals and rat models. The SH and SHHF rats used in our studies have not been fully genotyped and are polygenetic models of CVD. The response of these animal models to LA might also be influenced by genetic abnormalities in these models that do not pertain to the underlying state of Fe-overload. This causes an increased variability

in their responses to asbestos and other inhalable pollution exposures, giving an accurate depiction of the continuum of responses seen in the human subpopulation of CVD.

The ability of LA to bind Fe is not unique to this fiber type as other fibers have shown an ability to bind Fe. It has been postulated in other studies that macrophages are the source of Fe for the formation of ferruginous bodies on fibers (Koerten *et al.*, 1986). Specifically, it has been hypothesized that inflammatory macrophages that are recruited to the lung after fiber exposure are the source of Fe (Birgegard and Caro, 1984). This postulation is based on more abundant Fe in the inflammatory macrophage compared to resident lung macrophages due to uptake of damaged erythrocytes. The time required to form ferruginous bodies after exposure is not known, but some individuals are known to more readily deposit Fe on fibers. This variation in deposition of Fe on fibers has been thought to be related to differences in individual body Fe burden. Our data are consistent with this assumption and show that SHHF with Fe-overload accumulate Fe in fiber-laden macrophages as early as 3 months whereas other strains with less tissue Fe show minimal accumulation.

Chapter 3 demonstrates that in the presence of increased Fe levels, the inflammatory effect of LA is reduced. Interestingly, our findings in Chapter 6 not only support this by showing that animals with Fe-overload have a decreased LA-induced inflammatory gene expression, but also showing that animals with disease associated Fe-overload more readily coated fibers with Fe. This finding supports our hypothesis that the endogenous loading of Fe is dependent on the bio-availability of Fe and that individuals with CVD-associated Fe-overload more readily coat fibers. This also validates the increases seen in Chapter 5 of markers of Fe homeostasis in response to the enhanced movement of Fe in the SHHF. This finding may explain why often individuals with chronic diseases demonstrate reduced

inflammatory responses to particle exposures. Since accumulation of essential transition metals including Fe has been noted at the site of pathology and systemically, one might speculate on the role of these metals in the development of aberrant cell-cycle control and proliferative changes based on the increased hyperplastic lesions seen only in LA exposed SHHF. However, this association of Fe-overload in LA-exposed SHHF and the lack of inflammatory gene expression must be cautiously interpreted since numerous genetic abnormalities and the baseline presence of lung inflammation might also contribute to the lack of inflammatory gene induction in these rats.

In humans asbestos is known to cause a specific cancer of the pleural region of the lung well-known as mesothelioma. It is postulated that the migration of macrophages loaded with short fibers through lymphatics to pleural surface is involved in calcification and mesothelioma of the pleura. Rats after intratracheal instillation have also demonstrated the movement of short chrysotile fibers to the pleural region (Viallat *et al.*, 1986). Chronic inhalation studies of amosite and chrysotile have also demonstrated this translocation to the pleural region in hamsters and rats (Mast *et al.*, 1994, McConnell *et al.*, 1999). These studies, however, demonstrated strain specific differences with the hamster demonstrating greater translocation of fibers compared to rats and also pleural fibrosis and mesothelioma that were unseen in rats (Gelzleichter *et al.*, 1999). Thus, the rat is not considered the preferred model for the study of mesothelioma (Rodelsperger and Woitowitz, 1995) and the absence of pleural changes in our LA exposure studies appears to be a deficiency with our chosen rat models. Epidemiology, however, has determined a relationship between occupational and environmental exposure to LA and increased incidences of mesothelioma (Moolgavkar *et al.*, 2010). Donaldson *et al.*, 2010 hypothesized that the fibers that are more

biopersistent could move from the alveolar spaces to the pleural region and could eventually lead to carcinogenesis. Studies have also shown that injection of asbestos into the pleural region of rats can cause pleural changes, supporting this hypothesis (Hu *et al.*, 2010, Cullen *et al.*, 2002). Based on this hypothesis, the lack of pleural changes seen in our studies could be attributable to 1) a shorter timeframe after a single bolus instillation which may not have been long enough to see translocation of fibers to the pleura and 2) the lack of sensitivity of rats to the translocation of fibers.

In accordance with several other studies, we demonstrate progressive and concentration-dependent fibrotic changes in all rat strains exposed to LA. The development fibrosis after LA exposure has also been recently noted in Fisher 344 rats (Padilla-Carlin et al. 2011). The development of proliferative lesions, however, is unique to the SHHF. The development of the fibrosis has also been noted after exposure to crocidolite (Robledo *et al.*, 2000). Furthermore, it is known that other asbestos fibers deposit within the terminal bronchiolar region of the lung after acute inhalation exposure (Brody *et al.*, 1981). The fibrotic foci in all three strains and the proliferative lesions in SHHF were concentrated at the terminal bronchiolar junctions, indicating that the injury and disease occur at the site of fiber deposition in the lung. (Robledo *et al.*, 2000; Crouch, 1990).

The findings in SHHF, but not WKY or SH, of increased atypical hyperplasia and Fe accumulation within fiber-laden macrophages at 3 months post exposure prompted us to further examine the transcriptional activity of the lung using gene expression arrays. The results obtained from gene expression arrays do not allow the confirmation of a specific hypothesis, but serve as a hypotheses generating tool and provide insights into observed pathological findings. We postulated that a snap shot of global gene expression at the time

when these lesions begin to appear would allow us to get an insight into the role of Fe accumulation in the development of hyper plastic lesions in LA-exposed SHHF. While the Fe accumulation in macrophages and the development of atypical hyperplastic lesions are temporally associated in SHHF, one must also consider the role of underlying chronic baseline oxidative stress and inflammation and genetic abnormalities that contribute to the disease in interpretation of findings observed from gene expression patterns.

Even though genes regulating numerous metabolic and pathological processes have been noted to be abnormal at baseline in both SH and SHHF rats, it was surprising to note that the pathways involved in tumorogenesis were more altered in SHHF both at baseline and following LA exposure. TP53, an extensively characterized and a major tumor suppressor gene, was induced only in WKY exposed to LA, but not in SHHF that developed hyperplastic lesions. SHHF also was shown to have increased KRAS expression at baseline and a lack of cell-cycle control gene expression compared to WKY, supporting pathological findings. The lack of LA-induced changes in genes regulating Fe homeostasis suggests that Fe accumulation in animals with this Fe-overload condition may not be directly related to proliferative changes in the lungs of LA-exposed SHHF. Rather, the persistent inhibition of inflammatory gene induction likely due to Fe accumulation in LA-exposed SHHF might relate to their susceptibility to develop hypeplastic lesions. The SHHF seemed to be susceptible to the development of these lesions after asbestos exposure compared to the other animal models, possibly making the SHHF an appropriate model for the study of asbestos-induced cell proliferation. It would be of interest to determine if these proliferative lesions were unique to fiber exposure or could be repeated with other pollutant exposures.

The speculation that inhibition of inflammation by Fe might result in aberrant cell-cycle control and proliferation in SHHF goes against the common notion that inflammation is the key factor in development of cancer. Here, we try to go beyond the boundaries of the experimental results in postulating that the presence of chronic inflammation as a result of genetic predisposition, but not the inflammation induced by environmental insult might cause increased susceptibility to develop cancer. Rather, the inability to mount a robust inflammation as suggested earlier may predispose one to increased susceptibility through failing to initiate appropriate repair mechanisms. Future studies should examine the role of Fe accumulation at the site of disease and its contribution to regulation of cell-cycle control.

The role of Fe in the development of these hyperplastic lesions is unclear as indicated. In the literature, there are conflicting views about the role of Fe in proliferative changes leading to tumor progression. Studies have demonstrated increased levels of Fe at tumor sites; however, it is unclear if this accumulation of Fe is causal or a consequence of tumor development. Many studies believe that the ability of Fe to redox cycle and produce ROS may contribute to the oxidative damage to DNA (Hu *et al.*, 2010, Schurkes *et al.*, 2004, Toyokuni, 2011). Others believe that the accumulation of Fe is due to tumor associated oxidative stress and inflammation (Kukulj *et al.*, 2010). Our work at this time is unable to provide any insight into the role of Fe in cancer development, as we only assessed acute and sub-chronic time points and the proliferative lesions that did develop were not found to be progressive.

This work lays the foundation for multiple future research questions. Further assessment of the toxicity induced by other materials known to bind Fe would be of interest in order to determine if the availability of endogenous Fe modifies the inducible injury and

inflammation. We determined in our studies that the movement of Fe from cellular Fe pools was important in modulating the inflammatory response, however, it is necessary to understand specifically the pool of Fe that is susceptible to Fe sequestration by the fiber. We postulated in our studies that the fiber would initially take up Fe from the catalytically active Fe pool. Furthermore, we hypothesized that in the situation when no catalytically active cellular Fe is available to bind to inhaled fibers, the removal of Fe from more tightly bound protein coordination complexes would occur and may cause a different injury outcome. Future studies tracking the movement of Fe from the pools need to be done in order to understand specifically which pool this Fe is coming from and its biological implications. Due to the chronic nature of asbestos-induced diseases and the inability of many fibers to be removed from the lung, the implications of chronic Fe-overload requires further evaluation. Another future direction is the use of calculating Fe binding potentials for fibers with different physiochemical properties and assessing relative toxicities. This would allow for the determination of correlations between the ability of fibers to associated endogenous Fe and a fiber toxic potential given the host endogenous Fe concentrations remain constant. The use of different animal models of variable Fe regulation would also be of interest to study. All experiments we designed used a one-time intratracheal instillation of asbestos in order to control dosing between animal models with different minute volumes. However, studies assessing episodic inhalation exposures over a long period of time would be more realistic in mimicking the human exposure scenario.

We believe that this project, overall, has scientifically contributed to the field of toxicology. First, our project characterized the pulmonary disease states in commonly used rat models of CVD. We also were able to characterize a highly human relevant form of

asbestos, the LA sample, and determined its ability to associate Fe. We further determined a unique mechanism by which the acute inflammatory response may be mediated after fiber exposure and its inhibition by Fe. Lastly, we assessed the role of Fe and its contribution to LA-induced pulmonary disease susceptibility in models of Fe overload and demonstrated that Fe binds LA in vivo.

Since asbestos-induced diseases and the mechanisms of induction have been studied for decades but many aspects still remain unknown, the continued examination of asbestos toxicity is needed, as newer technologies for the evaluation of toxicity are made available. The information obtained from high throughput studies involving diverse animal models could allow us to determine how acute inflammation induced by asbestos or other pollutants can lead to the development of lung cancer and other diseases. These research findings may have implications influencing the treatment and prevention of asbestos-induced diseases.

REFERENCES

Abdalla, M. Y., Fawzi, M., Al-Maloul, S. R., El-Banna, N., Tayyem, R. F., and Ahmad, I. M. (2011). Increased oxidative stress and iron overload in Jordanian beta-thalassemic children. *Hemoglobin.* 35, 67-79.

Adamson, I.Y. & Bakowska, J. 2001, "KGF and HGF are growth factors for mesothelial cells in pleural lavage fluid after intratracheal asbestos", *Experimental lung research*, vol. 27, no. 7, pp. 605-616.

Adiseshaiah, P., Vaz, M., Machireddy, N., Kalvakolanu, D. V., and Reddy, S. P. (2008). A Fra-1-dependent, matrix metalloproteinase driven EGFR activation promotes human lung epithelial cell motility and invasion. *J. Cell. Physiol.* 216, 405-412.

Allen, K. (2010). Hereditary haemochromatosis - diagnosis and management. *Aust. Fam. Physician.* 39, 938-941.

Anderson, G.J. & Vulpe, C.D. 2009, "Mammalian iron transport", *Cellular and molecular life sciences : CMLS*, vol. 66, no. 20, pp. 3241-3261.

Anderson, M. E. 1985. Determination of glutathione and glutathione disulfide in biological samples. *Meth. Enzymol.*113: 548-555.

Blum, A. 2009. Heart failure--new insights. *Israel Med. Assoc. J.* 11: 105-111.

Bernstein, D. M., Chevalier, J., and Smith, P. (2005). Comparison of Calidria chrysotile asbestos to pure tremolite: final results of the inhalation biopersistence and histopathology examination following short-term exposure. *Inhal. Toxicol.* 17, 427-449.

Bernstein, D. M., Chevalier, J., and Smith, P. (2003). Comparison of Calidria chrysotile asbestos to pure tremolite: inhalation biopersistence and histopathology following short-term exposure. *Inhal. Toxicol.* 15, 1387-1419.

Bernstein, D. M., Rogers, R. A., Sepulveda, R., Donaldson, K., Schuler, D., Gaering, S., Kunzendorf, P., Chevalier, J., and Holm, S. E. (2010). The pathological response and fate in the lung and pleura of chrysotile in combination with fine particles compared to amosite asbestos following short-term inhalation exposure: interim results. *Inhal. Toxicol.* 22, 937-962.

Birgegard, G. and Caro, J. (1984). Increased ferritin synthesis and iron uptake in inflammatory mouse macrophages. *Scand. J. Haematol.* 33, 43-48.

Brody, A. R., Hill, L. H., Adkins, B., Jr, and O'Connor, R. W. (1981). Chrysotile asbestos inhalation in rats: deposition pattern and reaction of alveolar epithelium and pulmonary macrophages. *Am. Rev. Respir. Dis.* 123, 670-679.

Cassel, S. L., Eisenbarth, S. C., Iyer, S. S., Sadler, J. J., Colegio, O. R., Tephly, L. A., Carter, A. B., Rothman, P. B., Flavell, R. A., and Sutterwala, F. S. (2008). The Nalp3 inflammasome is essential for the development of silicosis. *Proc. Natl. Acad. Sci. U. S. A.* 105, 9035-9040.

Cheng, X. W., K. Okumura, M. Kuzuya, Z. Jin, K. Nagata, K. Obata, A. Inoue, A. Hirashiki, K. Takeshita, K. Unno, G.P. Shi, M. Yokota, and T. Murohara. 2009. Mechanism of diastolic stiffening of the failing myocardium and its prevention by angiotensin receptor and calcium channel blockers. *J. Cardiovasc. Pharmacol.* 54:47-56.

Conforti-Andreoni, C., Ricciardi-Castagnoli, P., and Mortellaro, A. (2011). The inflammasomes in health and disease: from genetics to molecular mechanisms of autoinflammation and beyond. *Cell. Mol. Immunol.*

Crouch, E. (1990). Pathobiology of pulmonary fibrosis. *Am. J. Physiol.* 259, L159-84.

Cruz, C. M., Rinna, A., Forman, H. J., Ventura, A. L., Persechini, P. M., and Ojcius, D. M. (2007). ATP activates a reactive oxygen species-dependent oxidative stress response and secretion of proinflammatory cytokines in macrophages. *J. Biol. Chem.* 282, 2871-2879.

Cullen, R. T., Miller, B. G., Clark, S., and Davis, J. M. (2002). Tumorigenicity of cellulose fibers injected into the rat peritoneal cavity. *Inhal. Toxicol.* 14, 685-703.

Driscoll, K.E., Carter, J.M., Howard, B.W., Hassenbein, D., Janssen, Y.M. & Mossman, B.T. 1998, "Crocidolite activates NF-kappa B and MIP-2 gene expression in rat alveolar epithelial cells. Role of mitochondrial-derived oxidants", *Environmental health perspectives,* vol. 106 Suppl 5, pp. 1171-1174.

Doggrell, S. A., and L. Brown. 1998. Rat models of hypertension, cardiac hypertrophy and failure. *Cardiovasc. Res.* 39: 89-105.

Dominici, F., A. McDermott, M. Daniels, S.L. Zeger, and J.M. Samet. 2005. Revised analyses of the national morbidity, mortality, and air pollution study: mortality among residents of 90 cities. *J. Toxicol. Enviorn. Health A.* 68: 1071-1092

Donaldson, K., Murphy, F. A., Duffin, R., and Poland, C. A. (2010). Asbestos, carbon nanotubes and the pleural mesothelium: a review of the hypothesis regarding the role of long fibre retention in the parietal pleura, inflammation and mesothelioma. *Part Fibre Toxicol.* 7, 5.

Dorger, M., Allmeling, A.M., Kiefmann, R., Munzing, S., Messmer, K., and Krombach, F. 2002. Early inflammatory response to asbestos exposure in rat and hamster lungs: role of inducible nitric oxide syntase. Toxicol. Appl. Pharmacol. 181, 93-105

Dostert, C. and Petrilli, V. (2008). Asbestos triggers inflammation by activating the Nalp3 inflammasome]. *Med. Sci. (Paris).* 24, 916-918.

Dostert, C., Petrilli, V., Van Bruggen, R., Steele, C., Mossman, B. T., and Tschopp, J. (2008). Innate immune activation through Nalp3 inflammasome sensing of asbestos and silica. *Science.* 320, 674-677.

Duncan, K.E., Ghio, A.J., Dailey, L.A., Bern, A.M., Gibbs-Flournoy, E.A., Padilla-Carlin, D.J., Roggli, V.L. & Devlin, R.B. 2010, "Effect of Size-Fractionation on the Toxicity of Amosite and Libby Amphibole Asbestos", *Toxicological sciences : an official journal of the Society of Toxicology,* .

Eborn, S. K. and Aust, A. E. (1995). Effect of iron acquisition on induction of DNA single-strand breaks by erionite, a carcinogenic mineral fiber. *Arch. Biochem. Biophys.* 316, 507-514.

Eisen, M. B., Spellman, P. T., Brown, P. O., and Botstein, D. (1998). Cluster analysis and display of genome-wide expression patterns. *Proc. Natl. Acad. Sci. U. S. A.* 95, 14863-14868.

Ellervik, C., Tybjaerg-Hansen, A., Appleyard, M., Ibsen, H. & Nordestgaard, B.G. 2010, "Haemochromatosis genotype and iron overload: association with hypertension and left ventricular hypertrophy", *Journal of internal medicine,* vol. 268, no. 3, pp. 252-264.

Emter, C.A., S.A. McCune, G.C. Sparagna, M.J. Radin, and R.L. Moore. 2005. Low-intensity exercise training delays onset of decompensated heart failure in spontaneously hypertensive heart rats. *Am. J. Physiol. Heart Dirc. Physiol*. 289:H2030-H2038

Fang, R. and Aust, A. E. (1997). Induction of ferritin synthesis in human lung epithelial cells treated with crocidolite asbestos. *Arch. Biochem. Biophys.* 340, 369-375.

Farraj, A. K., N. Haykal-Coates, D. W. Winsett, M. S. Hazari, A. P. Carll, W. H. Rowan, A. D. Ledbetter, W. E. Cascio, and D. L. Costa. 2009. Increased non-conducted P-wave arrhythmias after a single oil fly ash inhalation exposure in hypertensive rats. *Environ. Health Persp.* 117: 709-715.

Fattman, C.L., Tan, R.J., Tobolewski, J.M. & Oury, T.D. 2006, "Increased sensitivity to asbestos-induced lung injury in mice lacking extracellular superoxide dismutase", *Free radical biology & medicine,* vol. 40, no. 4, pp. 601-607.

Fomina, I. G., V. V. Matveev, and A. V. Lazarev. 2007. Changes of spiroergometric parameters in males under 30 years of age with a hypertensive reaction of arterial pressure to graduated exercise. *Terapevticheskii Arkhiv* 79: 9-12.

Galanello, R., Agus, A., Campus, S., Danjou, F., Giardina, P. J., and Grady, R. W. (2010). Combined iron chelation therapy. *Ann. N. Y. Acad. Sci.* 1202, 79-86.

Gazzano, E., Turci, F., Foresti, E., Putzu, M.G., Aldieri, E., Silvagno, F., Lesci, I.G., Tomatis, M., Riganti, C., Romano, C., Fubini, B., Roveri, N. & Ghigo, D. 2007a, "Iron-

loaded synthetic chrysotile: a new model solid for studying the role of iron in asbestos toxicity", *Chemical research in toxicology*, vol. 20, no. 3, pp. 380-387.

Gelzleichter, T. R., Bermudez, E., Mangum, J. B., Wong, B. A., Janszen, D. B., Moss, O. R., and Everitt, J. I. (1999). Comparison of pulmonary and pleural responses of rats and hamsters to inhaled refractory ceramic fibers. *Toxicol. Sci.* 49, 93-101.

Ghiazzo, M, Scherbart, A.M., Fenoglio, I, Grendene, F, Turci, F, Martra, G, Albrecht, C, Schins, R.P., and Fubini, B. (2011). Surface iron inhibits quartz-induced cytotoxic and inflammatory responses in alveolar macrophages. Chem, Res. Toxicol. 24, 99-110

Ghio, A. J., Zhang, J., and Piantadosi, C. A. (1992). Generation of hydroxyl radical by crocidolite asbestos is proportional to surface [Fe3+]. *Arch. Biochem. Biophys.* 298, 646-650.

Ghio, A.J., Carter, J.D., Richards, J.H., Brighton, L.E., Lay, J.C. & Devlin, R.B. 1998, "Disruption of normal iron homeostasis after bronchial instillation of an iron-containing particle", *The American Journal of Physiology*, vol. 274, no. 3 Pt 1, pp. L396-403.

Ghio, A. J., Roggli, V. L., Richards, J. H., Crissman, K. M., Stonehuerner, J. D., and Piantadosi, C. A. 2003, "Oxalate deposition on asbestos bodies", *Human. Pathology.* vol 34, pp. 737-742.

Ghio, A. J., A. Churg, and V. L. Roggli. 2004. Ferruginous bodies: Implications in the mechanism of fiber and particle toxicity. *Toxicol. Pathol.* 32: 643-649.

Ghio, A. J., and M. D. Cohen. 2005. Disruption of iron homeostasis as a mechanism of biologic effect by ambient air pollution particles. *Inhal. Toxicol.* 17: 709-716.

Ghio, A.J., Funkhouser, W., Pugh, C.B., Winters, S., Stonehuerner, J.G., Mahar, A.M. & Roggli, V.L. 2006, "Pulmonary fibrosis and ferruginous bodies associated with exposure to synthetic fibers", *Toxicologic pathology*, vol. 34, no. 6, pp. 723-729.

Ghio, A. J., E. D. Hilborn, J. G. Stonehuerner, L. A. Dailey, J. D. Carter, J. H. Richards, K. M. Crissman, R. F. Foronjy, D. L. Uyeminami, and K. E. Pinkerton. 2008a. Particulate matter in cigarette smoke alters iron homeostasis to produce a biological effect. *Am. Respir. Crit. Care Med.* 178: 1130-1138.

Ghio, A. J., J. Stonehuerner, J. Richards, and R. B. Devlin. 2008b. Iron homeostasis in the lung following asbestos exposure. *Antioxidants Redox Signal.* 10: 371-377.

Ghio, A., Tan, R. J., Ghio, K., Fattman, C. L., and Oury, T. D. (2009). Iron accumulation and expression of iron-related proteins following murine exposure to crocidolite. *J. Environ. Pathol. Toxicol. Oncol.* 28, 153-162.

Gibbs, A. R., Gardner, M. J., Pooley, F. D., Griffiths, D. M., Blight, B., and Wagner, J. C. (1994). Fiber levels and disease in workers from a factory predominantly using amosite. *Environ. Health Perspect.* 102 Suppl 5, 261-263.

Gilmour, P. S., Brown, D. M., Beswick, P. H., MacNee, W., Rahman, I., and Donaldson, K. (1997). Free radical activity of industrial fibers: role of iron in oxidative stress and activation of transcription factors. *Environ. Health Perspect.* 105 Suppl 5, 1313-1317.

Gómez-Amores, Lucía, Alfonso Mate, José L. Miguel-Carrasco, Luís Jiménez, Ángeles Jos, Ana M. Cameán, Elisa Revilla, Consuelo Santa-María, and Carmen M. Vázquez. 2007. l-carnitine attenuates oxidative stress in hypertensive rats. *J. Nutr. Biochem.* 18: 533-540.

Governa, M., Amati, M., Fontana, S., Visona, I., Botta, G.C., Mollo, F., Bellis, D. & Bo, P. 1999, "Role of iron in asbestos-body-induced oxidant radical generation", *Journal of toxicology and environmental health.Part A*, vol. 58, no. 5, pp. 279-287.

Gozzelino, R., Jeney, V. & Soares, M.P. 2010, "Mechanisms of cell protection by heme oxygenase-1", *Annual Review of Pharmacology and Toxicology*, vol. 50, pp. 323-354.

Haegens, A., Barrett, T. F., Gell, J., Shukla, A., Macpherson, M., Vacek, P., Poynter, M. E., Butnor, K. J., Janssen-Heininger, Y. M., Steele, C., and Mossman, B. T. (2007). Airway epithelial NF-kappaB activation modulates asbestos-induced inflammation and mucin production in vivo. *J. Immunol.* 178, 1800-1808.

Haegens, A., van der Vliet, A., Butnor, K. J., Heintz, N., Taatjes, D., Hemenway, D., Vacek, P., Freeman, B. A., Hazen, S. L., Brennan, M. L., and Mossman, B. T. (2005). Asbestos-induced lung inflammation and epithelial cell proliferation are altered in myeloperoxidase-null mice. *Cancer Res.* 65, 9670-9677.

Han, H., Du, B., Pan, X., Liu, J., Zhao, Q., Lian, X., Qian, M., and Liu, M. (2010). CADPE inhibits PMA-stimulated gastric carcinoma cell invasion and matrix metalloproteinase-9 expression by FAK/MEK/ERK-mediated AP-1 activation. Mol. Cancer. Res. 8, 1477-1488.

Harjai, K. J. 1999. Potential new cardiovascular risk factors: Left ventricular hypertrophy, homocysteine, lipoprotein(a), triglycerides, oxidative stress, and fibrinogen. *Annals of Intern. Med.* 131: 376-386.

Hardy, J. A. and Aust, A. E. (1995). The effect of iron binding on the ability of crocidolite asbestos to catalyze DNA single-strand breaks. *Carcinogenesis.* 16, 319-325.

Heyen, J.R.R., E.R. Blasi, K. Nikula, R. Rocha, H.A. Daust, G. Frierdich, J.F. Van Vleet, P. De Ciechi, E.G. McMahon, and A.E. Rudolph. 2002. Structural, functional, and molecular characterization of the shhf model of heart failure. *Am. J. Physiol. Heart Circ. Physiol.* 283: H1775-H1784

Hill, G.D., Mangum, J.B., Moss, O.R., & Everitt, J.I. 2003, "Soluble ICAM-1, MCP-1, and MIP-2 protein secretion by rat pleural mesothelial cells following exposure to amosite asbestos", *Experimental Lung Research*, vol. 29, no. 5, pp. 277-290.

Hillegass, J. M., Shukla, A., Lathrop, S. A., MacPherson, M. B., Beuschel, S. L., Butnor, K. J., Testa, J. R., Pass, H. I., Carbone, M., Steele, C., and Mossman, B. T. (2010). Inflammation precedes the development of human malignant mesotheliomas in a SCID mouse xenograft model. *Ann. N. Y. Acad. Sci.* 1203, 7-14.

Hirano, S., Ono, M. & Aimoto, A. 1988, "Functional and biochemical effects on rat lung following instillation of crocidolite and chrysotile asbestos", *Journal of toxicology and environmental health*, vol. 24, no. 1, pp. 27-39.

Hornung, V., Bauernfeind, F., Halle, A., Samstad, E. O., Kono, H., Rock, K. L., Fitzgerald, K. A., and Latz, E. (2008). Silica crystals and aluminum salts activate the NALP3 inflammasome through phagosomal destabilization. *Nat. Immunol.* 9, 847-856.

Hsieh, Y. C., Wu, T. Z., Liu, D. P., Shao, P. L., Chang, L. Y., Lu, C. Y., Lee, C. Y., Huang, F. Y., and Huang, L. M. (2006). Influenza pandemics: past, present and future. *J. Formos. Med. Assoc.* 105, 1-6.

Hu, Q., Akatsuka, S., Yamashita, Y., Ohara, H., Nagai, H., Okazaki, Y., Takahashi, T., and Toyokuni, S. (2010). Homozygous deletion of CDKN2A/2B is a hallmark of iron-induced high-grade rat mesothelioma. *Lab. Invest.* 90, 360-373.

Huang da, W., Sherman, B. T., and Lempicki, R. A. (2009). Systematic and integrative analysis of large gene lists using DAVID bioinformatics resources. *Nat. Protoc.* 4, 44-57.

Kakhlon, O., and Z. I. Cabantchik. 2002. The labile iron pool: Characterization, measurement, and participation in cellular processes(1). *Free Radic. Biol. Med.* 33: 1037-1046.

Kamp, D.W., Israbian, V.A., Preusen, S.E., Zhang, C.X. & Weitzman, S.A. 1995a, "Asbestos causes DNA strand breaks in cultured pulmonary epithelial cells: role of iron-catalyzed free radicals", *The American Journal of Physiology*, vol. 268, no. 3 Pt 1, pp. L471-80.

Kamp, D.W., Israbian, V.A., Yeldandi, A.V., Panos, R.J., Graceffa, P. & Weitzman, S.A. 1995b, "Phytic acid, an iron chelator, attenuates pulmonary inflammation and fibrosis in rats after intratracheal instillation of asbestos", *Toxicologic pathology*, vol. 23, no. 6, pp. 689-695.

Kamp, D.W. & Weitzman, S.A. 1999, "The molecular basis of asbestos induced lung injury", *Thorax*, vol. 54, no. 7, pp. 638-652.

Kapturczak, M.H., Wasserfall, C., Brusko, T., Campbell-Thompson, M., Ellis, T.M., Atkinson, M.A. & Agarwal, A. 2004, "Heme oxygenase-1 modulates early inflammatory

responses: evidence from the heme oxygenase-1-deficient mouse", *The American journal of pathology,* vol. 165, no. 3, pp. 1045-1053.

Kibel, A., Belovari, T. & Drenjancevic-Peric, I. 2008, "The role of transferrin in atherosclerosis", *Medical hypotheses,* vol. 70, no. 4, pp. 793-797.

Kitamura, H. and Okudela, K. (2010). Bronchioloalveolar neoplasia. *Int. J. Clin. Exp. Pathol.* 4, 97-99.

Kline, J. N., Schwartz, D. A., Monick, M. M., Floerchinger, C. S., and Hunninghake, G. W. (1993). Relative release of interleukin-1 beta and interleukin-1 receptor antagonist by alveolar macrophages. A study in asbestos-induced lung disease, sarcoidosis, and idiopathic pulmonary fibrosis. *Chest.* 104, 47-53.

Kodavanti, U. P., and D. L. Costa. 2001. Rodent models of susceptibility: What is their place in inhalation toxicology? *Respir. Physiol.* 128: 57-70.

Kodavanti, U. P., M. C. Schladweiler, A. D. Ledbetter, R. Hauser, D. C. Christiani, J. McGee, J. R. Richards, and D. L. Costa. 2002. Temporal association between pulmonary and systemic effects of particulate matter in healthy and cardiovascular compromised rats. *J. Toxicol. Environ. Health. A* 65: 1545-1569.

Kodavanti, U. P., M. C. Schladweiler, A. D. Ledbetter, J. K. McGee, L. Walsh, P. S. Gilmour, J. W. Highfill, D. Davies, K.E. Pinkerton, J.H. Richards, K. Crissman, D. Andrews, and D.L. Costa. 2005. Consistent pulmonary and systemic responses from inhalation of fine concentrated ambient particles: Roles of rat strains used and physicochemical properties. *Environ Health Persp.* 113: 1561-1568.

Kodavanti, U. P., M. C. Schladweiler, A. D. Ledbetter, R. V. Ortuno, M. Suffia, P. Evansky, J. H. Richards, R.H. Jaskot, R. Thomas, E. Karoly, Y.C. Huang, D.L. Costa, P.S. Gilmour, and K.E. Pinkerton. 2006. The spontaneously hypertensive rat: An experimental model of sulfur dioxide-induced airways disease. *Toxicol. Sci.* 94: 193-205.

Kodavanti, U. P., M. C. Schladweiler, A. D. Ledbetter, W. P. Watkinson, M. J. Campen, D. W. Winsett, J. R. Richards, K. M. Crissman, G. E. Hatch, and D. L. Costa. 2000. The spontaneously hypertensive rat as a model of human cardiovascular disease: Evidence of exacerbated cardiopulmonary injury and oxidative stress from inhaled emission particulate matter. *Toxicol. Appl. Pharmacol.* 164: 250-63.

Kodavanti, U. P., M. C. Schladweiler, J. R. Richards, and D. L. Costa. 2001. Acute lung injury from intratracheal exposure to fugitive residual oil fly ash and its constituent metals in normo- and spontaneously hypertensive rats. *Inhal. Toxicol.* 13: 37-54.

Koerten, H. K., Brederoo, P., Ginsel, L. A., and Daems, W. T. (1986). The endocytosis of asbestos by mouse peritoneal macrophages and its long-term effect on iron accumulation and labyrinth formation. *Eur. J. Cell Biol.* 40, 25-36.

Koorts, A.M. & Viljoen, M. 2007, "Ferritin and ferritin isoforms I: Structure-function relationships, synthesis, degradation and secretion", *Archives of Physiology and Biochemistry,* vol. 113, no. 1, pp. 30-54.

Kruszewski, M. 2003. Labile iron pool: The main determinant of cellular response to oxidative stress. *Mut. Res.* 531: 81-92.

Kruszewski, M. 2004. The role of labile iron pool in cardiovascular diseases. *Acta Biochim. Pol.* 51: 471-480.

Kukulj, S., Jaganjac, M., Boranic, M., Krizanac, S., Santic, Z., and Poljak-Blazi, M. (2010). Altered iron metabolism, inflammation, transferrin receptors, and ferritin expression in non-small-cell lung cancer. *Med. Oncol.* 27, 268-277.

Kuribayashi, T. 1987. Spontaneously occurring hypertrophic cardiomyopathy in the rat. I. pathologic features. *Japan. Circ. J.* 51: 573-588.

Lam, C. F., A. J. Croatt, D. M. Richardson, K. A. Nath, and Z. S. Katusic. 2005. Heart failure increases protein expression and enzymatic activity of heme oxygenase-1 in the lung. *Cardiovasc. Res.* 65: 203-210.

Lassègue, B., and K.K. Griendling. 2004. Reactive oxygen species in hypertension: An update. *Am. J. Hypertens.* 17: 852-860.

Leenen, F. H., and B. Yuan. 1998. Dietary-sodium-induced cardiac remodeling in spontaneously hypertensive rat versus wistar-kyoto rat. *J. Hypertens.* 16: 885-892.

Lindroos, P. M., Coin, P. G., Badgett, A., Morgan, D. L., and Bonner, J. C. (1997). Alveolar macrophages stimulated with titanium dioxide, chrysotile asbestos, and residual oil fly ash upregulate the PDGF receptor-alpha on lung fibroblasts through an IL-1beta-dependent mechanism. *Am. J. Respir. Cell Mol. Biol.* 16, 283-292.

Lopez, A. D., C. D. Mathers, M. Ezzati, D. T. Jamison, and C. J. Murray. 2006. Global and regional burden of disease and risk factors, 2001: Systematic analysis of population health data. *Lancet* 367: 1747-1757.

Lowers, H.A., and Bern, A.M. 2009, "Particle Size Characterization of Water-Elutriated Libby Amphibole 2000 and RTI International Amosite", USGS Open File Report 2009-1242

Lund, L. G., Williams, M. G., Dodson, R. F., and Aust, A. E. (1994). Iron associated with asbestos bodies is responsible for the formation of single strand breaks in phi X174 RFI DNA. *Occup. Environ. Med.* 51, 200-204.

Martinon, F., Burns, K., and Tschopp, J. (2002). The inflammasome: a molecular platform triggering activation of inflammatory caspases and processing of proIL-beta. *Mol. Cell.* 10, 417-426.

Mast, R. W., Hesterberg, T. W., Glass, L. R., McConnell, E. E., Anderson, R., and Bernstein, D. M. (1994). Chronic inhalation and biopersistence of refractory ceramic fiber in rats and hamsters. *Environ. Health Perspect.* 102 Suppl 5, 207-209.

McConnell, E. E., Axten, C., Hesterberg, T. W., Chevalier, J., Miiller, W. C., Everitt, J., Oberdorster, G., Chase, G. R., Thevenaz, P., and Kotin, P. (1999). Studies on the inhalation toxicology of two fiberglasses and amosite asbestos in the Syrian golden hamster. Part II. Results of chronic exposure. *Inhal. Toxicol.* 11, 785-835.

McCune, S.A., Baker, P.B., and Stills, H.F. 1990. SHHF/Mcc-cp rat: model of obesity, non-insulin dependent diabetes, and congestive heart failure. *Institute for Laboratory Animal Research Journal* V32(3) New Rat Models of Obesity and Type II Diabetes

McDonald, J. C. (1998). Mineral fibre persistence and carcinogenicity. *Ind. Health.* 36, 372-375.

McIntire, M. G., Santagata, S., Ligon, K., and Chirieac, L. R. (2010). Epidermal growth factor receptor gene amplification in atypical adenomatous hyperplasia of the lung. *Am. J. Transl. Res.* 2, 309-315.

Meeker, G.P., Bern, A.M., Brownfield, I.K., Lowers, H.A., Sutley, S.J., Hoefen, T.M. & Vance, J.S. 2003, "The Composition and Morphology of Amphiboles from the Rainy Creek Complex, Near Libby, Montana", *American Mineralogist*, vol. 88, no. 11-12, pp. 1955-1969.

Mojtahedi, Z. and Ghaderi, A. (2005). Role of interleukin-18 in allergy and autoimmunity: an explanation for the hygiene hypothesis. *Med. Hypotheses.* 65, 305-307.

Moolgavkar, S. H., Turim, J., Alexander, D. D., Lau, E. C., and Cushing, C. A. (2010). Potency factors for risk assessment at Libby, Montana. *Risk Anal.* 30, 1240-1248.

Morris, R. D., E. N. Naumova, and R. L. Munasinghe. 1995. Ambient air pollution and hospitalization for congestive heart failure among elderly people in seven large US cities. *American Journal of Public Health* 85, (10) (Oct): 1361-5.

Morris, G. F., Notwick, A. R., David, O., Fermin, C., Brody, A. R., and Friedman, M. (2004). Development of lung tumors in mutant p53-expressing mice after inhalation exposure to asbestos. *Chest.* 125, 85S-6S.

Mossman, B. T., Bignon, J., Corn, M., Seaton, A., and Gee, J. B. (1990). Asbestos: scientific developments and implications for public policy. *Science.* 247, 294-301.

Muravov, O. I., Kaye, W. E., Lewin, M., Berkowitz, Z., Lybarger, J. A., Campolucci, S. S., and Parker, J. E. (2005). The usefulness of computed tomography in detecting asbestos-related pleural abnormalities in people who had indeterminate chest radiographs: the Libby, MT, experience. *Int. J. Hyg. Environ. Health.* 208, 87-99.

Nikula, K. J., and F. H. Green. 2000. Animal models of chronic bronchitis and their relevance to studies of particle-induced disease. *Inhal. Toxicol.* 12 Suppl 4: 123-153.

Noonan, C. W., Pfau, J. C., Larson, T. C., and Spence, M. R. (2006). Nested case-control study of autoimmune disease in an asbestos-exposed population. *Environ. Health Perspect.* 114, 1243-1247.

Nyska, A., Murphy, E., Foley, J.F., Collins, B.J., Petranka, J., Howden, R., Hanlon, P. & Dunnick, J.K. 2005, "Acute hemorrhagic myocardial necrosis and sudden death of rats exposed to a combination of ephedrine and caffeine", *Toxicological sciences : an official journal of the Society of Toxicology*, vol. 83, no. 2, pp. 388-396.

O'Byrne, P. M. (1996). Airway inflammation and asthma. *Aliment. Pharmacol. Ther.* 10 Suppl 2, 18-24.

Okamoto, K., and Aoki, K. 1963. Development of a strain of spontaneously hypertensive rats. *Japan. Circ.* 27: 282-293.

Omiya, S., S. Hikoso, Y. Imanishi, A. Saito, O. Yamaguchi, T. Takeda, I. Mizote, et al. 2009. Downregulation of ferritin heavy chain increases labile iron pool, oxidative stress and cell death in cardiomyocytes. *J. Mol. Cell. Cardiol.* 46: 59-66.

Othman, A.I., M.A. El-Missiry, M.A. Amer, and M. Arafa. 2008. Melatonin conrols oxidative stress and modulates iron, ferritin, and transferrin levels in adriamycin treated rats. Life Sci. 83:563-568

Padilla-Carlin DJ, Schladweiler MCJ, Shannahan JH, Kodavanti UP, Nyska A, Burgoon LD, Gavett SH. Pulmonary inflammatory and fibrotic responses in Fischer 344 rats after intratracheal instillation exposure to Libby amphibole. J. Toxicol. Environ. Health (accepted for publication)

Pang, I. K. and Iwasaki, A. (2011). Inflammasomes as mediators of immunity against influenza virus. *Trends Immunol.* 32, 34-41.

Pascolo, L., Gianoncelli, A., Kaulich, B., Rizzardi, C., Schneider, M., Bottin, C., Polentarutti, M., Kiskinova, M., Longoni, A., and Melato, M. (2011). Synchrotron soft X-ray imaging and fluorescence microscopy reveal novel features of asbestos body morphology and composition in human lung tissues. *Part Fibre Toxicol.* 8, 7.

Peipins, L.A., Lewin, M., Campolucci, S., Lybarger, J.A., Miller, A., Middleton, D., Weis, C., Spence, M., Black, B. & Kapil, V. 2003, "Radiographic abnormalities and exposure to asbestos-contaminated vermiculite in the community of Libby, Montana, USA", *Environmental health perspectives*, vol. 111, no. 14, pp. 1753-1759.

Pope, C. A.,3rd, R. T. Burnett, G. D. Thurston, M. J. Thun, E. E. Calle, D. Krewski, and J. J. Godleski. 2004. Cardiovascular mortality and long-term exposure to particulate air pollution:

Epidemiological evidence of general pathophysiological pathways of disease. *Circulation* 109: 71-77.

Pooley, F. D. (1972). Asbestos bodies, their formation, composition and character. *Environ. Res.* 5, 363-379.

Poser, I., Rahman, Q., Lohani, M., Yadav, S., Becker, H. H., Weiss, D. G., Schiffmann, D., and Dopp, E. (2004). Modulation of genotoxic effects in asbestos-exposed primary human mesothelial cells by radical scavengers, metal chelators and a glutathione precursor. *Mutat. Res.* 559, 19-27.

Poss, K.D. & Tonegawa, S. 1997, "Reduced stress defense in heme oxygenase 1-deficient cells", *Proceedings of the National Academy of Sciences of the United States of America*, vol. 94, no. 20, pp. 10925-10930.

Putnam, E.A., Smartt, A., Groves, A., Schwanke, C., Brezinski, M. & Pershouse, M.A. 2008, "Gene expression changes after exposure to six-mix in a mouse model", *Journal of immunotoxicology*, vol. 5, no. 2, pp. 139-144.

Raval, C.M. & Lee, P.J. 2010, "Heme oxygenase-1 in Lung Disease", *Current Drug Targets*,.

Robledo, R. F., Buder-Hoffmann, S. A., Cummins, A. B., Walsh, E. S., Taatjes, D. J., and Mossman, B. T. (2000). Increased phosphorylated extracellular signal-regulated kinase immunoreactivity associated with proliferative and morphologic lung alterations after chrysotile asbestos inhalation in mice. *Am. J. Pathol.* 156, 1307-1316.

Rodelsperger, K. and Woitowitz, H. J. (1995). Airborne fibre concentrations and lung burden compared to the tumour response in rats and humans exposed to asbestos. *Ann. Occup. Hyg.* 39, 715-725.

Sabo-Attwood, T., Ramos-Nino, M., Bond, J., Butnor, K.J., Heintz, N., Gruber, A.D., Steele, C., Taatjes, D.J., Vacek, P. & Mossman, B.T. 2005, "Gene expression profiles reveal increased mClca3 (Gob5) expression and mucin production in a murine model of asbestos-induced fibrogenesis", *The American journal of pathology*, vol. 167, no. 5, pp. 1243-1256.

Sanchez, V.C., Pietruska, J.R., Miselis, N.R., Hurt, R.H. & Kane, A.B. 2009, "Biopersistence and potential adverse health impacts of fibrous nanomaterials: what have we learned from asbestos?", *Wiley interdisciplinary reviews.Nanomedicine and nanobiotechnology*, vol. 1, no. 5, pp. 511-529.

Salonen, J. T., K. Nyyssonen, H. Korpela, J. Tuomilehto, R. Seppanen, and R. Salonen. 1992. High stored iron levels are associated with excess risk of myocardial infarction in eastern Finnish men. *Circulation* 86: 803-811.

Samet, J., and D. Krewski. 2007. Health effects associated with exposure to ambient air pollution. *J. Toxicol. Environ. Health A.* 40: 227-242

Sans, S., H. Kesteloot, and D. Kromhout. 1997. The burden of cardiovascular diseases mortality in Europe. task force of the European society of cardiology on cardiovascular mortality and morbidity statistics in Europe. *Eur. Heart J.* 18: 1231-1248.

Scapellato, M. L., and M. Lotti. 2007. Short-term effects of particulate matter: An inflammatory mechanism? *Crit. Rev. Toxicol.* 37: 461-87.

Schmid-Schonbein, G. W., D. Seiffge, F. A. DeLano, K. Shen, and B. W. Zweifach. 1991. Leukocyte counts and activation in spontaneously hypertensive and normotensive rats. *Hypertension* 17: 323-330.

Schurkes, C., Brock, W., Abel, J., and Unfried, K. (2004). Induction of 8-hydroxydeoxyguanosine by man made vitreous fibres and crocidolite asbestos administered intraperitoneally in rats. *Mutat. Res.* 553, 59-65.

Sen, S., Roy, M., and Chakraborti, A. S. (2011). Ameliorative effects of glycyrrhizin on streptozotocin-induced diabetes in rats. *J. Pharm. Pharmacol.* 63, 287-296.

Shackelford, C., Long, G., Wolf, J., Okerberg, C. & Herbert, R. 2002, "Qualitative and quantitative analysis of nonneoplastic lesions in toxicology studies", *Toxicologic pathology*, vol. 30, no. 1, pp. 93-96.

Shannahan, J.H., Schladweiler, M.C., Richards, J.H., Ledbetter, A.D., Ghio, A.J. & Kodavanti, U.P. 2010, "Pulmonary oxidative stress, inflammation, and dysregulated iron homeostasis in rat models of cardiovascular disease", *Journal of toxicology and environmental health.Part A*, vol. 73, no. 10, pp. 641-656.

Shannahan, J.H., Ghio, A.J., Schladweiler, M.C., McGee, J.K., Richards, J.H., Gavett, S.H., & Kodavanti, U.P. 2011a "The Role of Iron in Libby Amphibole-Induced Toxicity" Submitted for Publication

Shannahan, J.H., Schladweiler, M.C., Padilla-Carlin, D.J., Nyska, A., Richards, J.H., Ghio, A.J., Gavett, S.H., and Kodavanti, U.P. 2011b. The role of cardiovascular disease-associated iron overload in Libby amphibole-induced pulmonary injury and inflammation. *Inhal. Toxicol*. (in press)

Shen, Z., Bosbach, D., Hochella, M. F.,Jr, Bish, D. L., Williams, M. G.,Jr, Dodson, R. F., and Aust, A. E. (2000). Using in vitro iron deposition on asbestos to model asbestos bodies formed in human lung. *Chem. Res. Toxicol.* 13, 913-921.

Shih, D. M., and A. J. Lusis. 2009. The roles of PON1 and PON2 in cardiovascular disease and innate immunity. *Curr. Opin. Lipidol.* 20: 288-292.

Smartt, A.M., Brezinski, M., Trapkus, M., Gardner, D. & Putnam, E.A. 2010, "Collagen accumulation over time in the murine lung after exposure to crocidolite asbestos or Libby amphibole", *Environmental toxicology*, vol. 25, no. 1, pp. 68-76.

Srivastava, R. K., Lohani, M., Pant, A. B., and Rahman, Q. (2010). Cyto-genotoxicity of amphibole asbestos fibers in cultured human lung epithelial cell line: role of surface iron. *Toxicol. Ind. Health.* 26, 575-582.

Sullivan, P.A. 2007, "Vermiculite, respiratory disease, and asbestos exposure in Libby, Montana: update of a cohort mortality study", *Environmental health perspectives,* vol. 115, no. 4, pp. 579-585.

Sun, L., Y. H. Gao, D. K. Tian, J. P. Zheng, C. Y. Zhu, Y. Ke, and K. Bian. 2006. Inflammation of different tissues in spontaneously hypertensive rats. *Sheng Li Xue Bao: [Acta Physiologica Sinica]* 58: 318-323.

Suzuki, H., A. Swei, B. W. Zweifach, and G. W. Schmid-Schonbein. 1995. In vivo evidence for microvascular oxidative stress in spontaneously hypertensive rats. hydroethidine microfluorography. *Hypertension* 25: 1083-1089.

Thomas, D. H., Attanoos, R. L., and Gibbs, A. R. (2004). Coexistent atypical adenomatous hyperplasia, primary lung adenocarcinoma and pleural mesothelioma in an asbestos-exposed subject. *Histopathology.* 45, 540-542.

Toyokuni, S. (2011). Mysterious link between iron overload and CDKN2A/2B. *J. Clin. Biochem. Nutr.* 48, 46-49.

Treffry, A., Harrison, P. M., Cleton, M. I., de Bruijn, W. C., and Mann, S. (1987). A note on the composition and properties of ferritin iron cores. *J. Inorg. Biochem.* 31, 1-6.

Tsuzuki, T., Ninomiya, H., Natori, Y., and Ishikawa, Y. (2008). Coalescent pleural malignant mesothelioma and adenocarcinoma of the lung, involving only minor asbestos exposure. *Pathol. Int.* 58, 451-455.

Tuomainen, T. P., K. Punnonen, K. Nyyssonen, and J. T. Salonen. 1998. Association between body iron stores and the risk of acute myocardial infarction in men. *Circulation* 97: 1461-1466.

Turi, S., A. Friedman, C. Bereczki, F. Papp, J. Kovacs, E. Karg, and I. Nemeth. 2003. Oxidative stress in juvenile essential hypertension. *J. Hypertens.* 21: 145-152.

Ulrich, M.M.W., G.M. Alink, P. Kumarathasan, R. Vincent, A.J.F. Boera, and F.R. Cassee. 2002. Health effects and time course of particulate matter on the cardiopulmonary system in rats with lung inflammation. *J. Toxicol. Environ. Health A.* 65: 1571-1595

U.S. EPA (2007). Method 200.7 Revision 4.4: Determination of metals and trace elements in water and wastes by inductively coupled plasma -atomic emission spectrometry. In: Methods for the determination of metals in environmental samples, supplement I. EPA/600/R-94/111. Available: http://www.epa.gov/waterscience/methods/method/files/200_7.pdf

U.S. EPA. 2010, "Particle size distribution data for Libby amphibole structures observed in air at the Libby asbestos Superfund site", Superfund Records Center, U.S. EPA Region 8, Denver, CO.

Viallat, J. R., Raybuad, F., Passarel, M., and Boutin, C. (1986). Pleural migration of chrysotile fibers after intratracheal injection in rats. *Arch. Environ. Health.* 41, 282-286.

Videan, E. N., C. B. Heward, K. Chowdhury, J. Plummer, Y. Su, and R. G. Cutler. 2009. Comparison of biomarkers of oxidative stress and cardiovascular disease in humans and chimpanzees (pan troglodytes). *Comp. Med.* 59: 287-296.

Vinikoor, L. C., Larson, T. C., Bateson, T. F., and Birnbaum, L. (2010). Exposure to asbestos-containing vermiculite ore and respiratory symptoms among individuals who were children while the mine was active in Libby, Montana. *Environ. Health Perspect.* 118, 1033-1028.

Wallenborn, J.G., Kovalcik, K.D., McGee, J.K., Landis, M.S. & Kodavanti, U.P. 2009, "Systemic translocation of (70)zinc: kinetics following intratracheal instillation in rats", *Toxicology and applied pharmacology,* vol. 234, no. 1, pp. 25-32.

Wang, X., Samet, J. M., and Ghio, A. J. (2006a). Asbestos-induced activation of cell signaling pathways in human bronchial epithelial cells. *Exp. Lung Res.* 32, 229-243.

Wang, X., Wu, Y., Stonehuerner, J. G., Dailey, L. A., Richards, J. D., Jaspers, I., Piantadosi, C. A., and Ghio, A. J. (2006b). Oxidant generation promotes iron sequestration in BEAS-2B cells exposed to asbestos. *Am. J. Respir. Cell Mol. Biol.* 34, 286-292.

Wang, Y., Faux, S. P., Hallden, G., Kirn, D. H., Houghton, C. E., Lemoine, N. R., and Patrick, G. (2004). Interleukin-1beta and tumour necrosis factor-alpha promote the transformation of human immortalised mesothelial cells by erionite. *Int. J. Oncol.* 25, 173-178.

Webber, J.S., Blake, D.J., Ward, T.J. & Pfau, J.C. 2008, "Separation and characterization of respirable amphibole fibers from Libby, Montana", *Inhalation toxicology,* vol. 20, no. 8, pp. 733-740.

Weinberg, E. D. (2009). Iron availability and infection. *Biochim. Biophys. Acta.* 1790, 600-605.

Weinrach, D. M., K. L. Wang, W. R. Wiseman, and L. K. Diaz. 2005. Ferruginous bodies on frozen section. *Arch. Pathol. Lab. Med.* 129: 266.

Whitehouse, A. C., Black, C. B., Heppe, M. S., Ruckdeschel, J., and Levin, S. M. (2008). Environmental exposure to Libby Asbestos and mesotheliomas. *Am. J. Ind. Med.* 51, 877-880.

Wichers, L. B., J. P. Nolan, D. W. Winsett, A. D. Ledbetter, U. P. Kodavanti, M. C. Schladweiler, D. L. Costa, and W. P. Watkinson. 2004. Effects of instilled combustion-derived particles in spontaneously hypertensive rats. part II: Pulmonary responses. *Inhal. Toxicol.* 16: 407-419.

Xie, X.M., Cao, X., Chen, M.F., Zhou, Y.C., Chen, X.B. & Jiang, H.Y. 2008, "Effect of chronic iron overload on atherosclerosis lesion in apolipoprotein E knockout mice", *Zhong nan da xue xue bao.Yi xue ban = Journal of Central South University.Medical sciences,* vol. 33, no. 1, pp. 57-62.

Yang, C., Y. Chen, C. Yang, and S. Ho. 2004. Relationship between ambient air pollution and hospital admissions for cardiovascular diseases in Kaohsiung, Taiwan. *J. Toxicol. Environ. Health A.* 67: 483-493.

Yang, W., B.L. Jennison, and S.T. Omaye. 1998. Cardiovasculat disease hospitalization and ambient levels of carbon monoxide. *J. Toxicol. Environ. Health A.* 55: 185-196.

Yao, H. and Rahman, I. (2011). Current concepts on oxidative/carbonyl stress, inflammation and epigenetics in pathogenesis of chronic obstructive pulmonary disease. *Toxicol. Appl. Pharmacol.*

Yasuda, T., Funakubo, A. & Fukui, Y. 2002, "An investigation of blood damage induced by static pressure during shear-rate conditions", *Artificial Organs,* vol. 26, no. 1, pp. 27-31.

Yu, B., U. P. Kodavanti, M. Takeuchi, H. Witschi, and K. E. Pinkerton. 2008. Acute tobacco smoke-induced airways inflammation in spontaneously hypertensive rats. *Inhal. Toxicol.* 20: 623-633.

Zhang, Y., Lee, T. C., Guillemin, B., Yu, M. C., and Rom, W. N. (1993). Enhanced IL-1 beta and tumor necrosis factor-alpha release and messenger RNA expression in macrophages from idiopathic pulmonary fibrosis or after asbestos exposure. *J. Immunol.* 150, 4188-4196.

Zhang, Y., W. Huang, S. J. London, G. Song, G. Chen, L. Jiang, N. Zhao, B. Chen, and H. Kan. 2006. Ozone and daily mortality in Shanghai, China. *Environ. Health Persp.* 114: 1227-1232.